In-situ temporospatial characterization of the neuroinflammatory response to prion infection in the murine brain

by

Alyona V. Michael

A dissertation submitted to the graduate faculty

in partial fulfillment of the requirements for the degree of

DOCTOR OF PHILOSOPHY

Major: Veterinary Pathology

Program of Study Committee:
Jodi D. Smith, Major Professor
Mark R. Ackermann
Matthew T. Brewer
M. Heather West Greenlee
Jesse M. Hostetter

The student author, whose presentation of the scholarship herein was approved by the program of study committee, is solely responsible for the content of this dissertation. The Graduate College will ensure this dissertation is globally accessible and will not permit alterations after a degree is conferred.

Iowa State University

Ames, Iowa

2018

TABLE OF CONTENTS

ABSTRACT

Transmissible spongiform encephalopathies constitute a group of mammalian neurodegenerative protein misfolding disorders, characterized by neuronal loss and gliosis in response to accumulation of an abnormal conformer (PrP^{sc}) of the native cellular prion protein (PrP^{c}). The nature of the local inflammatory response and the potential contributions of microgliosis and astrocytosis to the progression of neuropathology have not been fully resolved. Shifts in microglial and astrocytic immunophenotypes have been demonstrated in other human neurodegenerative protein misfolding diseases. Similarly, we anticipated a fluid glial activation profile, characterized by transitions in phenotype markers and immunoproteasome induction, over the course of prion infection. This dissertation sought to characterize the neuroinflammatory response to prion infection using a murine intracranial infection model.

Successive chromogenic immunolabeling and in-situ hybridization were employed in analyzing expression patterns of glial activation markers and a proteasomal subtype (PSMB10) over the timecourse of infection in a murine scrapie model. Our model successfully recapitulated classical patterns of TSE-associated neuropathology and demonstrated a precocious microglial response, relative to other studies. We also identified an upregulation of the proinflammatory enzyme iNOS in glial populations at late stages of disease incubation. Colocalization analysis of glial cytoplasmic and activation markers allowed us to resolve an astrocyte-associated increase in Arg1 expression in clinical disease, despite lack of significant changes in global Arg1 expression. Although quantification of immunoproteasome subunit PSMB10 expression failed to yield significant temporospatial trends, this analysis characterized baseline expression patterns across 16 brain regions. Combined, these findings constitute a comprehensive in-situ evaluation of glial activation and present techniques novel to prion research.

CHAPTER 1. LITERATURE REVIEW

Background

Transmissible spongiform encephalopathies

Transmissible spongiform encephalopathies (TSEs) constitute a group of insidious neurodegenerative diseases that afflict a range of mammalian species, including humans (Kuru, Creutzfeldt-Jacob, Gerstmann-Sträussler-Scheinker), bovines (bovine spongiform encephalopathy), small ruminants (scrapie), and cervids (chronic wasting disease, CWD). Prion diseases share a common pathology of prolonged incubation spanning months to decades, gradual loss of cognitive capacity, ataxia, emaciation and an invariably fatal outcome (Asher et al., 1976). The delayed symptomology of TSEs provides opportunities for unwitting dissemination of human infection through both vertical transmission of genetic variants (Webb et al., 2009; Owen et al., 2014; Schmitz et al., 2016), and horizontal spread of acquired disease phenotypes via routine medical procedures (Sushma et al., 2016; Bonda et al., 2016; Rudge et al., 2015; Davanipour et al., 2014; Bradford et al., 2014; Gnanajothy et al., 2013; Thomas et al., 2013; Urwin et al., 2016; H. L. Kim et al., 2011; Hall et al., 2014). Additionally, the environmental persistence of the prion protein (Gough et al., 2010; Marin-Moreno et al., 2016; Nagaoka et al., 2010), increased prevalence of CWD (Zabel et al., 2017), cases of sporadic atypical BSE (Sala et al., 2012; Seuberlich et al., 2010; Ono et al., 2011; Saunders et al., 2012), and potential underestimation of actual food-borne infection rate (Oraby et al., 2016; Al-Zoughool et al., 2016) maintain animal-derived prion agents as a credible zoonotic threat.

TSE's are not completely unique in their proteinaceous etiology, as there are increasing parallels between prion infections and a subset of chronic human neurodegenerative diseases. Even prior to the establishment of scientific consensus on the basic mechanism of prion

propagation, researchers remarked on a degree of clinical homology between human TSEs and Alzheimer's disease (P. Brown et al., 1982). Modern understanding of neurodegenerative pathology substantiates this recognition with the demonstration of prion-like 'propagons' of fibrils in Alzheimer's (AD), Parkinson's (PD), Huntington's (HD) diseases and amyotrophic lateral sclerosis (ALS) composed of amyloid beta (Aβ) and tau, α-synuclein, and huntingtin, respectively. As reviewed by Aguzzi and Erana (Aguzzi et al., 2016; Erana et al., 2016), these entities share an amyloidogenic pathophysiology, wherein soluble oligomers of misfolded proteins can form self-propagating fibrils and result in aggregate deposition within neurons and the neuropil. However, infectivity of these subunits has yet to be demonstrated between individuals. In light of this distinction, the term 'prionoid' was proposed by the authors to designate protein misfolding diseases where transmissibility has not been proven. Evaluation of potential mechanistic homology between 'prionoids' and TSEs may provide valuable insight into their pathogeneses and suggest avenues for treatment.

The contribution of glial activation to the progression of prion infection is controversial, with evidence for mediation of both protective and deleterious outcomes. Incomplete understanding of early disease mechanisms contributes to lack of effective early diagnostics and treatment options for these diseases. This review will seek to summarize current understanding of glial kinetics, immunophenotypes, and their effect on proteolysis and disease progression.

Cellular prion protein (PrP^C)

In spite of clinical recognition of TSEs spanning 200 years (Liberski, 2012), the causative agent remained a mystery until the late 20th century. The 'protein only' theory, first advanced in the 1980's (Prusiner, 1982), proposed that TSE's are caused by a proteinase K-resistant

*pro*teinaceous *in*fectious particle. Pursuit of this unprecedented model of infectivity has yielded a mechanism of neurotoxicity mediated by self-propagating corruption of a native cytoplasmic prion protein, PrP^{c} by a foreign peptide with an identical primary amino acid sequence (Hope et al., 1986; Stahl et al., 1993; Pan et al., 1993). Cellular prion protein is ubiquitously expressed on tissue membranes as a glycosylphosphatidylinositol (GPI)-linked glycoprotein with a predominance of alpha-helices in its secondary structure. The highest concentration of PrP^{c} is found in neural tissues, with increased expression in the hippocampus and thalamolimbic system (Benvegnu et al., 2010).

Proposed functions of PrP^{c} are varied and include cellular differentiation, neuronal excitability and metal homeostasis (Castle et al., 2017). Despite conserved expression of the protein across mammalian species, PrP^{c} does not appear necessary for survival. Murine PrP^{c} knock-out models display minimal phenotypic disturbance but are resistant to prion infection (Bueler et al., 1992; Bueler et al., 1993). A line of Norwegian dairy goats, the only known mammal naturally deficient in PrP^{c}, are also phenotypically normal, but display upregulation of proinflammatory genes (Malachin et al., 2017). As discussed below, exposure of PrP^{c} molecules to an aberrant PrP^{sc} with a high beta-sheet composition catalyzes misfolding of native proteins, accumulation of PrP^{sc} plaques and induction of neuronal degeneration by hitherto uncertain mechanisms.

Prion types and strains

Prion disease models can be subclassified by prion type and strain. Prion types are grouped according to structural features that can influence the physical properties of the agent identified in the original host, whereas prion strains are separated by the pathophysiologic profile of infection

in a new host (Wemheuer et al., 2017). For example, the Rocky Mountain Laboratories (RML) mouse-adapted strain of scrapie was obtained when ovine scrapie agent was inoculated into goats, resulting in a 'drowsy' phenotype, followed by serial passage in in mice (Striebel et al., 2011). Generation of new prion strains can be somewhat limited by the concept of a species transmission barrier, wherein infectivity of a strain within members of the same species is higher than between members of different species. Depending on factors such as inoculation route and host PrP^c conformation, interspecies infections may exhibit prolonged incubation times or fail to reproduce disease entirely (Greenlee et al., 2015). For example, despite the ready oral transmissibility of scrapie between sheep and CWD between cervids, passage of these agents to cattle is only successful if instilled intracranially, and no cases of human infection of either has been recorded, despite inevitable unwitting consumption of infected animals (Greenlee et al., 2015). However, Czub et al recently presented preliminary findings of an ongoing oral CWD trial in Cynomolgus macaques, which suggested transmission of clinical disease to non-human primates following consumption of muscle from subclinically infected cervids (Stefanie Czub, 2017).

Prohibitively long TSE incubation times required to study disease phenotypes in large mammals have driven the development of a vast variety of murine models capable of recapitulating infection patterns of different strains (Brandner et al., 2017). Murine models offer a homogenous genetic background with shortened disease timecourse, and genetic manipulation can reproduce species-specific disease patterns as well as permit evaluation of the effects of PrP conformation and PRNP polymorphisms on disease progression (Brandner et al., 2017). Murine models of scrapie infection have been extensively employed in exploring prion pathophysiology and have contributed to foundational understanding of TSE infection, including strain-specific patterns of

neurodegeneration (Fraser et al., 1973; Bruce et al., 1991) and neuroinflammatory reactions (Giese et al., 1998; Carroll et al., 2016; Vincenti et al., 2015).

Prion infection and pathogenesis

PrP^{sc} ingested in natural and experimental infection appear to enter Peyer's patches in the alimentary tract and undergo amplification in dendritic cells, which subsequently transfer PrP^{sc} to autonomic nerves in a proximity-dependent manner (Kujala, 2011; Prinz et al., 2003). Tissue distribution of the prion agent varies by species. Lymphotropic TSEs, such as CWD, scrapie and vCJD, accumulate broadly through lymphoid organs prior to detection in the CNS (Ersdal et al., 2003; Sigurdson et al., 1999; D. A. Hilton et al., 1998). In contrast, BSE appears to be directly neuroinvasive, forgoing initial peripheral amplification (Balkema-Buschmann et al., 2011). Mechanisms of intercellular PrP^{sc} transmission are not fully elucidated. As reviewed by Aguzzi (Aguzzi et al., 2016), proposed means of dissemination include exosomal transmission (Yim et al., 2015), shedding into the ECM following cleavage by ADAM proteases (Altmeppen et al., 2015), tunneling nanotubules (Gousset et al., 2009), and endocytosis (Goold et al., 2013).

Prion proteins exist in a variety of conformations and polymerization states that propagate under a model of recruitment and fragmentation (Collinge, 2016). Briefly, misfolded PrP^{sc} particles stimulate and stabilize a conformational shift in PrP^{c}, initiating a polymerization chain to form insoluble amyloidogenic fibrils (Collinge, 2016). These fibrils can undergo sporadic fragmentation into a mix of oligomeric species that subsequently seed further PrP^{c} conversion (Collinge, 2016). The physical properties and biologic activity of these species vary. While fibrillar aggregates are deemed biologically inert, it is hypothesized that infectivity and

neurotoxicity are mediated by oligomeric fragmentation species that, unlike fibrillar amyloid plaques, are soluble and partially PK sensitive (C. Kim, 2011; Mays et al., 2015).

The observation that TSEs undergo prolonged subclinical incubation, despite rapidly rising post-inoculation prion titers in experimental infections (Hill et al., 2000), prompted the evolution of the two-phase hypothesis of infection kinetics. Prion infections are characterized by an initial stage of rapidly propagating infectious moieties up to an infectivity plateau (Sandberg et al., 2011). This autocatalytic phase is clinically unremarkable. Upon reaching the infectivity plateau, a new toxic PrP^{sc} isoform characterized by PK sensitivity begins to proliferate until a toxic threshold is reached, manifesting as onset of rapidly progressive clinical disease (Sandberg et al., 2011). The rate of propagation for this toxic species is directly proportional to the level of cellular PrP expression, while the autocatalytic phase appears PrP^{c}-independent (Sandberg et al., 2011). Thus, transgenic mice with increased PrP^{c} density achieve infectivity plateau at a similar rate to wild type mice, but attain toxic threshold and exhibit disease more rapidly thereafter (Sandberg et al., 2011). The mechanism of toxic conversion is unknown. This model dissociates neuroinfectivity, which peaks in subclinical stages, from the symptoms and lesions of neurotoxicity that have been used to characterize prion strains in infection models (Sandberg et al., 2014).

Lesions

Despite species-dependent spatiotemporal variability in lesion expression, deposition of PrP^{sc}, neural vacuolation ("spongiform change") and gliosis are universally manifested in hosts succumbing to prion diseases (Bruce et al., 1991; Carroll et al., 2016; Fraser et al., 1968; Legname et al., 2005; Hainfellner et al., 1997; Spraker et al., 2004; Wood et al., 1997). Surprisingly, the pathoetiology of spongiform change histologically observed in terminal TSE brains remains

somewhat enigmatic. Electron microscopy studies performed by Liberski et al (2005) revealed the membrane-bound contents of fatal familial insomnia and CJD vacuoles to consist of curled membrane fragments and amorphous “fluff” (Liberski et al., 2005). Appearance of these predominantly intra-dendritic cavities was hypothesized to be a function of disrupted axonal transport (A. E. Williams et al., 1994) or lysosomal dysregulation (Betmouni et al., 1996). However, the variability of vacuole appearance relative to preservation technique prompted Betmouni et al to call this change “an informative artifact” (Betmouni et al., 1999). Despite incomplete characterization of the vacuolar change, its appearance correlates to the toxic phase of infection (Sandberg et al., 2014) and the specific distribution pattern is useful in differentiating prion strains (Fraser et al., 1973).

The eventual onset of neurologic symptoms in the clinical phase of prion infection occurs secondary to neuronotoxicity, manifesting histologically as regionally exacerbated synaptic loss and neuronal depletion (Cunningham et al., 2005; Reis et al., 2015; K. J. Hilton et al., 2013). Whether prion toxicity is exerted directly or through a secondary mechanism has not been fully elucidated. There is some limited evidence that PrP^{sc} can directly mediate neuron damage. NMDA receptor-mediated excitotoxity was documented in a mouse model of CJD infection, though the mechanism remains uncertain (Ratte et al., 2008). Several studies have additionally shown that PrP^{sc} conformers can induce neuronal pore formation, resulting in abnormal membrane ion fluxes (Kourie et al., 2000; Berest et al., 2003; Solomon et al., 2010). However, these effects appear to make a minor contribution to disease progression. Secondary neurotoxicity due to accumulation of misfolded proteins and activation of the unfolded protein response (UPR) are discussed later in this review.

Activation of glial cells in response to prion infection is a well-documented phenomenon (A. Williams et al., 1997). Microglia and astrocytes have been demonstrated to undergo reactive hypertrophy during the proposed autocatalytic phase, well in advance of clinical disease (Diedrich et al., 1991; Sandberg et al., 2014; Carroll et al., 2016). Marked increases in microglial numbers, most pronounced in the hippocampus and thalamus, are driven by local expansion of resident cells, rather than recruitment of circulating monocytes (Gomez-Nicola et al., 2013). Glial activation in the course of prion infection can produce a hostile pro-inflammatory environment that may contribute to degenerative change. As reviewed in greater depth below, astrocytes and microglia are known to secrete inflammatory cytokines and reactive oxygen species (Tribouillard-Tanvier et al., 2009; Tribouillard-Tanvier et al., 2012; Sorce et al., 2014). These environmental changes may exacerbate cellular oxidative stress incurred through loss of PrP^c's antioxidant function (Keshet et al., 1999; Choi et al., 1998; Guentchev et al., 2000).

Microglia in Prion Disease

Histology of microglia

Several decades after Metchnikoff's observations of tissue-specific phagocytes at the end of the 19th century (Gordon, 2008), Pío del Río-Hortega confirmed microglia as unique neural resident phagocytes (Tremblay et al., 2015). Microglial ontogeny has since been disputed alongside that of other members of the mononuclear phagocytic system. More recently, the theory of bone marrow derivation has been challenged by fate-mapping experiments that traced microglial origins to erythromyeloid progenitors in the yolk sac (Sheng et al., 2015; Ginhoux et al., 2016). Immunohistologic differentiation of microglia from bone marrow derived macrophages has been complicated by common antigen expression, including F4/80, CD68, CX3CR1, CD11b

and Iba1 (Ginhoux et al., 2015). More recently, TMEM119, a transmembrane protein of uncertain function, has been demonstrated to specifically label microglia, with no myeloid cross-reactivity (Satoh et al., 2016).

Murine microglial precursors undergo multiphasic colonization of the cortex and retina after embryonic day 10, with waves of invasion radiating from pial and ventricular linings (Swinnen et al., 2013). Population densities are unevenly distributed throughout the brain. In the adult murine brain, microglia concentrate in the gray matter, with the highest densities observed in the basal ganglia, substantia nigra, hippocampal dentate gyrus and olfactory tubercle, followed by the diencephalon (Lawson et al., 1990). The lowest numbers are observed in the rhombencephalon (Lawson et al., 1990). In contrast, human microglia preferentially populate telencephalic white matter and appear to be most numerous in the brainstem (Mittelbronn et al., 2001).

Microglia in the healthy brain

Microglia are dynamic cells that can shift along a spectrum of activation states. Morphologically, these cells exist on a continuum ranging from a ‘resting’ form, characterized by a small soma and thin ramified processes, to a round-bodied ‘active’ cell with thick processes, to a de-ramified phagocyte (Walker et al., 2014). A similar fluidity is observed functionally, with experimentally inducible extreme polarization states. In an adaptation of peripheral blood monocyte terminology, microglia can be characterized as inactive “surveillant” (Wake et al., 2009), or belonging to one of 2 main activation phenotypes: “classically activated” pro-inflammatory (M1), or “alternatively activated” anti-inflammatory (M2), with several functional subtypes described (Edwards et al., 2006).

In the developing brain, migrating amoeboid microglia (Swinnen et al., 2013) have been demonstrated to regulate neurogenesis via phagocytosis of neural precursors and driving of synaptic pruning (Cunningham, 2013; Zhan et al., 2014). Maturation, characterized by arborization of thin highly motile processes, produces a 'surveillant' phenotype that continuously monitors neuronal synapses (Nimmerjahn et al., 2005) and phagocytically modulates neurogenesis in the healthy adult brain (Sierra et al., 2014).

As demonstrated by Butovsky et al., development and maintenance of these quiescent cells is driven extensively by microglial response to TGFβ1 signaling (Butovsky et al., 2014). TGFβ1 secreted by neurons and astrocytes upregulates expression of the fractalkine receptor (CX3CR1) on microglia (Abutbul et al., 2012), which in turn interacts with its neuronal ligand to modify synaptic circuitry (Paolicelli et al., 2011). Loss of TGFβ1 in knockout studies resulted in decreased CX3CR1 expression (Abutbul et al., 2012), induced microgliosis and neurodegeneration (Brionne et al., 2003).

In addition to non-homogenous spatial density, microglial populations in the healthy brain appear to have regionally specialized morphology and physiology. Transcriptomic analysis performed by Grabert et al suggests that cerebellar and hippocampal microglia are more immunologically "alert" with increased expression of genes involved in antigen processing and pathogen killing (Grabert et al., 2016). These findings of functional niches are supported by Stowell et al's report of phenotypic differences between cerebellar and cortical microglia in vivo (Stowell et al., 2017). Cerebellar microglia were characterized by decreased density, relative de-ramification reminiscent of activated phenotypes, and increased somal mobility (Stowell et al., 2017). Similarly amoeboid subtypes have been reported as the primary resident microglial morphology in the circumventricular organs of healthy murine brains, a structure exposed to

circulating molecules due to lack of a blood-brain barrier (Takagi et al., 2017). These cells displayed increased activation markers, suggesting localized immunologic priming. Furthermore, phenotypic variation has been demonstrated on a substructural level. Work by De Baise et al showed marked variation in microglial morphology and density between well-demarcated regions of the basal ganglia (De Biase et al., 2017). Morphologic dimorphism was accompanied by significant localized variation in lysosomal content, membrane polarization, and levels of cellular metabolism-associated transcripts (De Biase et al., 2017). Findings of regional phenotypic variation carry implications toward structurally differentiated disease susceptibility.

Microglial response to injury

Neural insult, whether mechanical, infectious or senile, can induce microglia to undergo a hypertrophic change of somatic enlargement, thickening and retraction of cellular processes to assume an 'amoeboid' phagocytic morphology. Histologically characterized as 'active", these cells can be functionally polarized under experimental settings to produce reactive phenotypes similar to that of peripheral monocytes (Colton, 2009). As reviewed by Orihuela et al, IFNγ is understood to induce 'classical' inflammatory functions such as production of IL1β, IL6, TNFα, and NO (Orihuela et al., 2016). This phenotype is referred to as M1 microglia. Resolution of the inflammatory milieu and elaboration of IL4, IL13 by peripheral cells can change microglial profiles to an anti-inflammatory (M2) state that stimulates tissue repair (Orihuela et al., 2016). Similarly, exposure to IL10, TGFβ or apoptotic bodies promotes a subtly different immunosuppressive phenotype termed 'acquired deactivated' (Orihuela et al., 2016). These profiles are not fixed. Individual cells respond to local microclimates with dynamic transition

between states, whose balance may influence tissue pathology in a temporospatially dependent manner.

Although purely polarized populations are unlikely to exist *in vivo* and antigen expression can be mixed even on individual cells, histologic differentiation of M1 and M2 microglia can be attempted using prescribed functional marker subsets. M1 microglia express elevated CD86, iNOS, IFNy, TNFa and IL1b (Kobayashi et al., 2013; Colton, 2009). M2 polarization induces Arg1, Ym1, FIZZ1 and CD206 expression (Colton, 2009). Two canonical markers, iNOS and Arg1, competitively inhibit each other through mutual reliance on arginine metabolism (Rath et al., 2014).

The role of activated microglia in neurodegenerative diseases is complex, with evidence for mediation of both neuroprotective and neurotoxic effects. As reviewed by Harry et al and Sierra et al microglial activation can create a hostile environment through elaboration of reactive oxygen species and inflammatory cytokines, as well as through inappropriate phagoptosis of viable neurons (Harry et al., 2008; Sierra et al., 2014). However, they can also promote neurogenesis (Thored et al., 2009; De Lucia et al., 2016) and limit neurotoxic inhibitory signaling through synaptic stripping (Z. Chen et al., 2014).

Microgliosis in prion infection.

In prion-infected brains, microglial activation occurs well in advance of clinical disease, and is characterized by marked cellular hypertrophy and hyperplasia (Sandberg et al., 2014; Carroll et al., 2016; Gomez-Nicola et al., 2013; Giese et al., 1998). However, studies of tissue inflammatory signatures and microglial polarization in prion disease have yielded contradictory results.

In 2002, Cunningham et al. reported that a paradoxical lack of proinflammatory cytokine production in morphologically activated microglia in intracranial ME7 prion infection was governed by a high concentration of anti-inflammatory TGFβ1 in the extracellular matrix (Cunningham et al., 2002). Maintenance of this 'alternatively activated' M2 profile model was later supported by several other investigators (Perry et al., 2002; Boche et al., 2006; Hughes et al., 2010). It was proposed that these anti-inflammatory microglial profiles may promote synaptic dissolution in early prion infection, however synaptic loss was shown to occur independently of microglial involvement (Šišková et al., 2009). These results are in contrast to more recent studies evaluating transcriptomics and cytokine expression, which suggest a proinflammatory neurotoxic microglial profile, with elevation of a wide variety of inflammatory mediators, including IL1β, IL6, TNFα, IFNγ, caspase 4, TIMP1 and matrix metalloprotease 12 (Vincenti et al., 2016; Carroll et al., 2016; Tribouillard-Tanvier et al., 2009; Newsom et al., 2011; Moody et al., 2011; Song et al., 2012). Furthermore, microglial elaboration of reactive oxygen species, NO and oxygen bursts in even early preclinical stages has been demonstrated to induce lipid peroxidation and oxidative stress in surrounding tissues (Sorce et al., 2014; Hafner-Bratkovic et al., 2012; Yun et al., 2006). These discrepancies are likely attributable, at least in part, to strain/host/inoculation variation between these studies. Additionally, sampling technique may have been a contributing factor, as authors used homogenates of whole or partially dissected brains to analyze mRNA transcript and cytokine levels. Given the localized nature of prion lesions and glial distribution, subtle differences in cytokine microclimates would have been lost to signal dilution in these studies.

Studies evaluating the effects of microglial ablation on disease phenotype yielded divergent outcomes, depending on the method of microglial inactivation. Arrest of microglial proliferation by blockage of mitogenic signaling through CSF1 receptors resulted in decreased

neurodegeneration and prolonged survival in ME7-infected mice (Gomez-Nicola et al., 2013). However, a recent study repeating CSF1R inhibition with ME7 and 22L prion strains resulted in marked acceleration of neuropathology (Carroll et al., 2018). Similarly, when microglia were pharmacologically depleted from RML-infected cerebellar organotypic cultured slices, there was a marked increase in neuronal death (Zhu et al., 2016). Microglia also appear to modulate neurogenesis and slow disease progression through removal of apoptotic bodies (De Lucia et al., 2016; Kranich et al., 2010). In summary, reported microglial inflammatory phenotypes vary between studies and their effects on disease progression appear mixed.

Astrocytes

Histology of astrocytes

Astrocytes are a morphologically diverse neuroglial population arising from radial glial progenitors (Doetsch, 2003). As the most numerous neural cell type, they are highly represented in all brain regions, but appear to be most dense in the hippocampus, hypothalamus, corpus callosum and cerebellar white matter of the rodent brain (Savchenko et al., 2000). Initial morphology studies divided astrocytes into fibrous and protoplasmic subtypes, characterized by long thickened processes for the former and highly branched thin processes for the latter (Andriezen, 1893; Miller et al., 1984). Fibrous astrocytes concentrate in white matter tracts, while protoplasmic astrocytes are diffusely distributed through gray matter (Andriezen, 1893). Beyond this basic distinction, functional differentiation of astrocytes in the healthy brain is suggested by marked variability in physiologic parameters, including receptor expression (Cai et al., 2000; Höft et al., 2014; Reuss et al., 2000), electrophysiological profiles (McKhann et al., 1997; Hibino et al., 2004), proliferative capacity (Kriegstein et al., 2009), and gene expression (Yeh et al., 2009).

Astrocytic heterogeneity extends to surface marker expression, confounding comprehensive histologic identification of astroglial populations (Kimelberg, 2004; Ogata et al., 2002). For example, glial fibrillary acidic protein (GFAP), a canonical astrocytic marker, is expressed preferentially by fibrous astrocytes in white matter of healthy brains, with limited presence in protoplasmic gray matter astrocytes (Walz et al., 1998; Cahoy et al., 2008). Furthermore, immunohistochemical labeling for GFAP is confined largely to wide perisomal processes, representing only 15% of the total cell volume (Bushong et al., 2002). Similar regional immunoreactivity is observed with glutamate transporter markers (Macnab et al., 2007; Lehre et al., 1995). In contrast, aldehyde dehydrogenase 1 family, member L1 (Aldh1L1), an alternative astrocyte marker, labels fine astrocytic processes via IHC and is panastrocytic in transcriptomic expression (Cahoy et al., 2008). Markers specific for reactive astrocytes include the acute phase protein Lcn2 and Serpina2n, a proteinase inhibitor (Zamanian et al., 2012).

Astrocytes in the healthy brain

Astrocytes display a vast variety of homeostatic functions in the healthy brain, including guidance of neurite outgrowth (Powell et al., 1999), synaptogenesis (Ullian et al., 2001), glycogen metabolism (A. M. Brown et al., 2007), osmotic regulation (Simard et al., 2006) and maintenance of the blood-brain barrier (Abbott et al., 2006). Additionally, astrocytes recycle excess glutamate to limit its excitotoxic effects (Rothstein et al., 1996). Astrocytic signaling appears to involve both gap junctions (Giaume et al., 2010) and fluctuations in Ca^{2+} levels (Khakh et al., 2015), permitting rapid intercellular communication in the absence of action potentials. Disruption of astrocytic signaling networks and homeostatic functions in response to neuroinflammation can contribute to neurotoxicity (Giaume et al., 2010; Liddelow et al., 2017).

Astrocytic response to injury

Astrogliosis can be initiated by a large variety of peripherally and locally generated molecular stimuli elaborated in response to either neural or systemic disease (Sofroniew, 2015). Activated astrocytes undergo hypertrophy of their cellular processes, which corresponds to upregulation of cytoskeletal intermediate filaments, especially glial fibrillary acidic protein (GFAP) and vimentin (Wilhelmsson et al., 2004). Higher grades of neural insult can induce astrocytic proliferation and formation of a glial scar (Wanner et al., 2013; Bardehle et al., 2013). Activated astrocytes can secrete many classes of effector molecules, including growth factors, extracellular matrix modulators, neurotransmitters and cytokines, such as IL6, IL1β, TNFα, IFNγ, TGFβ (Sofroniew, 2015). Similar to microglia, different activation stimuli can result in formation of multiple phenotypes of astrocytes (Anderson et al., 2014). Transcriptomic analysis performed by Zamanian et al (2012) demonstrated marked differences in gene expression between ischemia and LPS-activated astrocytes. Ischemic damage seemed to induce astrocyte secretion of neurotrophic factors and repair-mediating cytokines, whereas LPS promoted expression of synaptolytic complement components (Zamanian et al., 2012). These proinflammatory astrocytes, termed A1, can be activated by IL1α, TNFα and C1q generated by "classically-activated" microglia (Liddelow et al., 2017). Unlike 'protective' A2 phenotypes, these cells appear to promote caspase-mediated neuronotoxicity and fail to perform homeostatic functions, such as phagocytosis and synaptic maintenance (Liddelow et al., 2017).

Astrocytosis in prion infection

Astrocytosis is one of the earliest changes associated with prion infection, with upregulation of intermediate filament transcripts as early as 40 days post inoculation and strain-dependent spatial correlation to PrP^{sc} deposition (Carroll et al., 2016). GFAP expression has even been proposed as a diagnostic infectivity bioassay when coupled to bioluminescent reporters in transgenic mice (Tamgüney et al., 2009). Timing of astrogliosis onset varies by strain, however, it appears to uniformly precede microgliosis, vacuolation and clinical symptoms (Carroll et al., 2016).

Astrocytes are the earliest accumulators of PrP^{sc} and appear to transmit infectious prions directly to neurons (Diedrich et al., 1991; Victoria et al., 2016; Sarasa et al., 2012; Krejciova et al., 2017). In fact, neuronal pathology could be induced in transgenic mice expressing PrP^{c} exclusively on astrocytes and in co-cultures of astrocytes with Prnp0/0 neurons (D. R. Brown, 1999; Jeffrey et al., 2004), suggesting a critical role for astrocytes in generation of toxic PrP^{sc} species.

During prion infection, astrocytes secrete inflammatory cytokines, such as IL1β, IL6, IL12 and TNFα, as well as a variety of chemokines (Tribouillard-Tanvier et al., 2009; Song et al., 2012). Astrocytes appear to promote microglial recruitment during preclinical stages of prion disease through elaboration of chemokines CCL4 and CCL5 (Marella et al., 2004). Furthermore, astrocytes display a 'priming' mechanism similar to microglia, whereupon glia activated by a 'sterile' prion infection secrete exaggerated levels of chemokines in response to subsequent inflammatory cytokine stimulation (Hennessy et al., 2015). Partial inhibition of astrocytic activation in an IL1RI knock-out mouse lead to a decrease in PrP^{sc} accumulation and extended survival times (Schultz et al., 2004).

In summary, astrogliosis is an early feature of prion infection that appears to promote PrP^{sc} propagation and may mediate neuropathology, either through loss of homeostatic function or exacerbation of neuroinflammation.

The Ubiquitin Proteasome System (UPS) and Immunoproteasomes in Prion Disease

Proteolytic inhibition as a mechanism of neurotoxicity

Prion-mediated neurotoxicity may occur secondary to accumulation of misfolded proteins and initiation of the unfolded protein response (UPR). Prion infection has been documented to trigger dysfunction of both major branches of cellular proteolysis – autophagy and the ubiquitin protease system. Autophagocytic activation and dysfunction have been documented in multiple infection models (Boellaard et al., 1991; Liberski, 2012; Xu et al., 2012), and PrP^{sc} oligomers have been demonstrated to inhibit the 26S proteasome (McKinnon et al., 2016; Kristiansen et al., 2007). Subsequent buildup of misfolded proteins can trigger the unfolded protein response, which, if unresolved, can initiate caspase-mediated apoptosis. Activation of UPR signaling mediators has been documented in prion infection models, and their selective inhibition appears to be neuroprotective (Moreno et al., 2012).

The Ubiquitin Proteasome System (UPS)

26S proteasome structure and function. The ubiquitin proteasome system (UPS) degrades up to 90% of the cell's defunct peptides and contributes to rapidly terminating signaling cascades, modifying transcriptional activity of the cell, and replenishing the amino acid pool in times of starvation (Kristensen et al., 2008; Rock et al., 1994; Schubert et al., 2000; Lecker et al., 2006). Prion infection, itself a disorder of protein misfolding, adversely affects cellular proteolysis

and capacity for removal of abnormal proteinaceous aggresomes. This last section will review the 26S proteasome, it's immunologically inducible subunits and their potential role in prion disease.

The UPS is composed of two enzyme subsets – the ubiquitinating and the proteolytic. Malformed and damaged peptides are tagged for degradation by the ubiquitin system, which sequentially catalyzes the addition of ubiquitin to a peptide substrate, labeling the peptide for degradation (Lecker et al., 2006).

The ubiquitinated peptides then enter the proteolytic half of the UPS pathway, mediated by the cytosolic 26S proteasome. This superstructure is composed of two parts – a 19S cap and a 20S proteasome. The barrel–shaped 20S proteasome is composed of 4 seven-membered rings: 2 rings of beta subunit rings sandwiched between a pair of alpha subunit rings (Lecker et al., 2006). The nineteen proteins of the 19S regulatory cap are primarily responsible for granting ubiquitinated peptides access to enter the proteasome barrel for degradation (Lecker et al., 2006).

Within the beta rings of the 20S barrel, three of the constitutively expressed beta subunits (β1, β2, β3) can cleave admitted peptides between specific patterns of amino acids, exhibiting activity akin to that of certain soluble proteases (caspase, trypsin, chymotrypsin, respectively) (Lecker et al., 2006). Once all recognized cleavage sites are catabolized, the 3-25 amino acid-long peptide fragments are released into the cytosol to be further degraded by soluble peptidases and recycled (Lecker et al., 2006).

The 26S proteasome and prion infection. Inhibition of the 26S proteasome by prion infection has been demonstrated both in vitro (Kristiansen et al., 2007) and in vivo (McKinnon et al., 2016), with consequences including increased rates of neuronal degeneration and PrP^{sc} deposition. Experimental inhibition of the 26S proteasome results in similarly increased formation

of PrP^{sc} aggresomes and exacerbated caspase-mediated neuronal apoptosis (Kristiansen et al., 2005). In these studies, neuronal toxicity and proteasomal impairment was associated with non-fibrillar PrP^{sc} aggregates, suggesting that this process is mediated by toxic oligomeric species (Kristiansen et al., 2007). Inhibition of the 26S proteasome was reported to parallel PrP^{sc} deposition, occurring well before onset of clinical disease, with initial aggregation of ubiquitinated proteins appearing in both neurons and astrocytes (McKinnon et al., 2016).

Immunoproteasomes

Immunoproteasome structure and function. In the 1990's, a structural analog of the classical 26S proteasome responsible for generating the majority of MHC I-peptides was characterized in antigen presenting cells (APCs), including microglia (Griffin et al., 1998). This phenotype is capable of higher rates of peptide degradation, and its altered cleavage pattern grants breakdown products increased affinity for MHC class I presentation (Raule et al., 2014).

It was discovered that assembly of this immunoproteasome phenotype could be induced in non-APCs under the influence of environmental conditions, such as inflammation, infection, hyperglycemia, oxidative and heat stress (Griffin et al., 1998; Hensley et al., 2010). Most notably, exposure of cells to the inflammatory cytokines IFNα/β/γ and TNFα was shown to trigger a phenotypic transition from the constitutive 26S proteasome to the immunoproteasome (Bose et al., 2001; Jakel et al., 2009; Gavilan et al., 2009).

Under cytokine stimulation, expression of the catabolic beta subunits in non-antigen-presenting-cells, and thus the proteolytic specificity of the 26S proteasome can be transcriptionally altered (Ferrington et al., 2012). The constitutive proteolytic subunits of the 26S proteasome, β1,

β2 and β3, are replaced in the beta rings by β1i (LMP2, PSMB9), β2i (MECL1, PSMB10), β5i (LMP7, PSMB8), respectively (Ferrington et al., 2012).

Immunoproteasome role in neurodegenerative diseases. While tissue expression is highest in immune organs, such as lymph nodes and thymus, low levels of immunoproteasome subunits are present in healthy murine and human brains (Stohwasser et al., 1997; Piccinini et al., 2003). Microglial induction of immunoproteasome subunits has been demonstrated to occur in response to IFNγ stimulation, resulting in increased production of inflammatory mediators, such as TNFα and IL6 (Stohwasser et al., 2000). Similarly, immunoproteasomal inhibition resulted in decreased microglial capacity to respond to inflammatory stimuli, resulting in dampening of NFκb and iNOS induction, and production of IL1β, NO and TNFα (Moritz et al., 2017; X. Chen et al., 2015).

Immunoproteasomes may additionally play a role in determining the immunophenotype of macrophages. A 2016 report by Chen et al found that functional inhibition of LMP2 (β1i, PSMB9), an immunoproteasome subunit, promoted M2 polarization in alveolar macrophages (S. Chen et al., 2016). While immunoproteasomal upregulation was demonstrated in both polarization states, this occurred in a transcriptionally independent manner in M2 macrophages, demonstrating increased signal on western blots with no concurrent elevation of mRNA transcripts (S. Chen et al., 2016).

Upregulation of immunoproteasome expression has been documented in ageing brains and in neurodegenerative diseases, including Alzheimer's, Huntington's and amyotrophic lateral sclerosis (Gavilan et al., 2009; Orre et al., 2013; Cheroni et al., 2009; Mishto et al., 2006; Diaz-Hernandez et al., 2003). The contribution of immunoproteasomes to these diseases is uncertain

and entity-specific. When immunoproteasomes were inhibited in murine models of Alzheimer's, traumatic brain injury and stroke, neuroinflammation was decreased (Orre et al., 2013; Wagner et al., 2017; X. Chen et al., 2015; Moritz et al., 2017). Similar inhibition in an ALS model resulted in exacerbation of disease (Ahtoniemi et al., 2007).

Immunoproteasomes in prion infection. Cellular prion proteins have been demonstrated to act as substrates for immunoproteasomes in-vitro (Tenzer et al., 2004). While pathogenic prions appear to impair constitutive proteasome function (Deriziotis et al., 2011; McKinnon et al., 2016), studies of immunoproteasome expression and impact on prion disease are limited. Given indications of immunoproteasomal involvement in other 'prionoid' diseases and the increasing evidence of proinflammatory signaling and oxidative damage in prion infection, immunoproteasome activation could be anticipated. However, a 2010 report by Amici et al. of scrapie infection in sheep demonstrated an overall increase of proteasomal activity in brainstems of infected animals, but did not observe a change in immunoblot immunoproteasome expression in brainstem homogenates (Amici et al., 2010). This study compared only clinical and unaffected animals and was limited by sample location (brainstem only) and lack of in-situ evaluation of subunit expression, thus potentially losing data to signal dilution (Amici et al., 2010).

REFERENCES

Abbott, N. J., Ronnback, L., & Hansson, E. (2006). Astrocyte-endothelial interactions at the blood-brain barrier. *Nat Rev Neurosci, 7*(1), 41-53. doi:10.1038/nrn1824

Abutbul, S., Shapiro, J., Szaingurten-Solodkin, I., Levy, N., Carmy, Y., Baron, R., . . . Monsonego, A. (2012). TGF-beta signaling through SMAD2/3 induces the quiescent microglial phenotype within the CNS environment. *Glia, 60*(7), 1160-1171. doi:10.1002/glia.22343

Aguzzi, A., & Lakkaraju, A. K. (2016). Cell Biology of Prions and Prionoids: A Status Report. *Trends Cell Biol, 26*(1), 40-51. doi:10.1016/j.tcb.2015.08.007

Ahtoniemi, T., Goldsteins, G., Keksa-Goldsteine, V., Malm, T., Kanninen, K., Salminen, A., & Koistinaho, J. (2007). Pyrrolidine dithiocarbamate inhibits induction of immunoproteasome and decreases survival in a rat model of amyotrophic lateral sclerosis. *Mol Pharmacol, 71*(1), 30-37. doi:10.1124/mol.106.028415

Al-Zoughool, M., Oraby, T., & Krewski, D. (2016). A Bayesian back-calculation method to estimate the risk of bovine spongiform encephalopathy (BSE) in Canada during the period 1996-2011. *J Toxicol Environ Health A, 79*(16-17), 700-712. doi:10.1080/15287394.2016.1174004

Altmeppen, H. C., Prox, J., Krasemann, S., Puig, B., Kruszewski, K., Dohler, F., . . . Glatzel, M. (2015). The sheddase ADAM10 is a potent modulator of prion disease. *Elife, 4*. doi:10.7554/eLife.04260

Amici, M., Cecarini, V., Cuccioloni, M., Angeletti, M., Barocci, S., Rossi, G., . . . Eleuteri, A. M. (2010). Interplay between 20S proteasomes and prion proteins in scrapie disease. *J Neurosci Res, 88*(1), 191-201. doi:10.1002/jnr.22186

Anderson, K. M., Olson, K. E., Estes, K. A., Flanagan, K., Gendelman, H. E., & Mosley, R. L. (2014). Dual destructive and protective roles of adaptive immunity in neurodegenerative disorders. *Transl Neurodegener, 3*(1), 25. doi:10.1186/2047-9158-3-25

Andriezen, W. L. (1893). The Neuroglia Elements in the Human Brain. *Br Med J, 2*(1700), 227-230.

Asher, D. M., Gibbs, C. J., Jr., & Gajdusek, D. C. (1976). Pathogenesis of subacute spongiform encephalopathies. *Ann Clin Lab Sci, 6*(1), 84-103.

Balkema-Buschmann, A., Fast, C., Kaatz, M., Eiden, M., Ziegler, U., McIntyre, L., . . . Groschup, M. H. (2011). Pathogenesis of classical and atypical BSE in cattle. *Prev Vet Med, 102*(2), 112-117. doi:10.1016/j.prevetmed.2011.04.006

Bardehle, S., Kruger, M., Buggenthin, F., Schwausch, J., Ninkovic, J., Clevers, H., . . . Gotz, M. (2013). Live imaging of astrocyte responses to acute injury reveals selective juxtavascular proliferation. *Nat Neurosci, 16*(5), 580-586. doi:10.1038/nn.3371

Benvegnu, S., Poggiolini, I., & Legname, G. (2010). Neurodevelopmental expression and localization of the cellular prion protein in the central nervous system of the mouse. *J Comp Neurol, 518*(11), 1879-1891. doi:10.1002/cne.22357

Berest, V., Rutkowski, M., Rolka, K., Legowska, A., Debska, G., Stepkowski, D., & Szewczyk, A. (2003). The prion peptide forms ion channels in planar lipid bilayers. *Cell Mol Biol Lett, 8*(2), 353-362.

Betmouni, S., Clements, J., & Perry, V. H. (1999). Vacuolation in murine prion disease: an informative artifact. *Curr Biol, 9*(18), R677-679.

Betmouni, S., Perry, V. H., & Gordon, J. L. (1996). Evidence for an early inflammatory response in the central nervous system of mice with scrapie. *Neuroscience, 74*(1), 1-5.

Boche, D., Cunningham, C., Docagne, F., Scott, H., & Perry, V. H. (2006). TGFbeta1 regulates the inflammatory response during chronic neurodegeneration. *Neurobiol Dis, 22*(3), 638-650. doi:10.1016/j.nbd.2006.01.004

Boellaard, J. W., Kao, M., Schlote, W., & Diringer, H. (1991). Neuronal autophagy in experimental scrapie. *Acta Neuropathol, 82*(3), 225-228.

Bonda, D. J., Manjila, S., Mehndiratta, P., Khan, F., Miller, B. R., Onwuzulike, K., . . . Cali, I. (2016). Human prion diseases: surgical lessons learned from iatrogenic prion transmission. *Neurosurg Focus, 41*(1), E10. doi:10.3171/2016.5.Focus15126

Bose, S., Brooks, P., Mason, G. G., & Rivett, A. J. (2001). gamma-Interferon decreases the level of 26 S proteasomes and changes the pattern of phosphorylation. *Biochem J, 353*(Pt 2), 291-297.

Bradford, B. M., Piccardo, P., Ironside, J. W., & Mabbott, N. A. (2014). Human prion diseases and the risk of their transmission during anatomical dissection. *Clin Anat, 27*(6), 821-832. doi:10.1002/ca.22403

Brandner, S., & Jaunmuktane, Z. (2017). Prion disease: experimental models and reality. *Acta Neuropathol, 133*(2), 197-222. doi:10.1007/s00401-017-1670-5

Brionne, T. C., Tesseur, I., Masliah, E., & Wyss-Coray, T. (2003). Loss of TGF-beta 1 leads to increased neuronal cell death and microgliosis in mouse brain. *Neuron, 40*(6), 1133-1145.

Brown, A. M., & Ransom, B. R. (2007). Astrocyte glycogen and brain energy metabolism. *Glia, 55*(12), 1263-1271. doi:10.1002/glia.20557

Brown, D. R. (1999). Prion protein peptide neurotoxicity can be mediated by astrocytes. *J Neurochem, 73*(3), 1105-1113.

Brown, P., Salazar, A. M., Gibbs, C. J., Jr., & Gajdusek, D. C. (1982). Alzheimer's disease and transmissible virus dementia (Creutzfeldt-Jakob disease). *Ann N Y Acad Sci, 396*, 131-143.

Bruce, M. E., McConnell, I., Fraser, H., & Dickinson, A. G. (1991). The disease characteristics of different strains of scrapie in Sinc congenic mouse lines: implications for the nature of the agent and host control of pathogenesis. *J Gen Virol, 72 (Pt 3)*, 595-603. doi:10.1099/0022-1317-72-3-595

Bueler, H., Aguzzi, A., Sailer, A., Greiner, R. A., Autenried, P., Aguet, M., & Weissmann, C. (1993). Mice devoid of PrP are resistant to scrapie. *Cell, 73*(7), 1339-1347.

Bueler, H., Fischer, M., Lang, Y., Bluethmann, H., Lipp, H. P., DeArmond, S. J., . . . Weissmann, C. (1992). Normal development and behaviour of mice lacking the neuronal cell-surface PrP protein. *Nature, 356*(6370), 577-582. doi:10.1038/356577a0

Bushong, E. A., Martone, M. E., Jones, Y. Z., & Ellisman, M. H. (2002). Protoplasmic astrocytes in CA1 stratum radiatum occupy separate anatomical domains. *J Neurosci, 22*(1), 183-192.

Butovsky, O., Jedrychowski, M. P., Moore, C. S., Cialic, R., Lanser, A. J., Gabriely, G., . . . Weiner, H. L. (2014). Identification of a unique TGF-beta-dependent molecular and functional signature in microglia. *Nat Neurosci, 17*(1), 131-143. doi:10.1038/nn.3599

Cahoy, J. D., Emery, B., Kaushal, A., Foo, L. C., Zamanian, J. L., Christopherson, K. S., . . . Barres, B. A. (2008). A transcriptome database for astrocytes, neurons, and oligodendrocytes: a new resource for understanding brain development and function. *J Neurosci, 28*(1), 264-278. doi:10.1523/jneurosci.4178-07.2008

Cai, Z., Schools, G. P., & Kimelberg, H. K. (2000). Metabotropic glutamate receptors in acutely isolated hippocampal astrocytes: developmental changes of mGluR5 mRNA and functional expression. *Glia, 29*(1), 70-80.

Carroll, J. A., Race, B., Williams, K., Striebel, J., & Chesebro, B. (2018). Microglia Are Critical in Host Defense Against Prion Disease. *J Virol*. doi:10.1128/jvi.00549-18

Carroll, J. A., Striebel, J. F., Rangel, A., Woods, T., Phillips, K., Peterson, K. E., . . . Chesebro, B. (2016). Prion Strain Differences in Accumulation of PrPSc on Neurons and Glia Are Associated with Similar Expression Profiles of Neuroinflammatory Genes: Comparison of Three Prion Strains. *PLoS Pathog, 12*(4), e1005551. doi:10.1371/journal.ppat.1005551

Castle, A. R., & Gill, A. C. (2017). Physiological Functions of the Cellular Prion Protein. *Front Mol Biosci, 4*, 19. doi:10.3389/fmolb.2017.00019

Chen, S., Kammerl, I. E., Vosyka, O., Baumann, T., Yu, Y., Wu, Y., . . . Stoeger, T. (2016). Immunoproteasome dysfunction augments alternative polarization of alveolar macrophages. *Cell Death Differ, 23*(6), 1026-1037. doi:10.1038/cdd.2016.3

Chen, X., Zhang, X., Wang, Y., Lei, H., Su, H., Zeng, J., . . . Huang, R. (2015). Inhibition of immunoproteasome reduces infarction volume and attenuates inflammatory reaction in a rat model of ischemic stroke. *Cell Death Dis, 6*, e1626. doi:10.1038/cddis.2014.586

Chen, Z., Jalabi, W., Hu, W., Park, H. J., Gale, J. T., Kidd, G. J., . . . Trapp, B. D. (2014). Microglial displacement of inhibitory synapses provides neuroprotection in the adult brain. *Nat Commun, 5*, 4486. doi:10.1038/ncomms5486

Cheroni, C., Marino, M., Tortarolo, M., Veglianese, P., De Biasi, S., Fontana, E., . . . Bendotti, C. (2009). Functional alterations of the ubiquitin-proteasome system in motor neurons of a mouse model of familial amyotrophic lateral sclerosis. *Hum Mol Genet, 18*(1), 82-96. doi:10.1093/hmg/ddn319

Choi, S. I., Ju, W. K., Choi, E. K., Kim, J., Lea, H. Z., Carp, R. I., . . . Kim, Y. S. (1998). Mitochondrial dysfunction induced by oxidative stress in the brains of hamsters infected with the 263 K scrapie agent. *Acta Neuropathol, 96*(3), 279-286.

Collinge, J. (2016). Mammalian prions and their wider relevance in neurodegenerative diseases. *Nature, 539*(7628), 217-226. doi:10.1038/nature20415

Colton, C. A. (2009). Heterogeneity of Microglial Activation in the Innate Immune Response in the Brain. *J Neuroimmune Pharmacol, 4*(4), 399-418. doi:10.1007/s11481-009-9164-4

Cunningham, C. (2013). Microglia and neurodegeneration: the role of systemic inflammation. *Glia, 61*(1), 71-90. doi:10.1002/glia.22350

Cunningham, C., Boche, D., & Perry, V. H. (2002). Transforming growth factor beta1, the dominant cytokine in murine prion disease: influence on inflammatory cytokine synthesis and alteration of vascular extracellular matrix. *Neuropathol Appl Neurobiol, 28*(2), 107-119.

Cunningham, C., Deacon, R. M., Chan, K., Boche, D., Rawlins, J. N., & Perry, V. H. (2005). Neuropathologically distinct prion strains give rise to similar temporal profiles of behavioral deficits. *Neurobiol Dis, 18*(2), 258-269. doi:10.1016/j.nbd.2004.08.015

Davanipour, Z., Sobel, E., Ziogas, A., Smoak, C., Bohr, T., Doram, K., & Liwnicz, B. (2014). Ocular Tonometry and Sporadic Creutzfeldt - Jakob Disease (sCJD): A Confirmatory Case-Control Study. *Br J Med Med Res, 4*(12), 2322-2333. doi:10.9734/bjmmr/2014/7247

De Biase, L. M., Schuebel, K. E., Fusfeld, Z. H., Jair, K., Hawes, I. A., Cimbro, R., . . . Bonci, A. (2017). Local Cues Establish and Maintain Region-Specific Phenotypes of Basal Ganglia Microglia. *Neuron, 95*(2), 341-356.e346. doi:10.1016/j.neuron.2017.06.020

De Lucia, C., Rinchon, A., Olmos-Alonso, A., Riecken, K., Fehse, B., Boche, D., . . . Gomez-Nicola, D. (2016). Microglia regulate hippocampal neurogenesis during chronic neurodegeneration. *Brain Behav Immun, 55*, 179-190. doi:10.1016/j.bbi.2015.11.001

Deriziotis, P., André, R., Smith, D. M., Goold, R., Kinghorn, K. J., Kristiansen, M., . . . Tabrizi, S. J. (2011). Misfolded PrP impairs the UPS by interaction with the 20S proteasome and inhibition of substrate entry. *Embo j, 30*(15), 3065-3077. doi:10.1038/emboj.2011.224

Diaz-Hernandez, M., Hernandez, F., Martin-Aparicio, E., Gomez-Ramos, P., Moran, M. A., Castano, J. G., . . . Lucas, J. J. (2003). Neuronal induction of the immunoproteasome in Huntington's disease. *J Neurosci, 23*(37), 11653-11661.

Diedrich, J. F., Bendheim, P. E., Kim, Y. S., Carp, R. I., & Haase, A. T. (1991). Scrapie-associated prion protein accumulates in astrocytes during scrapie infection. *Proc Natl Acad Sci U S A, 88*(2), 375-379.

Doetsch, F. (2003). The glial identity of neural stem cells. *Nat Neurosci, 6*(11), 1127-1134. doi:10.1038/nn1144

Edwards, J. P., Zhang, X., Frauwirth, K. A., & Mosser, D. M. (2006). Biochemical and functional characterization of three activated macrophage populations. *J Leukoc Biol, 80*(6), 1298-1307. doi:10.1189/jlb.0406249

Erana, H., Venegas, V., Moreno, J., & Castilla, J. (2016). Prion-like disorders and Transmissible Spongiform Encephalopathies: An overview of the mechanistic features that are shared by the

various disease-related misfolded proteins. *Biochem Biophys Res Commun*. doi:10.1016/j.bbrc.2016.08.166

Ersdal, C., Ulvund, M. J., Benestad, S. L., & Tranulis, M. A. (2003). Accumulation of pathogenic prion protein (PrPSc) in nervous and lymphoid tissues of sheep with subclinical scrapie. *Vet Pathol, 40*(2), 164-174. doi:10.1354/vp.40-2-164

Ferrington, D. A., & Gregerson, D. S. (2012). Immunoproteasomes: Structure, Function, and Antigen Presentation. *Prog Mol Biol Transl Sci, 109*, 75-112. doi:10.1016/b978-0-12-397863-9.00003-1

Fraser, H., & Dickinson, A. G. (1973). Scrapie in mice. Agent-strain differences in the distribution and intensity of grey matter vacuolation. *J Comp Pathol, 83*(1), 29-40.

Fraser, H., & Dickinson, A. G. (1968). The sequential development of the brain lesions of scrapie in three strains of mice. *J Comp Pathol, 78*(3), 301-311. doi:http://dx.doi.org/10.1016/0021-9975(68)90006-6

Gavilan, M. P., Castano, A., Torres, M., Portavella, M., Caballero, C., Jimenez, S., . . . Ruano, D. (2009). Age-related increase in the immunoproteasome content in rat hippocampus: molecular and functional aspects. *J Neurochem, 108*(1), 260-272. doi:10.1111/j.1471-4159.2008.05762.x

Giaume, C., Koulakoff, A., Roux, L., Holcman, D., & Rouach, N. (2010). Astroglial networks: a step further in neuroglial and gliovascular interactions. *Nat Rev Neurosci, 11*(2), 87-99. doi:10.1038/nrn2757

Giese, A., Brown, D. R., Groschup, M. H., Feldmann, C., Haist, I., & Kretzschmar, H. A. (1998). Role of microglia in neuronal cell death in prion disease. *Brain Pathol, 8*(3), 449-457.

Ginhoux, F., & Guilliams, M. (2016). Tissue-Resident Macrophage Ontogeny and Homeostasis. *Immunity, 44*(3), 439-449. doi:10.1016/j.immuni.2016.02.024

Ginhoux, F., & Prinz, M. (2015). Origin of microglia: current concepts and past controversies. *Cold Spring Harb Perspect Biol, 7*(8), a020537. doi:10.1101/cshperspect.a020537

Gnanajothy, R., Umashanker, D., Vega, M. C., & Wu, B. J. (2013). A case of Creutzfeldt-Jakob disease following cataract surgery: sporadic versus iatrogenic cause. *Conn Med, 77*(6), 335-337.

Gomez-Nicola, D., Fransen, N. L., Suzzi, S., & Perry, V. H. (2013). Regulation of microglial proliferation during chronic neurodegeneration. *J Neurosci, 33*(6), 2481-2493. doi:10.1523/jneurosci.4440-12.2013

Goold, R., McKinnon, C., Rabbanian, S., Collinge, J., Schiavo, G., & Tabrizi, S. J. (2013). Alternative fates of newly formed PrP(Sc) upon prion conversion on the plasma membrane. *J Cell Sci, 126*(16), 3552-3562. doi:10.1242/jcs.120477

Gordon, S. (2008). Elie Metchnikoff: father of natural immunity. *Eur J Immunol, 38*(12), 3257-3264. doi:10.1002/eji.200838855

Gough, K. C., & Maddison, B. C. (2010). Prion transmission: prion excretion and occurrence in the environment. *Prion, 4*(4), 275-282.

Gousset, K., Schiff, E., Langevin, C., Marijanovic, Z., Caputo, A., Browman, D. T., . . . Zurzolo, C. (2009). Prions hijack tunnelling nanotubes for intercellular spread. *Nat Cell Biol, 11*(3), 328-336. doi:10.1038/ncb1841

Grabert, K., Michoel, T., Karavolos, M. H., Clohisey, S., Baillie, J. K., Stevens, M. P., . . . McColl, B. W. (2016). Microglial brain region-dependent diversity and selective regional sensitivities to ageing. *Nat Neurosci, 19*(3), 504-516. doi:10.1038/nn.4222

Greenlee, J. J., & Greenlee, M. H. (2015). The transmissible spongiform encephalopathies of livestock. *Ilar j, 56*(1), 7-25. doi:10.1093/ilar/ilv008

Griffin, T. A., Nandi, D., Cruz, M., Fehling, H. J., Kaer, L. V., Monaco, J. J., & Colbert, R. A. (1998). Immunoproteasome assembly: cooperative incorporation of interferon gamma (IFN-gamma)-inducible subunits. *J Exp Med, 187*(1), 97-104.

Guentchev, M., Voigtlander, T., Haberler, C., Groschup, M. H., & Budka, H. (2000). Evidence for oxidative stress in experimental prion disease. *Neurobiol Dis, 7*(4), 270-273. doi:10.1006/nbdi.2000.0290

Hafner-Bratkovic, I., Bencina, M., Fitzgerald, K. A., Golenbock, D., & Jerala, R. (2012). NLRP3 inflammasome activation in macrophage cell lines by prion protein fibrils as the source of IL-1beta and neuronal toxicity. *Cell Mol Life Sci, 69*(24), 4215-4228. doi:10.1007/s00018-012-1140-0

Hainfellner, J. A., Liberski, P. P., Guiroy, D. C., Cervenakova, L., Brown, P., Gajdusek, D. C., & Budka, H. (1997). Pathology and immunocytochemistry of a kuru brain. *Brain Pathol, 7*(1), 547-553.

Hall, V., Brookes, D., Nacul, L., Gill, O. N., & Connor, N. (2014). Managing the risk of iatrogenic transmission of Creutzfeldt-Jakob disease in the UK. *J Hosp Infect, 88*(1), 22-27. doi:10.1016/j.jhin.2014.06.002

Harry, G. J., & Kraft, A. D. (2008). Neuroinflammation and Microglia: Considerations and approaches for neurotoxicity assessment. *Expert Opin Drug Metab Toxicol, 4*(10), 1265-1277. doi:10.1517/17425255.4.10.1265

Hennessy, E., Griffin É, W., & Cunningham, C. (2015). Astrocytes Are Primed by Chronic Neurodegeneration to Produce Exaggerated Chemokine and Cell Infiltration Responses to Acute Stimulation with the Cytokines IL-1β and TNF-α. *J Neurosci, 35*(22), 8411-8422. doi:10.1523/jneurosci.2745-14.2015

Hensley, S. E., Zanker, D., Dolan, B. P., David, A., Hickman, H. D., Embry, A. C., . . . Yewdell, J. W. (2010). Unexpected role for the immunoproteasome subunit LMP2 in antiviral humoral and innate immune responses. *J Immunol, 184*(8), 4115-4122. doi:10.4049/jimmunol.0903003

Hibino, H., Fujita, A., Iwai, K., Yamada, M., & Kurachi, Y. (2004). Differential assembly of inwardly rectifying K+ channel subunits, Kir4.1 and Kir5.1, in brain astrocytes. *J Biol Chem, 279*(42), 44065-44073. doi:10.1074/jbc.M405985200

Hill, A. F., Joiner, S., Linehan, J., Desbruslais, M., Lantos, P. L., & Collinge, J. (2000). Species-barrier-independent prion replication in apparently resistant species. *Proc Natl Acad Sci U S A, 97*(18), 10248-10253.

Hilton, D. A., Fathers, E., Edwards, P., Ironside, J. W., & Zajicek, J. (1998). Prion immunoreactivity in appendix before clinical onset of variant Creutzfeldt-Jakob disease. *Lancet, 352*(9129), 703-704. doi:10.1016/s0140-6736(98)24035-9

Hilton, K. J., Cunningham, C., Reynolds, R. A., & Perry, V. H. (2013). Early Hippocampal Synaptic Loss Precedes Neuronal Loss and Associates with Early Behavioural Deficits in Three Distinct Strains of Prion Disease. *PLoS One, 8*(6), e68062. doi:10.1371/journal.pone.0068062

Höft, S., Griemsmann, S., Seifert, G., & Steinhäuser, C. (2014). Heterogeneity in expression of functional ionotropic glutamate and GABA receptors in astrocytes across brain regions: insights from the thalamus. *Philos Trans R Soc Lond B Biol Sci, 369*(1654). doi:10.1098/rstb.2013.0602

Hope, J., Morton, L. J., Farquhar, C. F., Multhaup, G., Beyreuther, K., & Kimberlin, R. H. (1986). The major polypeptide of scrapie-associated fibrils (SAF) has the same size, charge distribution and N-terminal protein sequence as predicted for the normal brain protein (PrP). *Embo j, 5*(10), 2591-2597.

Hughes, M. M., Field, R. H., Perry, V. H., Murray, C. L., & Cunningham, C. (2010). Microglia in the degenerating brain are capable of phagocytosis of beads and of apoptotic cells, but do not efficiently remove PrPSc, even upon LPS stimulation. *Glia, 58*(16), 2017-2030. doi:10.1002/glia.21070

Jakel, S., Kuckelkorn, U., Szalay, G., Plotz, M., Textoris-Taube, K., Opitz, E., . . . Voigt, A. (2009). Differential interferon responses enhance viral epitope generation by myocardial immunoproteasomes in murine enterovirus myocarditis. *Am J Pathol, 175*(2), 510-518. doi:10.2353/ajpath.2009.090033

Jeffrey, M., Goodsir, C. M., Race, R. E., & Chesebro, B. (2004). Scrapie-specific neuronal lesions are independent of neuronal PrP expression. *Ann Neurol, 55*(6), 781-792. doi:10.1002/ana.20093

Keshet, G. I., Ovadia, H., Taraboulos, A., & Gabizon, R. (1999). Scrapie-infected mice and PrP knockout mice share abnormal localization and activity of neuronal nitric oxide synthase. *J Neurochem, 72*(3), 1224-1231.

Khakh, B. S., & McCarthy, K. D. (2015). Astrocyte Calcium Signaling: From Observations to Functions and the Challenges Therein. *Cold Spring Harb Perspect Biol, 7*(4). doi:10.1101/cshperspect.a020404

Kim, C. (2011). Protease-Sensitive Conformers in Broad Spectrum of Distinct PrP(Sc) Structures in Sporadic Creutzfeldt-Jakob Disease Are Indicator of Progression Rate. *7*(9). doi:10.1371/journal.ppat.1002242

Kim, H. L., Do, J. Y., Cho, H. J., Jeon, Y. C., Park, S. J., Ma, H. I., . . . Kim, Y. J. (2011). Dura mater graft-associated Creutzfeldt-Jakob disease: the first case in Korea. *J Korean Med Sci, 26*(11), 1515-1517. doi:10.3346/jkms.2011.26.11.1515

Kimelberg, H. K. (2004). The problem of astrocyte identity. *Neurochem Int, 45*(2-3), 191-202. doi:10.1016/j.neuint.2003.08.015

Kobayashi, K., Imagama, S., Ohgomori, T., Hirano, K., Uchimura, K., Sakamoto, K., . . . Kadomatsu, K. (2013). Minocycline selectively inhibits M1 polarization of microglia. *Cell Death Dis, 4*, e525. doi:10.1038/cddis.2013.54

Kourie, J. I., & Culverson, A. (2000). Prion peptide fragment PrP[106-126] forms distinct cation channel types. *J Neurosci Res, 62*(1), 120-133. doi:10.1002/1097-4547(20001001)62:1<120::Aid-jnr13>3.0.Co;2-2

Kranich, J., Krautler, N. J., Falsig, J., Ballmer, B., Li, S., Hutter, G., . . . Aguzzi, A. (2010). Engulfment of cerebral apoptotic bodies controls the course of prion disease in a mouse strain-dependent manner. *J Exp Med, 207*(10), 2271-2281. doi:10.1084/jem.20092401

Krejciova, Z., Alibhai, J., Zhao, C., Krencik, R., Rzechorzek, N. M., Ullian, E. M., . . . Chandran, S. (2017). Human stem cell-derived astrocytes replicate human prions in a PRNP genotype-dependent manner. *J Exp Med, 214*(12), 3481-3495. doi:10.1084/jem.20161547

Kriegstein, A., & Alvarez-Buylla, A. (2009). The Glial Nature of Embryonic and Adult Neural Stem Cells. *Annu Rev Neurosci, 32*, 149-184. doi:10.1146/annurev.neuro.051508.135600

Kristensen, A. R., Schandorff, S., Hoyer-Hansen, M., Nielsen, M. O., Jaattela, M., Dengjel, J., & Andersen, J. S. (2008). Ordered organelle degradation during starvation-induced autophagy. *Mol Cell Proteomics, 7*(12), 2419-2428. doi:10.1074/mcp.M800184-MCP200

Kristiansen, M., Deriziotis, P., Dimcheff, D. E., Jackson, G. S., Ovaa, H., Naumann, H., . . . Tabrizi, S. J. (2007). Disease-associated prion protein oligomers inhibit the 26S proteasome. *Mol Cell, 26*(2), 175-188. doi:10.1016/j.molcel.2007.04.001

Kristiansen, M., Messenger, M. J., Klohn, P. C., Brandner, S., Wadsworth, J. D., Collinge, J., & Tabrizi, S. J. (2005). Disease-related prion protein forms aggresomes in neuronal cells leading to caspase activation and apoptosis. *J Biol Chem, 280*(46), 38851-38861. doi:10.1074/jbc.M506600200

Kujala, P. (2011). Prion Uptake in the Gut: Identification of the First Uptake and Replication Sites. *7*(12). doi:10.1371/journal.ppat.1002449

Lawson, L. J., Perry, V. H., Dri, P., & Gordon, S. (1990). Heterogeneity in the distribution and morphology of microglia in the normal adult mouse brain. *Neuroscience, 39*(1), 151-170.

Lecker, S. H., Goldberg, A. L., & Mitch, W. E. (2006). Protein degradation by the ubiquitin-proteasome pathway in normal and disease states. *J Am Soc Nephrol, 17*(7), 1807-1819. doi:10.1681/asn.2006010083

Legname, G., Nguyen, H. O., Baskakov, I. V., Cohen, F. E., Dearmond, S. J., & Prusiner, S. B. (2005). Strain-specified characteristics of mouse synthetic prions. *Proc Natl Acad Sci U S A, 102*(6), 2168-2173. doi:10.1073/pnas.0409079102

Lehre, K. P., Levy, L. M., Ottersen, O. P., Storm-Mathisen, J., & Danbolt, N. C. (1995). Differential expression of two glial glutamate transporters in the rat brain: quantitative and immunocytochemical observations. *J Neurosci, 15*(3 Pt 1), 1835-1853.

Liberski, P. P. (2012). Historical overview of prion diseases: a view from afar. *Folia Neuropathol, 50*(1), 1-12.

Liberski, P. P., Streichenberger, N., Giraud, P., Soutrenon, M., Meyronnet, D., Sikorska, B., & Kopp, N. (2005). Ultrastructural pathology of prion diseases revisited: brain biopsy studies. *Neuropathol Appl Neurobiol, 31*(1), 88-96. doi:10.1111/j.1365-2990.2004.00595.x

Liddelow, S. A., & Barres, B. A. (2017). Reactive Astrocytes: Production, Function, and Therapeutic Potential. *Immunity, 46*(6), 957-967. doi:10.1016/j.immuni.2017.06.006

Macnab, L. T., & Pow, D. V. (2007). Expression of the exon 9-skipping form of EAAT2 in astrocytes of rats. *Neuroscience, 150*(3), 705-711. doi:10.1016/j.neuroscience.2007.09.049

Malachin, G., Reiten, M. R., Salvesen, O., Aanes, H., Kamstra, J. H., Skovgaard, K., . . . Bakkebo, M. K. (2017). Loss of prion protein induces a primed state of type I interferon-responsive genes. *PLoS One, 12*(6), e0179881. doi:10.1371/journal.pone.0179881

Marella, M., & Chabry, J. (2004). Neurons and astrocytes respond to prion infection by inducing microglia recruitment. *J Neurosci, 24*(3), 620-627. doi:10.1523/jneurosci.4303-03.2004

Marin-Moreno, A., Espinosa, J. C., Fernandez-Borges, N., Piquer, J., Girones, R., Andreoletti, O., & Torres, J. M. (2016). An assessment of the long-term persistence of prion infectivity in aquatic environments. *Environ Res, 151*, 587-594. doi:10.1016/j.envres.2016.08.031

Mays, C. E., van der Merwe, J., Kim, C., Haldiman, T., McKenzie, D., Safar, J. G., & Westaway, D. (2015). Prion Infectivity Plateaus and Conversion to Symptomatic Disease Originate from Falling Precursor Levels and Increased Levels of Oligomeric PrPSc Species. *J Virol, 89*(24), 12418-12426. doi:10.1128/jvi.02142-15

McKhann, G. M., 2nd, D'Ambrosio, R., & Janigro, D. (1997). Heterogeneity of astrocyte resting membrane potentials and intercellular coupling revealed by whole-cell and gramicidin-perforated patch recordings from cultured neocortical and hippocampal slice astrocytes. *J Neurosci, 17*(18), 6850-6863.

McKinnon, C., Goold, R., Andre, R., Devoy, A., Ortega, Z., Moonga, J., . . . Tabrizi, S. J. (2016). Prion-mediated neurodegeneration is associated with early impairment of the ubiquitin-proteasome system. *Acta Neuropathol, 131*(3), 411-425. doi:10.1007/s00401-015-1508-y

Miller, R. H., & Raff, M. C. (1984). Fibrous and protoplasmic astrocytes are biochemically and developmentally distinct. *J Neurosci, 4*(2), 585-592.

Mishto, M., Bellavista, E., Santoro, A., Stolzing, A., Ligorio, C., Nacmias, B., . . . Franceschi, C. (2006). Immunoproteasome and LMP2 polymorphism in aged and Alzheimer's disease brains. *Neurobiol Aging, 27*(1), 54-66. doi:10.1016/j.neurobiolaging.2004.12.004

Mittelbronn, M., Dietz, K., Schluesener, H. J., & Meyermann, R. (2001). Local distribution of microglia in the normal adult human central nervous system differs by up to one order of magnitude. *Acta Neuropathol, 101*(3), 249-255.

Moody, L. R., Herbst, A. J., & Aiken, J. M. (2011). Upregulation of interferon-gamma-induced genes during prion infection. *J Toxicol Environ Health A, 74*(2-4), 146-153. doi:10.1080/15287394.2011.529064

Moreno, J. A., Radford, H., Peretti, D., Steinert, J. R., Verity, N., Martin, M. G., . . . Mallucci, G. R. (2012). Sustained translational repression by eIF2alpha-P mediates prion neurodegeneration. *Nature, 485*(7399), 507-511. doi:10.1038/nature11058

Moritz, K. E., McCormack, N. M., Abera, M. B., Viollet, C., Yauger, Y. J., Sukumar, G., . . . Burnett, B. G. (2017). The role of the immunoproteasome in interferon-gamma-mediated microglial activation. *Sci Rep, 7*(1), 9365. doi:10.1038/s41598-017-09715-y

Nagaoka, K., Yoshioka, M., Shimozaki, N., Yamamura, T., Murayama, Y., Yokoyama, T., & Mohri, S. (2010). Sensitive detection of scrapie prion protein in soil. *Biochem Biophys Res Commun, 397*(3), 626-630. doi:10.1016/j.bbrc.2010.06.013

Newsom, D. M., Liggitt, H. D., O'Rourke, K., Zhuang, D., Schneider, D. A., & Harrington, R. D. (2011). Cytokine antibody array analysis in brain and periphery of scrapie-infected Tg338 mice. *Comp Immunol Microbiol Infect Dis, 34*(5), 387-397. doi:10.1016/j.cimid.2011.06.001

Nimmerjahn, A., Kirchhoff, F., & Helmchen, F. (2005). Resting microglial cells are highly dynamic surveillants of brain parenchyma in vivo. *Science, 308*(5726), 1314-1318. doi:10.1126/science.1110647

Ogata, K., & Kosaka, T. (2002). Structural and quantitative analysis of astrocytes in the mouse hippocampus. *Neuroscience, 113*(1), 221-233.

Ono, F., Tase, N., Kurosawa, A., Hiyaoka, A., Ohyama, A., Tezuka, Y., . . . Sata, T. (2011). Atypical L-type bovine spongiform encephalopathy (L-BSE) transmission to cynomolgus macaques, a non-human primate. *Jpn J Infect Dis, 64*(1), 81-84.

Oraby, T., Al-Zoughool, M., Elsaadany, S., & Krewski, D. (2016). A stochastic model of the bovine spongiform encephalopathy epidemic in Canada. *J Toxicol Environ Health A, 79*(16-17), 677-689. doi:10.1080/15287394.2016.1173988

Orihuela, R., McPherson, C. A., & Harry, G. J. (2016). Microglial M1/M2 polarization and metabolic states. *Br J Pharmacol, 173*(4), 649-665. doi:10.1111/bph.13139

Orre, M., Kamphuis, W., Dooves, S., Kooijman, L., Chan, E. T., Kirk, C. J., . . . Hol, E. M. (2013). Reactive glia show increased immunoproteasome activity in Alzheimer's disease. *Brain, 136*(Pt 5), 1415-1431. doi:10.1093/brain/awt083

Owen, J., Beck, J., Campbell, T., Adamson, G., Gorham, M., Thompson, A., . . . Mead, S. (2014). Predictive testing for inherited prion disease: report of 22 years experience. *Eur J Hum Genet, 22*(12), 1351-1356. doi:10.1038/ejhg.2014.42

Pan, K. M., Baldwin, M., Nguyen, J., Gasset, M., Serban, A., Groth, D., . . . et al. (1993). Conversion of alpha-helices into beta-sheets features in the formation of the scrapie prion proteins. *Proc Natl Acad Sci U S A, 90*(23), 10962-10966.

Paolicelli, R. C., Bolasco, G., Pagani, F., Maggi, L., Scianni, M., Panzanelli, P., . . . Gross, C. T. (2011). Synaptic pruning by microglia is necessary for normal brain development. *Science, 333*(6048), 1456-1458. doi:10.1126/science.1202529

Perry, V. H., Cunningham, C., & Boche, D. (2002). Atypical inflammation in the central nervous system in prion disease. *Curr Opin Neurol, 15*(3), 349-354.

Piccinini, M., Mostert, M., Croce, S., Baldovino, S., Papotti, M., & Rinaudo, M. T. (2003). Interferon-gamma-inducible subunits are incorporated in human brain 20S proteasome. *J Neuroimmunol, 135*(1-2), 135-140.

Powell, E. M., & Geller, H. M. (1999). Dissection of astrocyte-mediated cues in neuronal guidance and process extension. *Glia, 26*(1), 73-83.

Prinz, M., Heikenwalder, M., Junt, T., Schwarz, P., Glatzel, M., Heppner, F. L., . . . Aguzzi, A. (2003). Positioning of follicular dendritic cells within the spleen controls prion neuroinvasion. *Nature, 425*(6961), 957-962. doi:10.1038/nature02072

Prusiner, S. B. (1982). Novel proteinaceous infectious particles cause scrapie. *Science, 216*(4542), 136-144.

Rath, M., Müller, I., Kropf, P., Closs, E. I., & Munder, M. (2014). Metabolism via Arginase or Nitric Oxide Synthase: Two Competing Arginine Pathways in Macrophages. *Front Immunol, 5*. doi:10.3389/fimmu.2014.00532

Ratte, S., Prescott, S. A., Collinge, J., & Jefferys, J. G. (2008). Hippocampal bursts caused by changes in NMDA receptor-dependent excitation in a mouse model of variant CJD. *Neurobiol Dis, 32*(1), 96-104. doi:10.1016/j.nbd.2008.06.007

Raule, M., Cerruti, F., & Cascio, P. (2014). Enhanced rate of degradation of basic proteins by 26S immunoproteasomes. *Biochim Biophys Acta, 1843*(9), 1942-1947. doi:10.1016/j.bbamcr.2014.05.005

Reis, R., Hennessy, E., Murray, C., Griffin, E. W., & Cunningham, C. (2015). At the centre of neuronal, synaptic and axonal pathology in murine prion disease: degeneration of neuroanatomically linked thalamic and brainstem nuclei. *Neuropathol Appl Neurobiol, 41*(6), 780-797. doi:10.1111/nan.12232

Reuss, B., Leung, D. S., Ohlemeyer, C., Kettenmann, H., & Unsicker, K. (2000). Regionally distinct regulation of astroglial neurotransmitter receptors by fibroblast growth factor-2. *Mol Cell Neurosci, 16*(1), 42-58. doi:10.1006/mcne.2000.0857

Rock, K. L., Gramm, C., Rothstein, L., Clark, K., Stein, R., Dick, L., . . . Goldberg, A. L. (1994). Inhibitors of the proteasome block the degradation of most cell proteins and the generation of peptides presented on MHC class I molecules. *Cell, 78*(5), 761-771.

Rothstein, J. D., Dykes-Hoberg, M., Pardo, C. A., Bristol, L. A., Jin, L., Kuncl, R. W., . . . Welty, D. F. (1996). Knockout of glutamate transporters reveals a major role for astroglial transport in excitotoxicity and clearance of glutamate. *Neuron, 16*(3), 675-686.

Rudge, P., Jaunmuktane, Z., Adlard, P., Bjurstrom, N., Caine, D., Lowe, J., . . . Collinge, J. (2015). Iatrogenic CJD due to pituitary-derived growth hormone with genetically determined incubation times of up to 40 years. *Brain, 138*(Pt 11), 3386-3399. doi:10.1093/brain/awv235

Sala, C., Morignat, E., Oussaid, N., Gay, E., Abrial, D., Ducrot, C., & Calavas, D. (2012). Individual factors associated with L- and H-type Bovine Spongiform encephalopathy in France. *BMC Vet Res, 8*, 74. doi:10.1186/1746-6148-8-74

Sandberg, M. K., Al-Doujaily, H., Sharps, B., Clarke, A. R., & Collinge, J. (2011). Prion propagation and toxicity in vivo occur in two distinct mechanistic phases. *Nature, 470*(7335), 540-542. doi:10.1038/nature09768

Sandberg, M. K., Al-Doujaily, H., Sharps, B., De Oliveira, M. W., Schmidt, C., Richard-Londt, A., . . . Collinge, J. (2014). Prion neuropathology follows the accumulation of alternate prion protein isoforms after infective titre has peaked. *Nat Commun, 5*, 4347. doi:10.1038/ncomms5347

Sarasa, R., Martinez, A., Monleon, E., Bolea, R., Vargas, A., Badiola, J. J., & Monzon, M. (2012). Involvement of astrocytes in transmissible spongiform encephalopathies: a confocal microscopy study. *Cell Tissue Res, 350*(1), 127-134. doi:10.1007/s00441-012-1461-1

Satoh, J., Kino, Y., Asahina, N., Takitani, M., Miyoshi, J., Ishida, T., & Saito, Y. (2016). TMEM119 marks a subset of microglia in the human brain. *Neuropathology, 36*(1), 39-49. doi:10.1111/neup.12235

Saunders, S. E., Bartelt-Hunt, S. L., & Bartz, J. C. (2012). Occurrence, Transmission, and Zoonotic Potential of Chronic Wasting Disease. *Emerg Infect Dis, 18*(3), 369-376. doi:10.3201/eid1803.110685

Savchenko, V. L., McKanna, J. A., Nikonenko, I. R., & Skibo, G. G. (2000). Microglia and astrocytes in the adult rat brain: comparative immunocytochemical analysis demonstrates the efficacy of lipocortin 1 immunoreactivity. *Neuroscience, 96*(1), 195-203.

Schmitz, M., Dittmar, K., Llorens, F., Gelpi, E., Ferrer, I., Schulz-Schaeffer, W. J., & Zerr, I. (2016). Hereditary Human Prion Diseases: an Update. *Mol Neurobiol*. doi:10.1007/s12035-016-9918-y

Schubert, U., Anton, L. C., Gibbs, J., Norbury, C. C., Yewdell, J. W., & Bennink, J. R. (2000). Rapid degradation of a large fraction of newly synthesized proteins by proteasomes. *Nature, 404*(6779), 770-774. doi:10.1038/35008096

Schultz, J., Schwarz, A., Neidhold, S., Burwinkel, M., Riemer, C., Simon, D., . . . Baier, M. (2004). Role of interleukin-1 in prion disease-associated astrocyte activation. *Am J Pathol, 165*(2), 671-678. doi:10.1016/s0002-9440(10)63331-7

Seuberlich, T., Heim, D., & Zurbriggen, A. (2010). Atypical transmissible spongiform encephalopathies in ruminants: a challenge for disease surveillance and control. *J Vet Diagn Invest, 22*(6), 823-842.

Sheng, J., Ruedl, C., & Karjalainen, K. (2015). Most Tissue-Resident Macrophages Except Microglia Are Derived from Fetal Hematopoietic Stem Cells. *Immunity, 43*(2), 382-393. doi:10.1016/j.immuni.2015.07.016

Sierra, A., Beccari, S., Diaz-Aparicio, I., Encinas, J. M., Comeau, S., & Tremblay, M. E. (2014). Surveillance, phagocytosis, and inflammation: how never-resting microglia influence adult hippocampal neurogenesis. *Neural Plast, 2014*, 610343. doi:10.1155/2014/610343

Sigurdson, C. J., Williams, E. S., Miller, M. W., Spraker, T. R., O'Rourke, K. I., & Hoover, E. A. (1999). Oral transmission and early lymphoid tropism of chronic wasting disease PrPres in mule deer fawns (Odocoileus hemionus). *J Gen Virol, 80 (Pt 10)*, 2757-2764. doi:10.1099/0022-1317-80-10-2757

Simard, A. R., Soulet, D., Gowing, G., Julien, J. P., & Rivest, S. (2006). Bone marrow-derived microglia play a critical role in restricting senile plaque formation in Alzheimer's disease. *Neuron, 49*(4), 489-502. doi:10.1016/j.neuron.2006.01.022

Šišková, Z., Page, A., O'Connor, V., & Perry, V. H. (2009). Degenerating Synaptic Boutons in Prion Disease : Microglia Activation without Synaptic Stripping. *Am J Pathol, 175*(4), 1610-1621. doi:10.2353/ajpath.2009.090372

Sofroniew, M. V. (2015). Astrogliosis. *Cold Spring Harb Perspect Biol, 7*(2). doi:10.1101/cshperspect.a020420

Solomon, I. H., Huettner, J. E., & Harris, D. A. (2010). Neurotoxic mutants of the prion protein induce spontaneous ionic currents in cultured cells. *J Biol Chem, 285*(34), 26719-26726. doi:10.1074/jbc.M110.134619

Song, K., Na, J. Y., Oh, M. H., Kim, S., Kim, Y. H., Park, B. Y., . . . Kwon, J. (2012). Synthetic Prion Peptide 106-126 Resulted in an Increase Matrix Metalloproteinases and Inflammatory Cytokines from Rat Astrocytes and Microglial Cells. *Toxicol Res, 28*(1), 5-9. doi:10.5487/tr.2012.28.1.005

Sorce, S., Nuvolone, M., Keller, A., Falsig, J., Varol, A., Schwarz, P., . . . Aguzzi, A. (2014). The role of the NADPH oxidase NOX2 in prion pathogenesis. *PLoS Pathog, 10*(12), e1004531. doi:10.1371/journal.ppat.1004531

Spraker, T. R., Balachandran, A., Zhuang, D., & O'Rourke, K. I. (2004). Variable patterns of distribution of PrP(CWD) in the obex and cranial lymphoid tissues of Rocky Mountain elk (Cervus elaphus nelsoni) with subclinical chronic wasting disease. *Vet Rec, 155*(10), 295-302.

Stahl, N., Baldwin, M. A., Teplow, D. B., Hood, L., Gibson, B. W., Burlingame, A. L., & Prusiner, S. B. (1993). Structural studies of the scrapie prion protein using mass spectrometry and amino acid sequencing. *Biochemistry, 32*(8), 1991-2002.

Stefanie Czub, W. S.-S., Christiane Stahl-Hennig, Michael Beekes, Hermann Schaetzl, Dirk Morzkus. (2017). *First evidence of intracranial and peroral transmission of CWD into Cynomolgus macaques: a work in progress*. Prion 2017, annual meeting. Conference proceedings. Retrieved from https://www.youtube.com/embed/Vtt1kAVDhDQ

Stohwasser, R., Giesebrecht, J., Kraft, R., Muller, E. C., Hausler, K. G., Kettenmann, H., . . . Kloetzel, P. M. (2000). Biochemical analysis of proteasomes from mouse microglia: induction of immunoproteasomes by interferon-gamma and lipopolysaccharide. *Glia, 29*(4), 355-365.

Stohwasser, R., Standera, S., Peters, I., Kloetzel, P. M., & Groettrup, M. (1997). Molecular cloning of the mouse proteasome subunits MC14 and MECL-1: reciprocally regulated tissue expression of interferon-gamma-modulated proteasome subunits. *Eur J Immunol, 27*(5), 1182-1187. doi:10.1002/eji.1830270520

Stowell, R. D., Wong, E. L., Batchelor, H. N., Mendes, M. S., Lamantia, C. E., Whitelaw, B. S., & Majewska, A. K. (2017). Cerebellar microglia are dynamically unique and survey Purkinje neurons in vivo. *Dev Neurobiol*. doi:10.1002/dneu.22572

Striebel, J. F., Race, B., Meade-White, K. D., LaCasse, R., & Chesebro, B. (2011). Strain specific resistance to murine scrapie associated with a naturally occurring human prion protein polymorphism at residue 171. *PLoS Pathog, 7*(9), e1002275. doi:10.1371/journal.ppat.1002275

Sushma, B., Gugwad, S., Pavaskar, R., & Malik, S. A. (2016). Prions in dentistry: A need to be concerned and known. *J Oral Maxillofac Pathol, 20*(1), 111-114. doi:10.4103/0973-029x.180961

Swinnen, N., Smolders, S., Avila, A., Notelaers, K., Paesen, R., Ameloot, M., . . . Rigo, J. M. (2013). Complex invasion pattern of the cerebral cortex bymicroglial cells during development of the mouse embryo. *Glia, 61*(2), 150-163. doi:10.1002/glia.22421

Takagi, S., Furube, E., Nakano, Y., Morita, M., & Miyata, S. (2017). Microglia are continuously activated in the circumventricular organs of mouse brain. *J Neuroimmunol*. doi:10.1016/j.jneuroim.2017.10.008

Tamgüney, G., Francis, K. P., Giles, K., Lemus, A., DeArmond, S. J., & Prusiner, S. B. (2009). Measuring prions by bioluminescence imaging. *Proc Natl Acad Sci U S A, 106*(35), 15002-15006. doi:10.1073/pnas.0907339106

Tenzer, S., Stoltze, L., Schonfisch, B., Dengjel, J., Muller, M., Stevanovic, S., . . . Schild, H. (2004). Quantitative analysis of prion-protein degradation by constitutive and immuno-20S proteasomes indicates differences correlated with disease susceptibility. *J Immunol, 172*(2), 1083-1091.

Thomas, J. G., Chenoweth, C. E., & Sullivan, S. E. (2013). Iatrogenic Creutzfeldt-Jakob disease via surgical instruments. *J Clin Neurosci, 20*(9), 1207-1212. doi:10.1016/j.jocn.2013.01.007

Thored, P., Heldmann, U., Gomes-Leal, W., Gisler, R., Darsalia, V., Taneera, J., . . . Lindvall, O. (2009). Long-term accumulation of microglia with proneurogenic phenotype concomitant with persistent neurogenesis in adult subventricular zone after stroke. *Glia, 57*(8), 835-849. doi:10.1002/glia.20810

Tremblay, M., Lecours, C., Samson, L., Sánchez-Zafra, V., & Sierra, A. (2015). From the Cajal alumni Achúcarro and Río-Hortega to the rediscovery of never-resting microglia. *Front Neuroanat, 9*. doi:10.3389/fnana.2015.00045

Tribouillard-Tanvier, D., Carroll, J. A., Moore, R. A., Striebel, J. F., & Chesebro, B. (2012). Role of cyclophilin A from brains of prion-infected mice in stimulation of cytokine release by microglia and astroglia in vitro. *J Biol Chem, 287*(7), 4628-4639. doi:10.1074/jbc.M111.269480

Tribouillard-Tanvier, D., Striebel, J. F., Peterson, K. E., & Chesebro, B. (2009). Analysis of protein levels of 24 cytokines in scrapie agent-infected brain and glial cell cultures from mice differing in prion protein expression levels. *J Virol, 83*(21), 11244-11253. doi:10.1128/jvi.01413-09

Ullian, E. M., Sapperstein, S. K., Christopherson, K. S., & Barres, B. A. (2001). Control of synapse number by glia. *Science, 291*(5504), 657-661. doi:10.1126/science.291.5504.657

Urwin, P. J., Mackenzie, J. M., Llewelyn, C. A., Will, R. G., & Hewitt, P. E. (2016). Creutzfeldt-Jakob disease and blood transfusion: updated results of the UK Transfusion Medicine Epidemiology Review Study. *Vox Sang, 110*(4), 310-316. doi:10.1111/vox.12371

Victoria, G. S., Arkhipenko, A., Zhu, S., Syan, S., & Zurzolo, C. (2016). Astrocyte-to-neuron intercellular prion transfer is mediated by cell-cell contact. *Sci Rep, 6*, 20762. doi:10.1038/srep20762

Vincenti, J. E., Murphy, L., Grabert, K., McColl, B. W., Cancellotti, E., Freeman, T. C., & Manson, J. C. (2015). Defining the Microglia Response during the Time Course of Chronic Neurodegeneration. *J Virol, 90*(6), 3003-3017. doi:10.1128/jvi.02613-15

Vincenti, J. E., Murphy, L., Grabert, K., McColl, B. W., Cancellotti, E., Freeman, T. C., & Manson, J. C. (2016). Defining the Microglia Response during the Time Course of Chronic Neurodegeneration. *J Virol, 90*(6), 3003-3017. doi:10.1128/jvi.02613-15

Wagner, L. K., Gilling, K. E., Schormann, E., Kloetzel, P. M., Heppner, F. L., Kruger, E., & Prokop, S. (2017). Immunoproteasome deficiency alters microglial cytokine response and improves cognitive deficits in Alzheimer's disease-like APPPS1 mice. *Acta Neuropathol Commun, 5*(1), 52. doi:10.1186/s40478-017-0453-5

Wake, H., Moorhouse, A. J., Jinno, S., Kohsaka, S., & Nabekura, J. (2009). Resting microglia directly monitor the functional state of synapses in vivo and determine the fate of ischemic terminals. *J Neurosci, 29*(13), 3974-3980. doi:10.1523/jneurosci.4363-08.2009

Walker, F. R., Beynon, S. B., Jones, K. A., Zhao, Z., Kongsui, R., Cairns, M., & Nilsson, M. (2014). Dynamic structural remodelling of microglia in health and disease: a review of the models, the signals and the mechanisms. *Brain Behav Immun, 37*, 1-14. doi:10.1016/j.bbi.2013.12.010

Walz, W., & Lang, M. K. (1998). Immunocytochemical evidence for a distinct GFAP-negative subpopulation of astrocytes in the adult rat hippocampus. *Neurosci Lett, 257*(3), 127-130.

Wanner, I. B., Anderson, M. A., Song, B., Levine, J., Fernandez, A., Gray-Thompson, Z., . . . Sofroniew, M. V. (2013). Glial scar borders are formed by newly proliferated, elongated astrocytes that interact to corral inflammatory and fibrotic cells via STAT3-dependent mechanisms after spinal cord injury. *J Neurosci, 33*(31), 12870-12886. doi:10.1523/jneurosci.2121-13.2013

Webb, T. E., Whittaker, J., Collinge, J., & Mead, S. (2009). Age of onset and death in inherited prion disease are heritable. *Am J Med Genet B Neuropsychiatr Genet, 150b*(4), 496-501. doi:10.1002/ajmg.b.30844

Wemheuer, W. M., Wrede, A., & Schulz-Schaeffer, W. J. (2017). Types and Strains: Their Essential Role in Understanding Protein Aggregation in Neurodegenerative Diseases. *Front Aging Neurosci, 9*. doi:10.3389/fnagi.2017.00187

Wilhelmsson, U., Li, L., Pekna, M., Berthold, C. H., Blom, S., Eliasson, C., . . . Pekny, M. (2004). Absence of glial fibrillary acidic protein and vimentin prevents hypertrophy of astrocytic processes and improves post-traumatic regeneration. *J Neurosci, 24*(21), 5016-5021. doi:10.1523/jneurosci.0820-04.2004

Williams, A., Lucassen, P. J., Ritchie, D., & Bruce, M. (1997). PrP deposition, microglial activation, and neuronal apoptosis in murine scrapie. *Exp Neurol, 144*(2), 433-438. doi:10.1006/exnr.1997.6424

Williams, A. E., van Dam, A. M., Man, A. H. W. K., Berkenbosch, F., Eikelenboom, P., & Fraser, H. (1994). Cytokines, prostaglandins and lipocortin-1 are present in the brains of scrapie-infected mice. *Brain Res, 654*(2), 200-206.

Wood, J. L., McGill, I. S., Done, S. H., & Bradley, R. (1997). Neuropathology of scrapie: a study of the distribution patterns of brain lesions in 222 cases of natural scrapie in sheep, 1982-1991. *Vet Rec, 140*(7), 167-174.

Xu, Y., Tian, C., Wang, S. B., Xie, W. L., Guo, Y., Zhang, J., . . . Dong, X. P. (2012). Activation of the macroautophagic system in scrapie-infected experimental animals and human genetic prion diseases. *Autophagy, 8*(11), 1604-1620. doi:10.4161/auto.21482

Yeh, T. H., Lee, D. Y., Gianino, S. M., & Gutmann, D. H. (2009). Microarray analyses reveal regional astrocyte heterogeneity with implications for neurofibromatosis type 1 (NF1)-regulated glial proliferation. *Glia, 57*(11), 1239-1249. doi:10.1002/glia.20845

Yim, Y. I., Park, B. C., Yadavalli, R., Zhao, X., Eisenberg, E., & Greene, L. E. (2015). The multivesicular body is the major internal site of prion conversion. *J Cell Sci, 128*(7), 1434-1443. doi:10.1242/jcs.165472

Yun, S. W., Gerlach, M., Riederer, P., & Klein, M. A. (2006). Oxidative stress in the brain at early preclinical stages of mouse scrapie. *Exp Neurol, 201*(1), 90-98. doi:10.1016/j.expneurol.2006.03.025

Zabel, M., & Ortega, A. (2017). The Ecology of Prions. *Microbiol Mol Biol Rev, 81*(3). doi:10.1128/mmbr.00001-17

Zamanian, J. L., Xu, L., Foo, L. C., Nouri, N., Zhou, L., Giffard, R. G., & Barres, B. A. (2012). Genomic analysis of reactive astrogliosis. *J Neurosci, 32*(18), 6391-6410. doi:10.1523/jneurosci.6221-11.2012

Zhan, Y., Paolicelli, R. C., Sforazzini, F., Weinhard, L., Bolasco, G., Pagani, F., . . . Gross, C. T. (2014). Deficient neuron-microglia signaling results in impaired functional brain connectivity and social behavior. *Nat Neurosci, 17*(3), 400-406. doi:10.1038/nn.3641

Zhu, C., Herrmann, U. S., Falsig, J., Abakumova, I., Nuvolone, M., Schwarz, P., . . . Aguzzi, A. (2016). A neuroprotective role for microglia in prion diseases. *J Exp Med, 213*(6), 1047-1059. doi:10.1084/jem.20151000

CHAPTER 2: IN-SITU TEMPOROSPATIAL CHARACTERIZATION OF THE GLIAL RESPONSE TO PRION INFECTION

A manuscript to be submitted to *Veterinary Pathology*

Alyona V. Michael[1], Justin J. Greenlee[2], Tyler A. Harm[1], S.J. Moore[2], Min Zhang[3], Melissa S. Lind M. Heather West Greenlee[4], Jodi D. Smith[1]

Author affiliations
[1] Department of Veterinary Pathology, College of Veterinary Medicine, Iowa State University, Ames, IA
[2] Virus and Prion Research Unit, National Animal Disease Center, Agricultural Research Service, US Department of Agriculture, Ames, IA
[3] Department of Statistics, College of Liberal Arts and Sciences, Iowa State University, Ames, IA
[4] Department of Biomedical Sciences, College of Veterinary Medicine, Iowa State University, Ames, IA

Abstract

Mammalian transmissible spongiform encephalopathies (TSEs) induce marked activation of astrocytes and microglia that precedes neuronal loss and cognitive decline. Investigation of clinical parallels between TSEs and other neurodegenerative protein misfolding diseases, such as Alzheimer's, has revealed similar patterns of neuroinflammatory responses to accumulation of self-propagating amyloids. The contribution of glial activation to the progression of protein misfolding diseases is controversial, with evidence for mediation of both protective and deleterious effects. Glial populations exhibit a heterogeneous distribution throughout the brain, and are capable of dynamic transitions along a spectrum of functional activation states between pro- and anti-inflammatory polarization extremes. Using a murine model of scrapie (RML), this study sought to characterize the neuroinflammatory response to prion infection by evaluating glial activation across 15 brain regions over time, and correlating it to traditional markers of prion neuropathology, including neuropil vacuolation and PrP^{sc} deposition. We used quantitative

immunohistochemistry to evaluate glial expression of iNOS and Arg1, markers of classical and alternative glial activation, respectively. Our results indicate progressive upregulation of iNOS in microglia, consistent with a pro-inflammatory phenotype, and a mixed astrocytic profile featuring iNOS expression in white matter tracts and detection of Arg1-positive populations throughout the brain. These data establish a comprehensive temporospatial lesion profile for this infection model, and contribute evidence of multiple glial activation states.

Introduction

Transmissible spongiform encephalopathies are an insidious, invariably fatal group of neurodegenerative diseases known to afflict a variety of mammalian species, including humans (Kuru, Creutzfeldt-Jacob, Gerstmann-Sträussler-Scheinker), bovines (bovine spongiform encephalopathy, BSE), small ruminants (scrapie), and cervids (chronic wasting disease, CWD). Although the exact mechanism of neurotoxicity is uncertain, infectivity and eventual neurodegeneration in prion infection is mediated by self-propagating corruption of a native cytoplasmic prion protein, PrP^{c}, by a misfolded protein with an identical primary amino acid sequence, PrP^{sc}. [56, 66] Misfolded PrP^{sc} particles stimulate and stabilize a conformational shift in PrP^{c}, initiating a polymerization chain to form insoluble amyloidogenic fibrils. [16] These fibrils can undergo sporadic fragmentation into a mix of oligomeric species that subsequently seed further PrP^{c} conversion. [16] Elements of this proteinaceous etiology are increasingly recognized in other classes of human neurodegenerative diseases,[1, 22] such as Alzheimer's (AD), [47, 75] Parkinson's (PD),[69 83] and Huntington's (HD)[43, 60] diseases and Amyotrophic Lateral Sclerosis (ALS).[42]

Microglia, yolk-sac derived resident neural phagocytes,[26] undergo activation and proliferation in response to misfolded oligomers in human neurodegenerative protein misfolding

diseases and classical prion disease alike. [25, 32, 47, 60, 83] The contribution of microgliosis to neuroinflammation is incompletely elucidated. There is evidence for mediation of both deleterious effects, such as through generation of reactive oxygen species and inappropriate neuronal phagoptosis,[8, 31] as well as neuroprotective mechanisms, including neurogenesis[20] and synaptic stripping [13]. The study of neuroinflammation is further complicated by the apparent physiologic fluidity of microglial populations, which can undergo dynamic transition between activation states. Phenotypic polarity can be induced in cultured microglia resulting in manifestation of pro-inflammatory "M1" or anti-inflammatory "M2" activation states characterized by divergent secretory and phagocytic profiles.[55] M1-polarized microglia, which can be experimentally stimulated by IFNy to generate pro-inflammatory IL1β, IL6, TNFα and NO [17] have been reported in models of AD,[50] PD,[41, 83] and ALS [5]. However, there is evidence for spatial and temporal variation of microglial phenotypes during disease progression. M2 microglia, which can be generated in-vitro in response to Th2 cytokines, appear to cluster around Aβ plaques in AD,[35] and predominate in early pre-clinical stages of both AD and ALS, with a shift to M1-skewed phenotypes in late disease.[29, 35]

Studies characterizing the inflammatory profiles of microglia in experimental prion infections have yielded contradictory results, with earlier evidence suggesting a paradoxical M2 microglial profile despite an activated morphology,[6, 18, 33, 77] while more recent transcriptomic and cytokine array analyses support a neurotoxic microglial profile and a pro-inflammatory cytokine milieu associated with M1 activation.[10, 11, 27, 51, 53, 64, 71, 74] These discrepancies are likely attributable, at least in part, to strain, host, and collection time-point variation between these studies. Additionally, sampling technique may have been a confounding factor, as authors used homogenates of whole or partially dissected brains to analyze mRNA transcript and cytokine

levels. Microglial distribution is non-homogeneous throughout the brain, with marked variation in population density,[40] transcriptomes,[28] surface activation markers,[67] and physiologic parameters[19]. Microglial subsets are highly localized and can be resolved to a substructural level with sharp lines of border demarcation,[19] suggesting that microglial response to neurodegenerative disease could vary markedly on a regional level.

Astrocytosis is one of the earliest changes observed in prion infection,[11] and astrocytes have been implicated in PrP^{sc} accumulation and transmission to neurons.[21, 39, 61, 72] Activated astrocytes can secrete either neuroprotective molecules or pro-inflammatory cytokines, depending on the inciting stimulus.[4, 63, 82] An activation scheme similar to M1/M2 differentiation has been proposed for astrocytes, with "A1" phenotypes associated with neuronotoxicity and "A2" phenotypes with neuroprotection.[45, 46] Experimental astrocytic polarization into "classical" and "alternative" activation patterns with differential expression of iNOS and Arg1 has been demonstrated in culture.[34] Astrocyte subclasses have not been investigated in prion disease.

The aim of this study was to characterize the glial response to prion infection using a mouse model of scrapie (RML) by evaluating glial activation over time and correlating it to classical markers of prion neuropathology, including neuropil vacuolation, and PrP^{sc} deposition. Although gliosis is a well-documented phenomenon in prion infection,[11, 25, 59] this study represents a comprehensive time course investigation across 15 brain regions with in-situ expression analysis for iNOS and Arg1, canonical markers of glial polarization. [57, 68] We found that microgliosis late in the clinical time course is associated with pro-inflammatory upregulation of iNOS, and minimal Arg1 expression. Colocalization analysis revealed predominantly astrocytic Arg1 expression in the cerebellum and medulla, with isolated iNOS-positive astrocyte populations in the cerebellar peduncles and internal capsule. This was an unexpected finding indicating the possible existence

of multiple astrocytic inflammatory phenotypes. These data provide a detailed temporospatial characterization of neuropathology and gliosis in the RML scrapie infection model, contributing insight into glial activation dynamics and evidence for multiple activation states.

Materials and Methods

Animals and Tissue Preparation

This experiment was performed in accordance with the *Guide for the Care and Use of Laboratory Animals,* and approved by the Institutional Animal Care and Use Committee at the National Animal Disease Center (protocol #3985).

C57BL/6 mice aged 6 to 8 weeks from an inbred colony maintained at the USDA National Animal Disease Center were inoculated intracranially into the right cerebral hemisphere with 20 μL of 10% w/v brain homogenate in PBS pooled from C57BL/6 mice terminally ill with the mouse-adapted Rocky Mountain Laboratories (RML) strain of the scrapie agent. Groups of mice were euthanized at predetermined time points of 30 (n=4), 60 (n=4), 90 (n=4), and 120 (n=5) days post inoculation (DPI), along with a group of animals that was allowed to survive until clinical signs necessitated euthanasia at 155 DPI (n=5). Age-matched C57BL/6 negative controls were inoculated with 10% w/v normal brain homogenate (NBH) in PBS and included at each time point (30, 90, 120 DPI n=2; 60 DPI n=4; 155 DPI n=2). Brains were collected into 10% neutral buffered formalin. After 24 hours of fixation, brains were transversely sectioned at four levels: mid-cerebellum, rostral colliculus, thalamus and hypothalamus, and rostral cerebrum at level of septal nuclei. Tissues were processed by routine histologic methods, embedded in paraffin, sectioned at 5 μm, and mounted on glass slides for hematoxylin and eosin staining or immunohistochemistry.

Vacuolation Scoring

Brain sections from 4 infected and 2 mock-inoculated animals from each time-point (30, 60, 90, 120, 155 DPI) were mounted and stained with hematoxylin and eosin. 15 regions of interest, 12 grey matter and 3 white matter, were evaluated per animal and scored on a scale of 0 (no vacuoles) to 5 (maximal vacuolation) for grey matter and 0 to 3 for white matter, as described by Fraser and Dickinson (1973). Scores were averaged among timepoint cohorts, and mean values ≥2 (grey matter) and ≥1 (white matter) were considered definitive for spongiform change. Regions of interest analyzed for this and subsequent immunohistochemistry studies included the following, from caudal to rostral: vestibular nuclei (VestNuc), cerebellar peduncles (CerPed), cerebellar nuclei (CerNuc), superior colliculus (Coll), medial longitudinal fasciculus (MLF), midbrain reticular nucleus (MRN), lateral thalamus (LatThal), medial thalamus (MedThal), hypothalamus (Hypothal), dentate gyrus of hippocampus (HDG), CA1 of hippocampus (HCA1), internal capsule (IntCap), cerebral cortex at level of thalamus (Cthal), septal nuclei (SepNuc) and cerebral cortex at level of septal nuclei (Csep).

Immunohistochemistry

Brain sections were immunolabeled to detect PrP^{sc} as previously described[79] using mouse anti-PrP primary antibody 6C2 (CVI-WUR, Lelystad). Sequential multiple immunolabeling was performed on two sets of serial tissue sections using primary antibodies against Arg1 (rabbit anti-Arg1, ab91279, Abcam), iNOS (rabbit anti-iNOS, ab15323, Abcam), Iba1 (rabbit anti-Iba1, ab178847, Abcam) and GFAP (rabbit anti-GFAP, Z022429, Dako). Each set was labeled first with either Arg1 or iNOS, followed by Iba1 and GFAP. For each set, slides were baked for 1h in a 60C oven and rehydrated. Antigen retrieval was performed in a rice cooker using citrate-EDTA-10%

w/v sucrose buffer (pH 6) for 15 minutes, followed by Tris-EDTA -10% w/v sucrose buffer (pH 9) for 20 minutes. Next, sections were incubated for 10 minutes in a 3% hydrogen peroxide solution, followed by a 30 min incubation in 5% bovine serum albumin in Tris-buffered saline. iNOS and Arg1 primary antibodies were each applied at a dilution of 1:250, and incubated overnight at 4˚C. Tissues were then washed with TBST-10% w/v sucrose buffer, and incubated at 37˚C with an HRP-conjugated goat anti-rabbit secondary antibody (ImmPRESS, MP-7500, Vector Laboratories) diluted 1:3 in TBST. After washing, slides were developed with ImmPACT AEC Peroxidase (HRP) Substrate (SK-4205, Vector Laboratories) according to kit instructions. Tissues were counterstained with 1:1 deionized water:Gill's #2 hematoxylin (Sigma-Aldrich) for 2 minutes and stored in TBS buffer at 4C through the duration of image acquisition. On completing image capture for each staining round, as described below, slides were stripped of chromogen and antibody by adapting a beta-mercaptoethanol buffer incubation protocol described by Gendusa et al. [24] as follows: doubling the concentration of beta-mercaptoethanol (1.8ml per 100ml buffer) and extending elution buffer incubation to 90 minutes. After removing bound iNOS or Arg1 antibody complexes, tissues were re-blocked by incubating for 1 hour with 5% BSA in TBS, and then re-labeled with rabbit anti-Iba1 primary (1:5000), as described above. Following image acquisition of Iba1 immunoreactivity, tissues were again stripped of chromogen and antibody complexes, and submitted to a final round of immunolabeling for GFAP (1:5000). On completing image capture, GFAP-stained slides were coverslipped with aqueous permanent mounting medium for long-term storage (VectaMount AQ, H-5501, Vector Laboratories).

Image Analysis

Immunohistochemical staining was imaged using an Olympus DP73 camera mounted on an Olympus BX53 microscope, operated with cellSens imaging software (v1.15, Olympus Corporation). TBST-wetted slides were coverslipped and 4800x3600ppi brightfield images were acquired at 200x magnification for the medial thalamus and 400x magnification for the remaining 14 regions of interest. Following image capture, coverslips were gently floated off tissue sections and slides were returned to storage in TBST at 4C in anticipation of the next IHC round. Images of successive IHC rounds were acquired from the same subanatomic location by visually aligning nuclei. Captured images were processed using the Area Quantification module v1.0 within the HALO image analysis platform (v2.0.1145.19, Indica Labs). Briefly, hematoxylin nuclear stain and AEC chromogen were selected as stain 1 and 2, respectively, and adequate deconvolution was confirmed visually. A base threshold intensity value was assigned to image sets and manually adjusted, as needed, for each image to accurately reflect chromogen distribution in the regions of interest. Total chromogen deposition in the region of interest was quantified by the module algorithm as % Stain 2 Positive Tissue. Colocalization of enzymatic and glial staining was achieved by assigning an opaque red and yellow pseudocolor to thresholded regions in HALO's Area Quantification module, respectively, and importing the resulting .tif images into Photoshop CC (Adobe). The Layer Auto-Align command was used to overlay paired images from each region of interest. An opacity value of 50% was assigned to the glial stain image, generating an orange zone in regions of colocalization. Layers were flattened, and the exported image was reanalyzed in HALO's Area Quantification module v1.0 to obtain a % Stain Positive Tissue for the orange colocalization zone.

Statistical Analysis

Data were analyzed using a generalized linear model to detect significant differences in quantified immunoreactivity between mock-inoculated and RML-infected animal groups. DPI, brain location and treatment condition were included as fixed effects in the model. Simple effect comparisons between the least squares (LS) means of mock-inoculated and infected animal groups were conducted at each DPI for each within all brain regions to determine the degree of significance. Similarly, simple effect comparisons were conducted between LS means of DPI 30 and DPI 60, 90, 120, 155 within infected groups at each location. These later comparisons were used to determine significance of increases in immunoreactivity in late disease at locations where the brain region of interest was not represented in mock-inoculated slides. Pearson correlation analysis was used to evaluate for temporal associations between stains at each location. Results were considered statistically significant if $p<0.05$. The software for conducting statistical analysis was SAS version 9.4.

Results

PrPsc deposition and spongiform change

Infected animals developed classic neuropathologic changes of PrP^{sc} accumulation and vacuolation (**Fig. 1-5).** Definitive spongiform change (**Fig. 6**) was first observed at 120 DPI in the three evaluated white matter regions (cerebellar peduncles, MLF, internal capsule), the lateral and medial thalamus, CA1 of the hippocampus and septal nuclei. By 155 DPI (clinical disease), spongiform change was additionally present in the vestibular nuclei and the dentate gyrus of the hippocampus. Definitive vacuolation was not observed in other evaluated brain regions in infected animals, nor in control brains.

Quantitative immunohistochemistry was used to determine changes in PrP^{sc} immunoreactivity over time. Significant increases between RML-infected and control groups were determined by one tail Student's t-tests of simple effects comparisons between group least squares means. PrPsc immunoreactivity (Fig. 7) was first significantly increased over age-matched controls at 60 DPI in the cerebellar nuclei ($p<.05$), midbrain reticular nucleus (MRN) ($p<.01$), lateral thalamus ($p<.05$), septal nuclei ($p<.05$) and cortex at the level of the septal nuclei ($p<.01$). PrP^{sc} remained progressively elevated through clinical disease in the cerebellar nuclei, MRN and lateral thalamus ($p<.001$). A significant and sustained increase in PrP^{sc} immunoreactivity was first detected at 90 days in the vestibular nuclei ($p<.01$) and medial thalamus ($p<.001$), and a transient increase was detected in the hypothalamus ($p<.01$). Significant PrP^{sc} immunoreactivity was ubiquitous in all grey matter regions by 155 DPI ($p<.001$ for all brain regions, except hypothalamus $p<.05$). PrP^{sc} deposition in white matter tracts was minimal, only achieving significance above controls at 155 DPI in the MLF ($p<.05$)

Gliosis

RML-inoculated animals developed microgliosis and astrocytosis over the course of infection. (**Fig. 8-12**) Qualitative changes in microglial morphology were observed over the course of infection. (**Fig. 13**) Quiescent ramified microglia were gradually replaced by hypertrophied phenotypes with thick processes, a change first observed in the MLF and, to a lesser degree, thalamus at 60 DPI. By 120 DPI, all examined regions contained a preponderance of hypertrophied microglia. Retraction of processes and a marked increase in somal volume ("amoeboid" microglia) was first observed at 120 DPI and sustained through clinical infection, where present. This

morphology did not appear until 155 DPI in the hippocampus and never manifested in examined sections of the colliculus, hypothalamus, cortex or septal nuclei.

Significant increases in Iba1 and GFAP immunoreactivity between infected and control animals were determined by one tail Student's t-tests of simple effects comparisons between group least squares means. In the absence of HCA1 representation in control slides at 155 DPI, RML-inoculated animals were instead compared to the 30 DPI cohort.

Iba1 immunoreactivity (**Fig. 14**) was significantly increased in infected brains as early as 30 DPI in the cortex at the level of the thalamus ($p>.05$) and 60 DPI in the MLF ($p<.05$). By 90 DPI, significant upregulation was detected in the vestibular nuclei ($p<.01$), MLF ($p<.001$), MRN ($p<.001$), medial and lateral thalamus ($p<.001$), hypothalamus ($p<.001$), and cortex at the level of the thalamus ($p<.05$). With exception of septal nuclei which failed to maintain significance at clinical disease ($p=.0631$), microgliosis was diffusely distributed through all brain regions by 155 DPI ($p<.001$ for all brain regions, excepting $p<.05$ for hypothalamus).

Astrocytic GFAP expression (**Fig. 15**) underwent a transient increase above age-matched controls at 60 DPI in the cerebellar peduncles ($p<.05$), HCA1 of the hippocampus ($p<.01$), and septal nuclei ($p<.001$). Sustained upregulation was not observed until 90 DPI in the MLF ($p<.001$), MRN ($p<.001$), and medial and lateral thalamus ($p<.001$). A significant increase in GFAP immunoreactivity was first detected at 120 DPI in the vestibular nuclei ($p<.001$), cerebellar nuclei ($p<.001$), colliculus ($p<.001$), cortex at the level of the thalamus ($p<.001$), and the cortex at the level of the septal nuclei ($p<.05$). Increased labeling was not measured at any point in the dentate gyrus, internal capsule or hypothalamus. The cerebellar peduncles, hippocampus, hypothalamus and internal capsule in control animals demonstrated elevated GFAP immunoreactivity at all timepoints relative to other brain regions.

Temporospatial distribution of iNOS and Arg1

Quantitative IHC was similarly used to evaluate total iNOS and Arg1 immunoreactivity (**Fig. 16-20**) and the degree of colocalization with Iba1 and GFAP within each brain region. Significant differences in iNOS and Arg1 immunoreactivity between infected and control mice were determined by two tail Student's t-tests of simple effects comparisons between group least squares means for total enzyme. One tail Student's t-tests were used to compare increases in colocalized enzyme expression between group least squares means. In the absence of HCA1 representation in control slides at 155DPI, RML-inoculated animals were compared to the 30DPI cohort.

Total iNOS expression was varied across the brain regions, with no significant change in infected mice in 7/15 regions (**Fig. 21**). A transient increase in total iNOS was observed at 60 DPI in the vestibular nuclei ($p<.01$) and cerebellar nuclei ($p<.01$). From 60-155 DPI, there was a sustained and progressive increase in iNOS in the cerebellar peduncles ($p<.05$). Expression was not significantly elevated until 120 DPI in the MLF ($p<.01$), MRN ($p<.01$), and lateral thalamus ($p<.05$). Late increases in iNOS immunoreactivity were first observed at 155 DPI in CA1 of the hippocampus ($p<.01$, compared to 30 DPI infected cohort) and internal capsule ($p<.001$).

To determine the degree of microglial and astrocytic expression of iNOS, colocalization of iNOS with Iba1 and GFAP was quantified (**Fig. 22**). iNOS colocalized primarily with microglial Iba1. (**Fig. 23**). A significant increase in colocalization of Iba1 with iNOS was first observed at 120 DPI in the vestibular nuclei ($p<.05$), MLF ($p<.001$), MRN ($p<.001$) and internal capsule ($p<.01$). By 155 DPI, microglial iNOS was upregulated in 9/15 brain regions, including the vestibular nuclei ($p<.001$), cerebellar peduncles ($p<.001$), cerebellar nuclei ($p<.001$), MLF

($p<.001$), MRN ($p<.001$), lateral thalamus ($p<.001$), medial thalamus ($p<.05$), CA1 ($p<.05$, compared to 30 DPI infected cohort) and the internal capsule ($p<.001$). A significant increase in colocalization of iNOS and GFAP was present only at 155 DPI in the white matter tracts of the cerebellar peduncles ($p<.001$) and the internal capsule ($p<.001$), with a transient increase at 120 DPI in the lateral thalamus ($p<.05$) (**Fig. 24**). iNOS immunoreactivity that did not colocalize with either Iba1 or GFAP was primarily observed along vascular endothelium and forming halos around small nuclei of uncertain cellular identity.

Total Arg1 expression demonstrated no statistically significant change over time in the majority (13/15) of evaluated brain regions (**Fig. 25**). Vestibular nuclei displayed increased Arg1 immunoreactivity over controls at 30 DPI ($p<.05$). A significant decrease in Arg1 was detected in this region at 120 DPI ($p<.001$); however, this was likely due to one outlying control value that contained a concentration of strongly Arg1-immunoreactive neurons. Cerebellar nuclei displayed a similar transient increase in Arg1 expression at 30 DPI ($p<.05$) and another significant increase at 155 DPI ($p<.001$).

To determine the degree of microglial and astrocytic expression of Arg1, colocalization of Arg1 with Iba1 and GFAP was quantified. In areas of highest Arg1 expression, such as the medulla oblongata and cerebellum, neuronal and vascular Arg1 expression accounted for the majority of immunoreactivity (**Fig. 26**). Overall, the amount of glial Arg1 expression was low, but Arg1 colocalized to a greater extent with astrocytic GFAP than microglial Iba1. Low quantities of Arg1 colocalization with Iba1 were detected at significant levels over controls in the vestibular nuclei at 90 ($p<.01$) and 120DPI ($p<.05$) (**Fig. 28**). A similar increase in Iba1-colocalized Arg1 at 120DPI ($p<.05$) with concurrent increases in control and clinical animals at 155DPI was observed in the cerebellar peduncles. Iba1-colocalized Arg1 expression was significantly increased at 120 ($p<.05$)

and 155DPI ($p<.001$) in the cerebellar nuclei. Microglial Iba1 colocalization represented a fraction of total glial Arg1. At such low levels of quantified coreactivity, incidental overlap (e.g. overlap of neuronal cytoplasm and microglial process) could be a confounding factor for meaningful interpretation. GFAP colocalization with Arg1 represented the majority of glial coimmunoreactivity (**Fig 27**). A significant increase in astrocytic expression of Arg1, beginning at 120DPI and sustained through clinical disease, was observed in the vestibular nuclei ($p<.01$), cerebellar peduncles ($p<.05$), and cerebellar nuclei ($p<.05$) **(Fig. 29**). Astrocytic Arg1 was transiently upregulated at 120DPI in the medial thalamus ($p<.01$), dentate gyrus ($p<.05$) and CA1 ($p<.01$). Although trends towards sustained upregulation of astrocytic Arg1 at 120DPI were observed in the colliculus and MRN, and suggestions of a transient elevation at 120DPI were present in the lateral thalamus, internal capsule and septal nuclei, the quantified signal did not achieve statistical significance over controls.

Correlation analysis between immunohistochemical stains

To determine whether iNOS and Arg1 immunoreactivity is correlated to regional neuropathology development, Pearson's correlation matrices were calculated for immunohistochemical stains at each location in infected mice (Table A1). Additionally, iNOS and Arg1 were compared to each other at each location to identify any relationship between expression patterns of this mutually inhibitory enzyme pair. Stain pairs with $r>|.8|$ were evaluated as having a strong linear relationship. Only relationships with $p<.05$ are presented below. All significant relationships observed in this model displayed a positive correlation. It is important to note that because r values do not reflect the slope of temporal trends in immunoreactivity, some strong positive correlations corresponded to an absence of change for both stains at the analyzed location.

Total iNOS exhibited positive correlations at the largest number of locations with PrP^{sc} and Iba1, and displayed less association with spongiform change and GFAP. Immunoreactivity was positively associated over time with PrP^{sc} in the cerebellar peduncles ($p<.05$), dentate gyrus ($p<.001$), CA1 ($p<.001$), internal capsule ($p<.001$) and the cortex at the level of the thalamus ($p<.05$). Little significant interaction was present between total iNOS and vacuolation, as a positive relationship was observed only in 2/9 locations that developed spongiform change. These included the MLF and the dentate gyrus ($p<.05$ for both). Total iNOS was positively associated with Iba1 in the cerebellar peduncles ($p<.05$), lateral thalamus ($p<.05$), hippocampus ($p<.05$) and internal capsule ($p<.05$). A positive correlation between total iNOS and GFAP was observed only in the MLF, CA1 and cortex at the level of the thalamus ($p<.05$ for all).

Microglial iNOS displayed little difference in the strength of association with PrP^{sc} and glial stains, as positive correlations were observed in 4-5 scattered brain regions for any stain pair. Microglial iNOS was moderately correlated to spongiform change. Positive relationships were observed in 4/9 areas where definitive vacuolation was present, including the vestibular nuclei, the cerebellar peduncles, MLF, and internal capsule ($p<.05$ for all). A positive correlation was observed with PrP^{sc} deposition in 5/9 areas, including the vestibular nuclei ($p<.05$), cerebellar peduncles ($p<.01$), medial thalamus ($p<.05$), CA1 of the hippocampus ($p<.01$) and the internal capsule ($p<.001$). Astrocytic iNOS was positively correlated to spongiform change in only 3/9 areas with definitive vacuolation, including the medial ($p<.01$) and lateral ($p<.01$) thalamus and CA1 ($p<.05$). Sporadic associations were observed with PrP^{sc} in 3 brain regions.

Total Arg1 displayed marginally more association with spongiform change and Iba1, compared to PrP^{sc} and GFAP. Total Arg1 was positively correlated to PrP^{sc} in 4/15 regions, including the vestibular nuclei ($p<.05$), cerebellar peduncles ($p<.05$), colliculus ($p<.05$), and cortex

at the level of the thalamus ($p<.001$). Arg1 was positively correlated to spongiform change in 5/9 brain regions that developed definitive vacuolation. These included the vestibular nuclei ($p<.05$), cerebellar peduncles ($p<.05$), medial and lateral thalamus ($p<.05$) and the dentate gyrus ($p<.01$). Of the glial stains, total Arg1 displayed the most correlation with Iba1 immunoreactivity. Despite only displaying statistically significant increases in immunoreactivity in the vestibular and cerebellar nuclei, total Arg1 was additionally positively correlated to Iba1 in the colliculus ($p<.05$), medial and lateral thalamus ($p<.05$), dentate gyrus ($p<.001$) and cortex at the level of the thalamus ($p<.05$). Significant positive correlation with GFAP was observed only in the colliculus ($p<.001$), MLF ($p<.05$) and hypothalamus ($p<.001$).

Microglial Arg1 represented a minor fraction of glial colocalization, but displayed strong positive correlation with PrP^{sc} in 6/15 brain regions and with spongiform change in 5/9 regions where vacuolation was definitively observed. Astrocytic Arg1 displayed markedly less association with PrP^{sc} deposition and spongiform change, with positive correlation observed in only 2/15 and 1/9 regions, respectively.

Correlation coefficients between total iNOS and Arg1 were evaluated for evidence of reciprocal trends. Overall, there was little correlation between global enzyme expression across brain regions, as only the MLF and thalamus displayed a strong positive relationship between total iNOS and Arg1 ($p<.05$). Interestingly, despite apparently strong positive correlation in immunoreactivity between total enzymatic stains in the MLF ($p<.05$, $n=5$), no association between iNOS and glial Arg1 was observed in this region. No significant negative linear relationships between total iNOS and Arg1 were present in these data. There were few significant interactions between glial Arg1 and glial iNOS across the brain. No reciprocal relationships suggestive of temporal inhibition were observed between glia-colocalized stains.

Discussion

This study sought to characterize the temporospatial distribution of salient prion neuropathology in an intracranial infection model of murine scrapie and correlate changes to canonical markers of glial polarization.

Prion infection is known to induce a patterned progression of neuropathology in the brain, wherein PrP^{sc} accumulation is followed by glial activation and finally by spongiform change, neuronal and synaptic loss.[11, 80] While this infection model reproduced histologic changes classically associated with scrapie infection, the order of lesion development deviated somewhat from previous reports.

In the present work, PrP^{sc} deposition preceded gliosis in 4/15 regions, and was the first pathologic change observed at 60DPI in the cerebellar nuclei, lateral thalamus, and rostral cortex, with delayed detection at 120DPI in the dentate gyrus. In the remaining regions, gliosis was detected either in advance of, or contemporaneously with the first significant increases in PrP^{sc} immunoreactivity between 60 and 90DPI.

Astrocytic accumulation of PrP^{sc} has been demonstrated early in disease progression,[21, 72] and previous works have detected an upregulation of GFAP as early as 40DPI,[11] well in advance of microgliosis.[11] Astrocytosis was detected at 60DPI prior to microgliosis in only 4/15 of the evaluated brain regions, including the cerebellar peduncles, midbrain reticular nucleus (MRN), CA1 and septal nuclei. In remaining regions, microgliosis either preceded or was detected at the same time as the first appreciable increase in GFAP immunoreactivity. Notably, in the vestibular nuclei, MLF, internal capsule, and cortex at the level of the thalamus, microgliosis was quantifiably increased before upregulation of either GFAP or PrP^{sc} immunoreactivity. The timing

and distribution of prion-associated neurodegenerative changes are dictated by incompletely understood strain-host interactions, but are highly conserved within an infection model.[23] Our demonstration of a precocious microglial response relative to other studies that employed RML scrapie agent in C57BL/6 mice[11] may be attributed to variations in harvest timepoints, sampling location or genetic polymorphisms arising from the long-term (>20 generations) inbreeding of the originating colony.[49]

Spongiform change, where detected, occurred subsequent to PrP^{sc} deposition and gliosis, consistent with RML progression in other models. In the 9 areas where definitive vacuolation was detected, spongiform change had the highest degree of correlation with Iba1 immunoreactivity, exhibiting a strong positive relationship with 8/9 brain regions, excepting the MLF. A lesser degree of association was observed between spongiform change, PrP^{sc} and Arg1, with 5/9 regions of each of these stains exhibiting strong positive relationships with vacuolation. In contrast GFAP only demonstrated strong positive correlation with vacuolation in 3/9 areas, including the vestibular nuclei, lateral thalamus and cortex at the level of the septal nuclei. These findings suggest that microgliosis is more strongly associated with development of spongiform change than astrocytosis.

Neuropathology was most pronounced in the dorsal medulla, sensory midbrain and the thalamus. These regions demonstrated marked PrP^{sc} accumulation and gliosis by 90 days post-inoculation, with the MRN exhibiting PrP^{sc} accumulation and astrocytosis by 60DPI. Of the 15 evaluated brain regions, the hypothalamus exhibited the least pathology, with only a transient increase in PrP^{sc} and Iba1 at 90DPI, and a second, smaller, peak for both at 155DPI.

The hippocampus, a region commonly evaluated in experimental prion infection due to its involvement in behavioral alterations, exhibited a relatively late onset of lesion development and

inconsistent pathology between the closely apposed dentate gyrus and CA1. Delayed PrP^{sc} accumulation was the first indicator of pathology in the dentate gyrus at 120 DPI, with spongiform change and upregulation of Iba1 appearing at 155DPI. No significant astrocytosis was detected in this region. CA1, however, exhibited an early transient spike in GFAP at 60 DPI ($p<.01$), which was followed by microgliosis and spongiform change at 120DPI. PrPsc deposition did not achieve significant levels and GFAP upregulation wasn't observed again in the CA1 until 155DPI ($p<.001$ for both).

The neuroinflammatory profile of prion disease has been a subject of continued debate, and published results vary with infection model.[54] Several studies have reported that prion infection incites a marked upregulation of genes mediating cell motility, proliferation, homeostatic mechanisms and inflammatory responses that are primarily attributed to microglia.[3, 65] Furthermore, two patterns of upregulation were detected: non-lesioned areas were associated with a homeostasis-mediating cluster, while lesioned brain regions overexpressed genes related to proteolysis, cell stress and activation of innate immunity.[3, 73] This apparent dichotomy in microglial activation profiles lends support for the potential benefits of localized in-situ analysis. Infected brains in recent comprehensive transcriptomic and cytokine array analyses demonstrated a definitively proinflammatory signature, with upregulation of IL1β, TNFα, Csf1, IFNγ, caspase 4, TIMP1 and MMP12.[10, 51, 53, 64, 71, 73] Such an inflammatory milieu would be anticipated to promote pro-inflammatory polarization of microglia and induce iNOS expression.[58] Indeed, microglia have been shown to elaborate nitric oxide in response to PrP^{sc}.[30] However, phagocytosis of apoptotic neurons in late disease[38] could bias microglia towards alternative activation, which is associated with Arg1 expression.[68] Mixed populations of microglia mediating pro-and anti-inflammatory effects have been demonstrated in Alzheimer's disease[14, 48] and ALS[44]. We used

quantitative immunohistochemistry to spatiotemporally characterize iNOS and Arg1 labeling through the infection timecourse and correlate expression to lesion patterns. Colocalization analysis of enzyme immunoreactivity with Iba1 and GFAP was furthermore employed to differentiate between microglial and astrocytic expression.

iNOS induction in the brain results in elaboration of neuronotoxic nitric oxide (NO).[7] iNOS expression is associated with classically activated proinflammatory glia[15, 34], and has been demonstrated in AD[48, 76], PD[37, 70] and ALS[62]. Total iNOS expression was upregulated late in disease incubation, with significantly increased expression detected by 120 DPI in 4/15 regions and in an additional 4 locations at terminal disease, representing the dorsal medulla, cerebellum, midbrain, lateral thalamus, HCA1 and internal capsule. No iNOS upregulation was observed in the colliculus, medial thalamus, hypothalamus, dentate gyrus, septal nuclei or cerebral cortex. It is notable that closely apposed regions, such as the dentate gyrus and CA1 of the hippocampus, and the medial and lateral thalamus had statistically significant variation in iNOS expression. Among brain regions exhibiting iNOS upregulation, the strongest positive correlation between iNOS and other immunohistochemical targets was observed with Iba1, a finding supported by colocalization data. Additionally, neither total nor microglial iNOS upregulation was detected in brain regions that failed to demonstrate a transition to amoeboid microglial morphology by clinical disease. These included the colliculus, hypothalamus, dentate gyrus, septal nuclei and both cortical locations. iNOS detection in this model contrasts with previous reports detailing lack of iNOS upregulation[77] or transient upregulation followed by descending expression in terminal disease.[12] However, these studies used ME7 scrapie, which has been associated with a dampened inflammatory profile, [6, 18] and analyzed signal from whole or partially dissected brain homogenate.

The spatial distribution of iNOS expression in our model supports the possibility of signal dilution as a confounding factor in these study designs.

iNOS immunoreactivity was observed to colocalize with both Iba1 and GFAP. Significant increases in microglial iNOS expression were observed by 155 DPI in all regions of global iNOS upregulation, with the addition of medial thalamus. Increased astrocytic iNOS expression was only observed in white matter of the cerebellar peduncles and internal capsule. Curiously, a concomitant increase in total GFAP immunoreactivity was not observed in the internal capsule at 155 DPI. Inversely, there is a lack of significant astrocytic iNOS at 155 DPI in the MLF, despite marked GFAP upregulation as early as 90 DPI. Combined, these findings indicate that astrocytic iNOS induction is not directly associated with the density of activated fibrous astrocytes and is driven by unknown location-dependent factors. Sporadic iNOS immunoreactivity was also observed in GFAP- and Iba1-negative cells with filamentous processes that strongly resembled astrocytes. GFAP has been demonstrated to underestimate astrocyte densitiy[36], as it can fail to label up to 40% of cells[78] and only associates with an estimated 15% of total cell volume[9]. Thus, the colocalization results may not fully reflect astrocytic contribution to iNOS expression. In sum, our results support the existence of a pro-inflammatory iNOS-high environment primarily generated by microglia at clinical disease. This is consistent with an M1 “classically activated” microglial phenotype.

Expression of Arg1, used to identify M2 microglia,[15] is associated with extracellular matrix repair, suppression of inflammation, and has been demonstrated in both astrocytes and monocytes during the reparative phase of spinal cord injury.[2, 52, 68] Arginase-1 expression did not reflect the same widespread distribution as iNOS and displayed markedly different cell association. Global Arg1 expression was unremarkable rostral to cerebellum. The highest immunoreactivity levels

were noted in the grey matter regions of the dorsal medulla and cerebellum, in control and infected animals alike, relative to the rest of the brain. Here, Arg1 immunoreactivity was primarily observed in neuronal cytoplasm with variable expression in vascular endothelium. This finding coincides with Yu et al.'s report of high basal arginase expression in the grey matter of the cerebellum and dorsal medulla, however hippocampal and cerebral cortical immunoreactivity was not recapitulated in the present timecourse.[81] In this study, as in ours, Arg1 was primarily expressed by neurons.[81]

In areas with significant Arg1 upregulation, glial expression colocalized predominantly with GFAP. In-situ colocalization permitted detection of a small but statistically significant transient rise in astrocytic Arg1 at 120 DPI in the medial thalamus, dentate gyrus and CA1 of the hippocampus, areas where there was no concurrent increase in total or microglial Arg1, and no hippocampal GFAP upregulation. Activated astrocytes can elaborate either neurotrophic factors promoting repair, or pro-inflammatory synaptolytic compounds, depending on the nature of the activating stimulus.[34, 63, 82] An activation spectrum similar to the M1/M2 paradigm has been advanced for astrocytes, broadly characterizing neurotoxic "A1" and neuroprotective "A2" phenotypes.[45] Arg1 production has been demonstrated in healthy and reactive astrocytes in a model of spinal cord trauma,[2] and can be induced in experimental polarization of cultured astrocytes.[34] Analysis of tissues from patients with protein misfolding neurodegenerative diseases including AD, HD, PD and ALS demonstrated presence of proinflammatory A1 astrocytes in lesioned brain regions.[46] Previous reports of astrocytic response to prion infection have similarly demonstrated a pro-inflammatory phenotype with secretion of IL1β, IL6, IL12 and TNFα,[64, 71] thus our finding of predominantly astrocytic Arg1 expression associated with an anti-inflammatory profile is unexpected.

Interestingly, total Arg1 exhibited a strong positive relationship with spongiform change in 5/9 regions where definitive spongiform change was detected. However, this relationship was not reflected by astrocytic Arg1, which was only positively correlated with spongiform change in the cerebellar peduncles. A strong positive correlation was similarly observed with microglial Arg1, however, Iba1-Arg1 colocalization represented an exceedingly small fraction of total Arg1 expression, suggesting that increased neuronal, rather than glial, expression contributed to any potential causality in this relationship. Additionally, on retrospective image analysis of regions with increased calculated Iba1-Arg1, colocalization frequently corresponded to areas of high neuronal density and could be attributed to coincidental overlap of cell processes and neurons, rather than true colocalization within a single glial species. Study design did not accommodate case-by-case exclusion of incidental colocalization. Thus, the Arg1-Iba1 colocalization data may not present significant evidence of an M2-polarized population.

iNOS and Arg1 exert opposing effects on the inflammatory status of surrounding cells. The possible association between expression of these enzymes and progression of regional pathology was explored through correlation analysis. Positive relationships were identified between iNOS/Arg1 and markers of neuropathology and gliosis at sporadic locations, however overwhelming evidence that either enzyme is more strongly associated with lesion development on a global scale was not present in our data.

Arg1 and iNOS rely on arginine metabolism and are mutually inhibitory, both through substrate competition and suppressive effects of downstream metabolites.[57] In the present study, an inverse temporal relationship between total NOS and Arg1 was not observed at any location. Furthermore, immunoreactivity was largely segregated by cell type, with significant coexpression of both Arg1 and iNOS in one glial population limited to astrocytes in the cerebellar peduncles.

Although transient upregulation of astrocytic Arg1 at 120 DPI was detected in several locations, these observations were not paired with a reciprocal rise in astrocytic iNOS at 155 DPI. Thus, there is no evidence that suppression of astrocytic Arg1 in clinical disease is mediated by iNOS.

In summary, our data support strong spatiotemporal associations between lesion development and proliferation of microglia demonstrating a pro-inflammatory iNOS-high phenotype. In contrast, astrocytic iNOS expression appears limited to cerebellar and diencephalic white matter, with trends towards anti-inflammatory Arg1 production in medullary and cerebellar regions, and transient upregulation in the diencephalon in late incubation. To our knowledge, this timecourse represents the first in-situ characterization of glial immunophenotypes in RML scrapie infection using sequential chromogenic immunohistochemistry. Our findings corroborate previous reports of a predominantly pro-inflammatory microglial profile in prion infection and contribute new evidence of location-dependent mixed astrocytic activation.

References

1. Aguzzi A, Lakkaraju AK. Cell Biology of Prions and Prionoids: A Status Report. Trends in cell biology. 2016 Jan;26(1):40-51. doi: 10.1016/j.tcb.2015.08.007. PubMed PMID: 26455408; eng.

2. Ahn M, Lee C, Jung K, et al. Immunohistochemical study of arginase-1 in the spinal cords of rats with clip compression injury. Brain research. 2012 Mar 22;1445:11-9. doi: 10.1016/j.brainres.2012.01.045. PubMed PMID: 22325098; eng.

3. Alibhai J, Blanco RA, Barria MA, et al. Distribution of Misfolded Prion Protein Seeding Activity Alone Does Not Predict Regions of Neurodegeneration. PLoS biology. 2016 Nov;14(11):e1002579. doi: 10.1371/journal.pbio.1002579. PubMed PMID: 27880767; PubMed Central PMCID: PMCPMC5120774. eng.

4. Anderson MA, Ao Y, Sofroniew MV. Heterogeneity of reactive astrocytes. Neuroscience letters. 2014 Apr 17;0:23-9. doi: 10.1016/j.neulet.2013.12.030. PubMed PMID: 24361547; PubMed Central PMCID: PMCPMC3984948. eng.

5. Beers DR, Zhao W, Liao B, et al. Neuroinflammation modulates distinct regional and temporal clinical responses in ALS mice. Brain, behavior, and immunity. 2011 Jul;25(5):1025-35. doi: 10.1016/j.bbi.2010.12.008. PubMed PMID: 21176785; PubMed Central PMCID: PMCPMC3096756. eng.

6. Boche D, Cunningham C, Docagne F, et al. TGFbeta1 regulates the inflammatory response during chronic neurodegeneration. Neurobiology of disease. 2006 Jun;22(3):638-50. doi: 10.1016/j.nbd.2006.01.004. PubMed PMID: 16510291; eng.

7. Brown GC. Mechanisms of inflammatory neurodegeneration: iNOS and NADPH oxidase. Biochemical Society transactions. 2007 Nov;35(Pt 5):1119-21. doi: 10.1042/bst0351119. PubMed PMID: 17956292; eng.

8. Brown GC, Neher JJ. Microglial phagocytosis of live neurons. Nature reviews Neuroscience. 2014 Apr;15(4):209-16. doi: 10.1038/nrn3710. PubMed PMID: 24646669; eng.

9. Bushong EA, Martone ME, Jones YZ, et al. Protoplasmic astrocytes in CA1 stratum radiatum occupy separate anatomical domains. The Journal of neuroscience : the official journal of the Society for Neuroscience. 2002 Jan 1;22(1):183-92. PubMed PMID: 11756501; eng.

10. Carroll JA, Striebel JF, Race B, et al. Prion infection of mouse brain reveals multiple new upregulated genes involved in neuroinflammation or signal transduction. Journal of virology. 2015 Feb;89(4):2388-404. doi: 10.1128/jvi.02952-14. PubMed PMID: 25505076; PubMed Central PMCID: PMCPMC4338885. eng.

11. Carroll JA, Striebel JF, Rangel A, et al. Prion Strain Differences in Accumulation of PrPSc on Neurons and Glia Are Associated with Similar Expression Profiles of Neuroinflammatory Genes: Comparison of Three Prion Strains. PLoS pathogens. 2016 Apr;12(4):e1005551. doi: 10.1371/journal.ppat.1005551. PubMed PMID: 27046083; PubMed Central PMCID: PMCPMC4821575. eng.

12. Chen LN, Sun J, Yang XD, et al. The Brain NO Levels and NOS Activities Ascended in the Early and Middle Stages and Descended in the Terminal Stage in Scrapie-Infected Animal Models. Molecular neurobiology. 2017 Apr;54(3):1786-1796. doi: 10.1007/s12035-016-9755-z. PubMed PMID: 26887380; eng.

13. Chen Z, Jalabi W, Hu W, et al. Microglial displacement of inhibitory synapses provides neuroprotection in the adult brain. Nature communications. 2014 Jul 22;5:4486. doi: 10.1038/ncomms5486. PubMed PMID: 25047355; PubMed Central PMCID: PMCPMC4109015. eng.

14. Cherry JD, Olschowka JA, O'Banion MK. Arginase 1+ microglia reduce Aβ plaque deposition during IL-1β-dependent neuroinflammation. Journal of neuroinflammation. 2015;12. doi: 10.1186/s12974-015-0411-8. PubMed PMID: 26538310; PubMed Central PMCID: PMCPMC4634600. eng.

15. Chhor V, Le Charpentier T, Lebon S, et al. Characterization of phenotype markers and neuronotoxic potential of polarised primary microglia in vitro. Brain, behavior, and immunity. 2013 Aug;32:70-85. doi: 10.1016/j.bbi.2013.02.005. PubMed PMID: 23454862; PubMed Central PMCID: PMCPMC3694309. eng.

16. Collinge J. Mammalian prions and their wider relevance in neurodegenerative diseases. Nature. 2016 Nov 10;539(7628):217-226. doi: 10.1038/nature20415. PubMed PMID: 27830781; eng.

17. Colton CA. Heterogeneity of Microglial Activation in the Innate Immune Response in the Brain. Journal of Neuroimmune Pharmacology. 2009 Dec;4(4):399-418. doi: 10.1007/s11481-009-9164-4. PubMed PMID: 19655259; PubMed Central PMCID: PMCPMC2773116. eng.

18. Cunningham C, Boche D, Perry VH. Transforming growth factor beta1, the dominant cytokine in murine prion disease: influence on inflammatory cytokine synthesis and alteration of vascular extracellular matrix. Neuropathology and applied neurobiology. 2002 Apr;28(2):107-19. PubMed PMID: 11972797; eng.

19. De Biase LM, Schuebel KE, Fusfeld ZH, et al. Local Cues Establish and Maintain Region-Specific Phenotypes of Basal Ganglia Microglia. Neuron. 2017 Jul 19;95(2):341-356.e6. doi: 10.1016/j.neuron.2017.06.020. PubMed PMID: 28689984; PubMed Central PMCID: PMCPMC5754189. eng.

20. De Lucia C, Rinchon A, Olmos-Alonso A, et al. Microglia regulate hippocampal neurogenesis during chronic neurodegeneration. Brain, behavior, and immunity. 2016 Jul;55:179-90. doi: 10.1016/j.bbi.2015.11.001. PubMed PMID: 26541819; PubMed Central PMCID: PMCPMC4907582. eng.

21. Diedrich JF, Bendheim PE, Kim YS, et al. Scrapie-associated prion protein accumulates in astrocytes during scrapie infection. Proceedings of the National Academy of Sciences of the United States of America. 1991 Jan 15;88(2):375-9. PubMed PMID: 1671170; PubMed Central PMCID: PMCPMC50813. eng.

22. Erana H, Venegas V, Moreno J, et al. Prion-like disorders and Transmissible Spongiform Encephalopathies: An overview of the mechanistic features that are shared by the various disease-related misfolded proteins. Biochemical and biophysical research communications. 2016 Aug 30. doi: 10.1016/j.bbrc.2016.08.166. PubMed PMID: 27590581; Eng.

23. Fraser H, Dickinson AG. Scrapie in mice. Agent-strain differences in the distribution and intensity of grey matter vacuolation. Journal of comparative pathology. 1973 Jan;83(1):29-40. PubMed PMID: 4199908; eng.

24. Gendusa R, Scalia CR, Buscone S, et al. Elution of High-affinity (>10(-9) K(D)) Antibodies from Tissue Sections: Clues to the Molecular Mechanism and Use in Sequential Immunostaining. Journal of Histochemistry and Cytochemistry. 2014 Jul;62(7):519-31. doi: 10.1369/0022155414536732. PubMed PMID: 24794148; PubMed Central PMCID: PMCPMC4174624. eng.

25. Giese A, Brown DR, Groschup MH, et al. Role of microglia in neuronal cell death in prion disease. Brain pathology (Zurich, Switzerland). 1998 Jul;8(3):449-57. PubMed PMID: 9669696; eng.

26. Ginhoux F, Guilliams M. Tissue-Resident Macrophage Ontogeny and Homeostasis. Immunity. 2016 Mar 15;44(3):439-49. doi: 10.1016/j.immuni.2016.02.024. PubMed PMID: 26982352; Eng.

27. Gomez-Nicola D, Fransen NL, Suzzi S, et al. Regulation of microglial proliferation during chronic neurodegeneration. The Journal of neuroscience : the official journal of the Society for Neuroscience. 2013 Feb 6;33(6):2481-93. doi: 10.1523/jneurosci.4440-12.2013. PubMed PMID: 23392676; eng.

28. Grabert K, Michoel T, Karavolos MH, et al. Microglial brain region-dependent diversity and selective regional sensitivities to ageing. Nature neuroscience. 2016 Mar;19(3):504-16. doi: 10.1038/nn.4222. PubMed PMID: 26780511; PubMed Central PMCID: PMCPMC4768346. eng.

29. Gravel M, Beland LC, Soucy G, et al. IL-10 Controls Early Microglial Phenotypes and Disease Onset in ALS Caused by Misfolded Superoxide Dismutase 1. The Journal of neuroscience : the official journal of the Society for Neuroscience. 2016 Jan 20;36(3):1031-48. doi: 10.1523/jneurosci.0854-15.2016. PubMed PMID: 26791230; eng.

30. Hafner-Bratkovic I, Bencina M, Fitzgerald KA, et al. NLRP3 inflammasome activation in macrophage cell lines by prion protein fibrils as the source of IL-1beta and neuronal toxicity. Cellular and molecular life sciences : CMLS. 2012 Dec;69(24):4215-28. doi: 10.1007/s00018-012-1140-0. PubMed PMID: 22926439; PubMed Central PMCID: PMCPMC3508391. eng.

31. Harry GJ, Kraft AD. Neuroinflammation and Microglia: Considerations and approaches for neurotoxicity assessment. Expert opinion on drug metabolism & toxicology. 2008 Oct;4(10):1265-77. doi: 10.1517/17425255.4.10.1265. PubMed PMID: 18798697; PubMed Central PMCID: PMCPMC2658618. eng.

32. Henkel JS, Engelhardt JI, Siklos L, et al. Presence of dendritic cells, MCP-1, and activated microglia/macrophages in amyotrophic lateral sclerosis spinal cord tissue. Annals of neurology. 2004 Feb;55(2):221-35. doi: 10.1002/ana.10805. PubMed PMID: 14755726; eng.

33. Hughes MM, Field RH, Perry VH, et al. Microglia in the degenerating brain are capable of phagocytosis of beads and of apoptotic cells, but do not efficiently remove PrPSc, even upon LPS stimulation. Glia. 2010 Dec;58(16):2017-30. doi: 10.1002/glia.21070. PubMed PMID: 20878768; PubMed Central PMCID: PMCPMC3498730. eng.

34. Jang E, Kim JH, Lee S, et al. Phenotypic polarization of activated astrocytes: the critical role of lipocalin-2 in the classical inflammatory activation of astrocytes. Journal of immunology (Baltimore, Md : 1950). 2013 Nov 15;191(10):5204-19. doi: 10.4049/jimmunol.1301637. PubMed PMID: 24089194; eng.

35. Jimenez S, Baglietto-Vargas D, Caballero C, et al. Inflammatory response in the hippocampus of PS1M146L/APP751SL mouse model of Alzheimer's disease: age-dependent switch in the microglial phenotype from alternative to classic. The Journal of neuroscience : the official journal of the Society for Neuroscience. 2008 Nov 5;28(45):11650-61. doi: 10.1523/jneurosci.3024-08.2008. PubMed PMID: 18987201; eng.

36. Kimelberg HK. The problem of astrocyte identity. Neurochemistry international. 2004 Jul-Aug;45(2-3):191-202. doi: 10.1016/j.neuint.2003.08.015. PubMed PMID: 15145537; eng.

37. Knott C, Stern G, Wilkin GP. Inflammatory Regulators in Parkinson's Disease: iNOS, Lipocortin-1, and Cyclooxygenases-1 and -2. Molecular and Cellular Neuroscience. 2000 2000/12/01/;16(6):724-739. doi: https://doi.org/10.1006/mcne.2000.0914.

38. Kranich J, Krautler NJ, Falsig J, et al. Engulfment of cerebral apoptotic bodies controls the course of prion disease in a mouse strain-dependent manner. The Journal of experimental medicine. 2010 Sep 27;207(10):2271-81. doi: 10.1084/jem.20092401. PubMed PMID: 20837697; PubMed Central PMCID: PMCPMC2947076. eng.

39. Krejciova Z, Alibhai J, Zhao C, et al. Human stem cell-derived astrocytes replicate human prions in a PRNP genotype-dependent manner. The Journal of experimental medicine. 2017 Dec 4;214(12):3481-3495. doi: 10.1084/jem.20161547. PubMed PMID: 29141869; PubMed Central PMCID: PMCPMC5716027. eng.

40. Lawson LJ, Perry VH, Dri P, et al. Heterogeneity in the distribution and morphology of microglia in the normal adult mouse brain. Neuroscience. 1990;39(1):151-70. PubMed PMID: 2089275; Eng.

41. Lee EJ, Woo MS, Moon PG, et al. Alpha-synuclein activates microglia by inducing the expressions of matrix metalloproteinases and the subsequent activation of protease-activated receptor-1. Journal of immunology (Baltimore, Md : 1950). 2010 Jul 1;185(1):615-23. doi: 10.4049/jimmunol.0903480. PubMed PMID: 20511551; eng.

42. Lee S, Kim HJ. Prion-like Mechanism in Amyotrophic Lateral Sclerosis: are Protein Aggregates the Key? Experimental Neurobiology. 2015 Mar;24(1):1-7. doi: 10.5607/en.2015.24.1.1. PubMed PMID: 25792864; PubMed Central PMCID: PMCPMC4363329. eng.

43. Leitman J, Ulrich Hartl F, Lederkremer GZ. Soluble forms of polyQ-expanded huntingtin rather than large aggregates cause endoplasmic reticulum stress. Nature communications. 2013;4:2753. doi: 10.1038/ncomms3753. PubMed PMID: 24217578; eng.

44. Lewis KE, Rasmussen AL, Bennett W, et al. Microglia and motor neurons during disease progression in the SOD1(G93A) mouse model of amyotrophic lateral sclerosis: changes in arginase1 and inducible nitric oxide synthase. Journal of neuroinflammation. 2014;11:55. doi: 10.1186/1742-2094-11-55. PubMed PMID: 24655927; PubMed Central PMCID: PMCPMC3994340. eng.

45. Liddelow SA, Barres BA. Reactive Astrocytes: Production, Function, and Therapeutic Potential. Immunity. 2017 Jun 20;46(6):957-967. doi: 10.1016/j.immuni.2017.06.006. PubMed PMID: 28636962; eng.

46. Liddelow SA, Guttenplan KA, Clarke LE, et al. Neurotoxic reactive astrocytes are induced by activated microglia. Nature. 2017 Jan 26;541(7638):481-487. doi: 10.1038/nature21029. PubMed PMID: 28099414; PubMed Central PMCID: PMCPMC5404890. eng.

47. Maezawa I, Zimin PI, Wulff H, et al. Amyloid-beta protein oligomer at low nanomolar concentrations activates microglia and induces microglial neurotoxicity. The Journal of biological chemistry. 2011 Feb 4;286(5):3693-706. doi: 10.1074/jbc.M110.135244. PubMed PMID: 20971854; PubMed Central PMCID: PMCPMC3030372. eng.

48. Martin E, Boucher C, Fontaine B, et al. Distinct inflammatory phenotypes of microglia and monocyte-derived macrophages in Alzheimer's disease models: effects of aging and amyloid pathology. Aging Cell. 2017 Feb;16(1):27-38. doi: 10.1111/acel.12522. PubMed PMID: 27723233; PubMed Central PMCID: PMCPMC5242297. eng.

49. Mekada K, Abe K, Murakami A, et al. Genetic differences among C57BL/6 substrains. Experimental animals. 2009 Apr;58(2):141-9. PubMed PMID: 19448337; eng.

50. Michelucci A, Heurtaux T, Grandbarbe L, et al. Characterization of the microglial phenotype under specific pro-inflammatory and anti-inflammatory conditions: Effects of oligomeric and fibrillar amyloid-beta. Journal of neuroimmunology. 2009 May 29;210(1-2):3-12. doi: 10.1016/j.jneuroim.2009.02.003. PubMed PMID: 19269040; eng.

51. Moody LR, Herbst AJ, Aiken JM. Upregulation of interferon-gamma-induced genes during prion infection. Journal of toxicology and environmental health Part A. 2011;74(2-4):146-53. doi: 10.1080/15287394.2011.529064. PubMed PMID: 21218343; PubMed Central PMCID: PMCPMC4621959. eng.

52. Munder M. Arginase: an emerging key player in the mammalian immune system. British Journal of Pharmacology. 2009 Oct;158(3):638-51. doi: 10.1111/j.1476-5381.2009.00291.x. PubMed PMID: 19764983; PubMed Central PMCID: PMCPMC2765586. eng.

53. Newsom DM, Liggitt HD, O'Rourke K, et al. Cytokine antibody array analysis in brain and periphery of scrapie-infected Tg338 mice. Comparative immunology, microbiology and infectious diseases. 2011 Sep;34(5):387-97. doi: 10.1016/j.cimid.2011.06.001. PubMed PMID: 21788075; eng.

54. Obst J, Simon E, Mancuso R, et al. The Role of Microglia in Prion Diseases: A Paradigm of Functional Diversity. Frontiers in aging neuroscience. 2017;9:207. doi: 10.3389/fnagi.2017.00207. PubMed PMID: 28690540; PubMed Central PMCID: PMCPMC5481309. eng.

55. Orihuela R, McPherson CA, Harry GJ. Microglial M1/M2 polarization and metabolic states. British Journal of Pharmacology. 2016 Feb;173(4):649-65. doi: 10.1111/bph.13139. PubMed PMID: 25800044; PubMed Central PMCID: PMCPMC4742299. eng.

56. Pan KM, Baldwin M, Nguyen J, et al. Conversion of alpha-helices into beta-sheets features in the formation of the scrapie prion proteins. Proceedings of the National Academy of Sciences of the United States of America. 1993 Dec 1;90(23):10962-6. PubMed PMID: 7902575; PubMed Central PMCID: PMCPMC47901. Eng.

57. Rath M, Müller I, Kropf P, et al. Metabolism via Arginase or Nitric Oxide Synthase: Two Competing Arginine Pathways in Macrophages. Frontiers in immunology. 2014;5. doi: 10.3389/fimmu.2014.00532. PubMed PMID: 25386178; PubMed Central PMCID: PMCPMC4209874. eng.

58. Saha RN, Pahan K. Regulation of Inducible Nitric Oxide Synthase Gene in Glial Cells. Antioxidants & redox signaling. 2006;8(5-6):929-47. doi: 10.1089/ars.2006.8.929. PubMed PMID: 16771683; PubMed Central PMCID: PMCPMC1963415. eng.

59. Sandberg MK, Al-Doujaily H, Sharps B, et al. Prion neuropathology follows the accumulation of alternate prion protein isoforms after infective titre has peaked. Nature communications. 2014 Jul 09;5:4347. doi: 10.1038/ncomms5347. PubMed PMID: 25005024; PubMed Central PMCID: PMCPMC4104459. eng.

60. Sapp E, Kegel KB, Aronin N, et al. Early and progressive accumulation of reactive microglia in the Huntington disease brain. Journal of neuropathology and experimental neurology. 2001 Feb;60(2):161-72. PubMed PMID: 11273004; eng.

61. Sarasa R, Martinez A, Monleon E, et al. Involvement of astrocytes in transmissible spongiform encephalopathies: a confocal microscopy study. Cell and tissue research. 2012 Oct;350(1):127-34. doi: 10.1007/s00441-012-1461-1. PubMed PMID: 22821398; eng.

62. Sasaki S, Shibata N, Komori T, et al. iNOS and nitrotyrosine immunoreactivity in amyotrophic lateral sclerosis. Neuroscience letters. 2000 2000/09/08/;291(1):44-48. doi: https://doi.org/10.1016/S0304-3940(00)01370-7.

63. Sofroniew MV. Astrogliosis. Cold Spring Harbor perspectives in biology. 2015 Feb;7(2). doi: 10.1101/cshperspect.a020420. PubMed PMID: 25380660; PubMed Central PMCID: PMCPMC4315924. eng.

64. Song K, Na JY, Oh MH, et al. Synthetic Prion Peptide 106-126 Resulted in an Increase Matrix Metalloproteinases and Inflammatory Cytokines from Rat Astrocytes and Microglial Cells. Toxicological Research. 2012 Mar;28(1):5-9. doi: 10.5487/tr.2012.28.1.005. PubMed PMID: 24278583; PubMed Central PMCID: PMCPMC3834397. eng.

65. Sorensen G, Medina S, Parchaliuk D, et al. Comprehensive transcriptional profiling of prion infection in mouse models reveals networks of responsive genes. BMC genomics. 2008 Mar 3;9:114. doi: 10.1186/1471-2164-9-114. PubMed PMID: 18315872; PubMed Central PMCID: PMCPMC2294129. eng.

66. Stahl N, Baldwin MA, Teplow DB, et al. Structural studies of the scrapie prion protein using mass spectrometry and amino acid sequencing. Biochemistry. 1993 Mar 2;32(8):1991-2002. PubMed PMID: 8448158; Eng.

67. Takagi S, Furube E, Nakano Y, et al. Microglia are continuously activated in the circumventricular organs of mouse brain. Journal of neuroimmunology. 2017 Oct 19. doi: 10.1016/j.jneuroim.2017.10.008. PubMed PMID: 29107327; eng.

68. Tang Y, Le W. Differential Roles of M1 and M2 Microglia in Neurodegenerative Diseases. Molecular neurobiology. 2016 Mar;53(2):1181-94. doi: 10.1007/s12035-014-9070-5. PubMed PMID: 25598354; eng.

69. Tarutani A, Arai T, Murayama S, et al. Potent prion-like behaviors of pathogenic alpha-synuclein and evaluation of inactivation methods. Acta neuropathologica communications. 2018 Apr 18;6(1):29. doi: 10.1186/s40478-018-0532-2. PubMed PMID: 29669601; eng.

70. Tieu K, Ischiropoulos H, Przedborski S. Nitric oxide and reactive oxygen species in Parkinson's disease. IUBMB life. 2003 Jun;55(6):329-35. doi: 10.1080/1521654032000114320. PubMed PMID: 12938735; eng.

71. Tribouillard-Tanvier D, Striebel JF, Peterson KE, et al. Analysis of protein levels of 24 cytokines in scrapie agent-infected brain and glial cell cultures from mice differing in prion protein expression levels. Journal of virology. 2009 Nov;83(21):11244-53. doi: 10.1128/jvi.01413-09. PubMed PMID: 19710140; PubMed Central PMCID: PMCPMC2772806. eng.

72. Victoria GS, Arkhipenko A, Zhu S, et al. Astrocyte-to-neuron intercellular prion transfer is mediated by cell-cell contact. Scientific reports. 2016 Feb 09;6:20762. doi: 10.1038/srep20762. PubMed PMID: 26857744; PubMed Central PMCID: PMCPMC4746738. eng.

73. Vincenti JE, Murphy L, Grabert K, et al. Defining the Microglia Response during the Time Course of Chronic Neurodegeneration. Journal of virology. 2015 Dec 30;90(6):3003-17. doi: 10.1128/jvi.02613-15. PubMed PMID: 26719249; PubMed Central PMCID: PMCPMC4810622. eng.

74. Vincenti JE, Murphy L, Grabert K, et al. Defining the Microglia Response during the Time Course of Chronic Neurodegeneration. Journal of virology. 2016 Mar;90(6):3003-17. doi: 10.1128/jvi.02613-15. PubMed PMID: 26719249; PubMed Central PMCID: PMCPMC4810622. eng.

75. Walker DG, Link J, Lue LF, et al. Gene expression changes by amyloid beta peptide-stimulated human postmortem brain microglia identify activation of multiple inflammatory processes. Journal of leukocyte biology. 2006 Mar;79(3):596-610. doi: 10.1189/jlb.0705377. PubMed PMID: 16365156; eng.

76. Wallace MN, Geddes JG, Farquhar DA, et al. Nitric oxide synthase in reactive astrocytes adjacent to beta-amyloid plaques. Experimental neurology. 1997 Apr;144(2):266-72. doi: 10.1006/exnr.1996.6373. PubMed PMID: 9168828; eng.

77. Walsh DT, Betmouni S, Perry VH. Absence of detectable IL-1beta production in murine prion disease: a model of chronic neurodegeneration. Journal of neuropathology and experimental neurology. 2001 Feb;60(2):173-82. PubMed PMID: 11273005; eng.

78. Walz W, Lang MK. Immunocytochemical evidence for a distinct GFAP-negative subpopulation of astrocytes in the adult rat hippocampus. Neuroscience letters. 1998 Dec 4;257(3):127-30. PubMed PMID: 9870336; eng.

79. West Greenlee MH, Lind M, Kokemuller R, et al. Temporal Resolution of Misfolded Prion Protein Transport, Accumulation, Glial Activation, and Neuronal Death in the Retinas of Mice Inoculated with Scrapie. The American journal of pathology. 2016 Sep;186(9):2302-9. doi: 10.1016/j.ajpath.2016.05.018. PubMed PMID: 27521336; PubMed Central PMCID: PMCPMC5012505. eng.

80. Williams A, Lucassen PJ, Ritchie D, et al. PrP deposition, microglial activation, and neuronal apoptosis in murine scrapie. Experimental neurology. 1997 Apr;144(2):433-8. doi: 10.1006/exnr.1997.6424. PubMed PMID: 9168844; eng.

81. Yu H, Iyer RK, Kern RM, et al. Expression of arginase isozymes in mouse brain. Journal of neuroscience research. 2001 Nov 1;66(3):406-22. doi: 10.1002/jnr.1233. PubMed PMID: 11746358; eng.

82. Zamanian JL, Xu L, Foo LC, et al. Genomic analysis of reactive astrogliosis. The Journal of neuroscience : the official journal of the Society for Neuroscience. 2012 May 2;32(18):6391-410. doi: 10.1523/jneurosci.6221-11.2012. PubMed PMID: 22553043; PubMed Central PMCID: PMCPMC3480225. eng.

83. Zhang W, Wang T, Pei Z, et al. Aggregated alpha-synuclein activates microglia: a process leading to disease progression in Parkinson's disease. FASEB journal : official publication of the Federation of American Societies for Experimental Biology. 2005 Apr;19(6):533-42. doi: 10.1096/fj.04-2751com. PubMed PMID: 15791003; eng.

Figures and Figure Legends

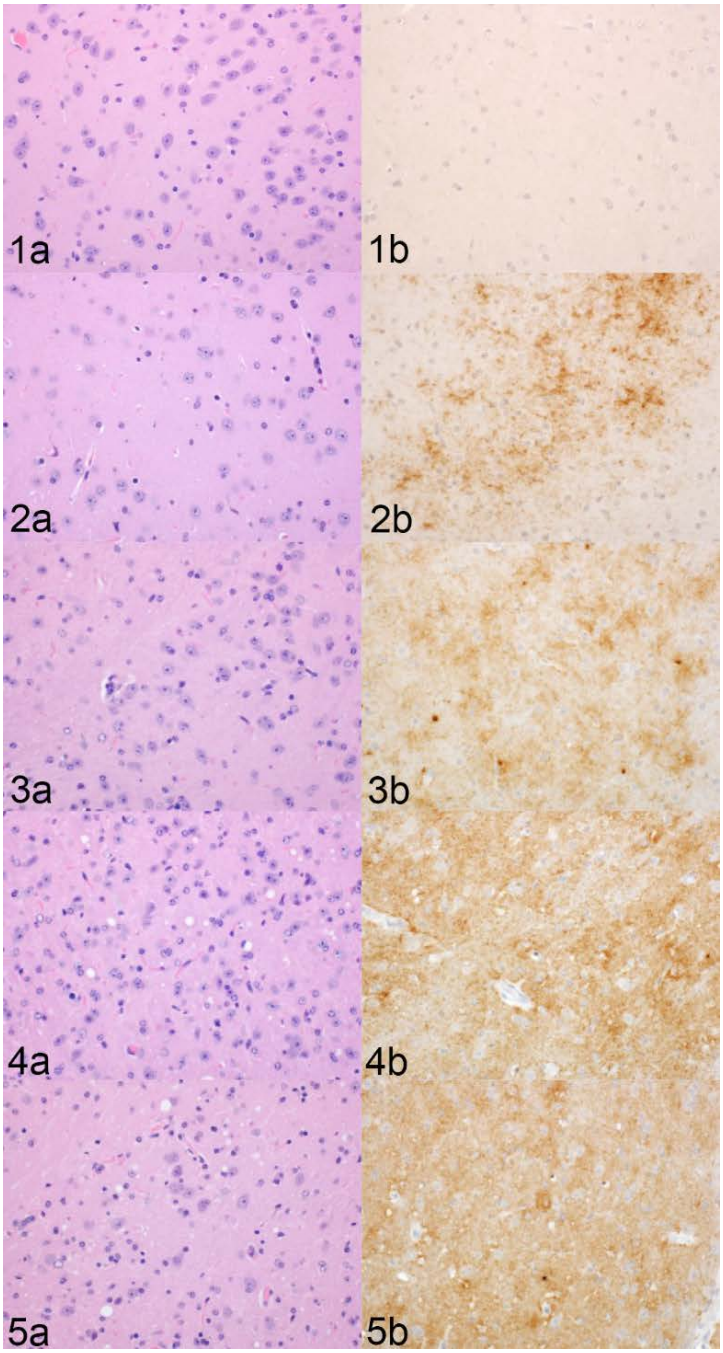

Figures 1-5. Representative images of thalamic vacuolation and PrP^{sc} immunoreactivity in RML-infected murine brain at 30 (Figure 1), 60 (Figure 2), 90 (Figure 3), 120 (Figure 4) and 155 DPI (Figure 5). Figures **1a-5a** Definitive spongiform change, characterized by well-demarcated empty vacuoles, was first detected at 120 DPI (4a). Histologic sections of thalamus, 400x, H&E. Figures

1b-5b. Immunohistochemistry for PrP^{sc}, monoclonal antibody 6C2. PrPsc labeling first appears at 60 DPI (2b) as punctate to granular immunoreactivity. Lateral thalamus, 400x, DAB.

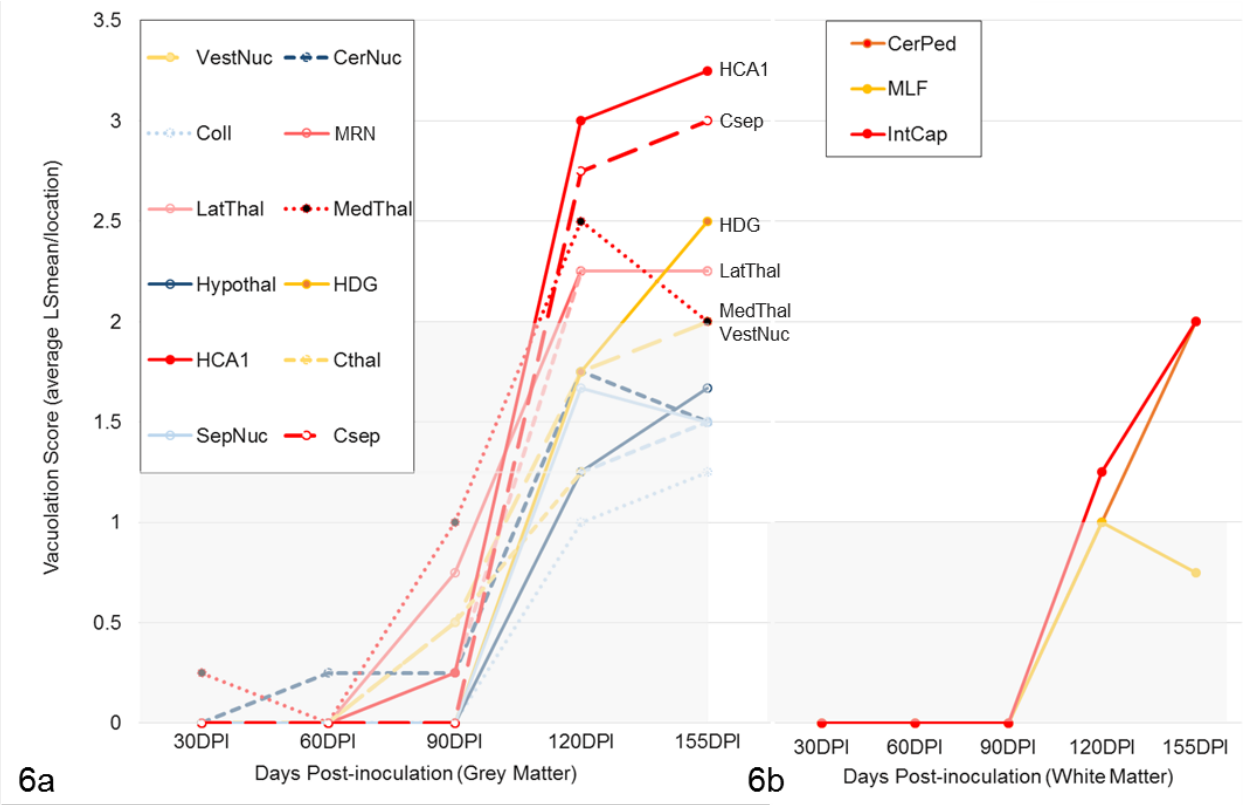

Figure 6. Neuronal vacuolation scores of RML-infected mice in grey (A) and white matter (B) regions over time. Data points for each brain region represent simple means for integer scores assigned to RML-infected cohorts at each timepoint. **A.** Grey matter vacuolation for a brain region was considered definitive for spongiform change when sample means ≥2, observed first at 120 DPI. **B.** White matter vacuolation was considered definitive for spongiform change when sample means ≥1; observed in all 3 regions at 120 DPI. Vestibular nuclei (VestNuc), cerebellar peduncles (CerPed), cerebellar nuclei (CerNuc), superior colliculus (Coll), medial longitudinal fasciculus (MLF), midbrain reticular nucleus (MRN), lateral thalamus (LatThal), medial thalamus (MedThal), hypothalamus (Hypothal), dentate gyrus of hippocampus (HDG), CA1 of hippocampus (HCA1), internal capsule (IntCap), cerebral cortex at level of thalamus (Cthal), septal nuclei (SepNuc), cerebral cortex at level of septal nuclei (Csep).

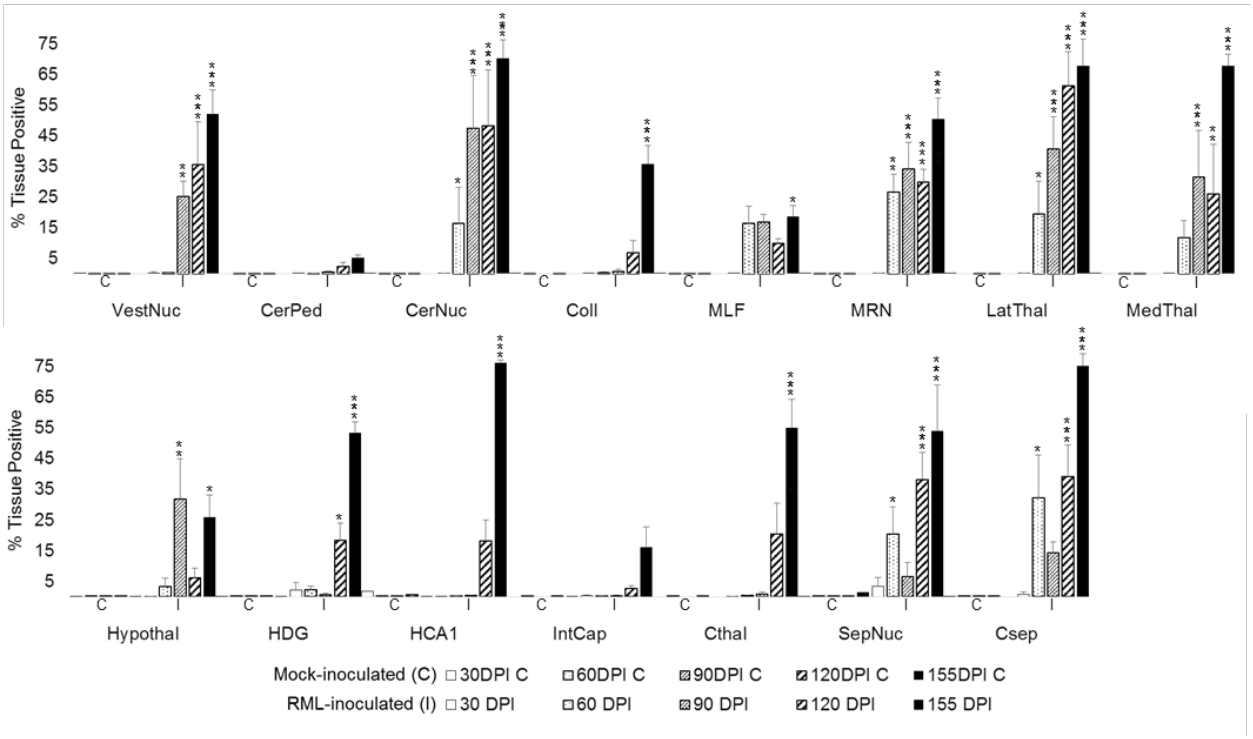

Figure 7. PrP^{sc} immunoreactivity in 15 brain regions over RML infection timecourse. Bars represent mean±SE values for control (C) and RML-inoculated (I) animal cohorts at each timepoint (30, 60, 90, 120, 155 DPI). *$p < 0.05$, **$p < 0.01$, ***$p < 0.001$; significant differences compared with control animals. Vestibular nuclei (VestNuc), cerebellar peduncles (CerPed), cerebellar nuclei (CerNuc), superior colliculus (Coll), medial longitudinal fasciculus (MLF), midbrain reticular nucleus (MRN), lateral thalamus (LatThal), medial thalamus (MedThal), hypothalamus (Hypothal), dentate gyrus of hippocampus (HDG), CA1 of hippocampus (HCA1), internal capsule (IntCap), cerebral cortex at level of thalamus (Cthal), septal nuclei (SepNuc), cerebral cortex at level of septal nuclei (Csep).

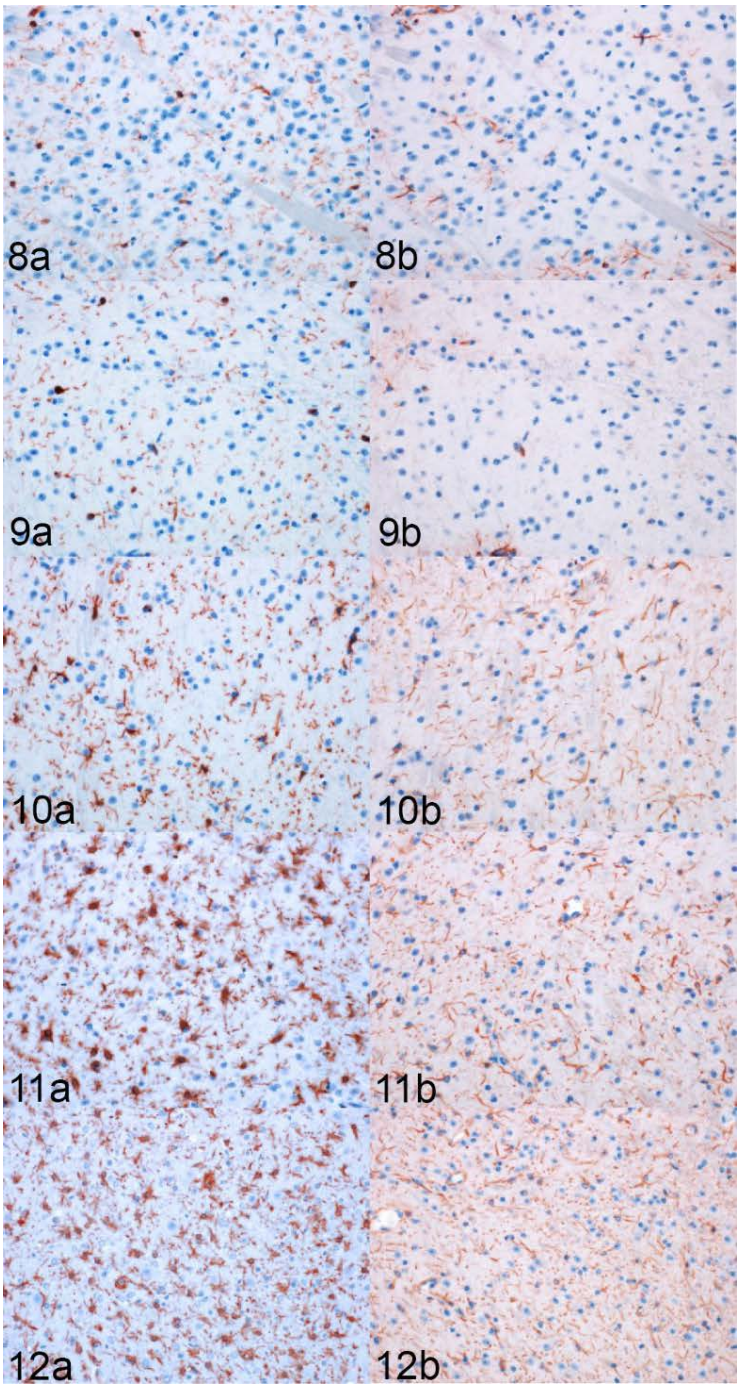

Figures 8-12. Representative images of Iba1 and GFAP immunoreactivity in the thalamus of infected mice 30 (Figure 8), 60 (Figure 9), 90 (Figure 10), 120 (Figure 11) and 155 DPI (Figure 12). **Figures 8a-12a.** Microglia undergo a hypertrophic and hyperplastic response to prion

infection at later timepoints, first appreciated here at 90 DPI (10a). Lateral thalamus, 400x, IHC for Iba1, AEC**. Figures 8b-12b.** Proliferative astrocytic reaction to scrapie infection visible at 90 DPI (10b). Lateral thalamus, 400x, IHC for GFAP, AEC.

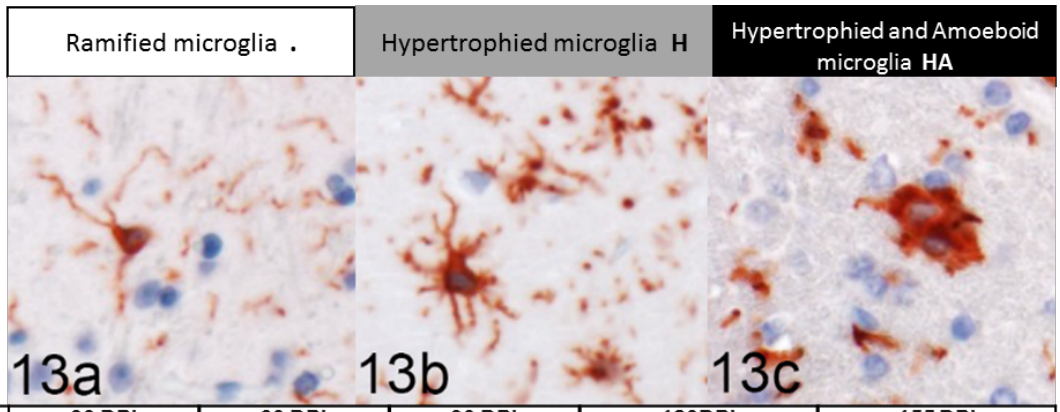

Brain Region	30 DPI				60 DPI				90 DPI				120DPI					155 DPI				
VestNuc	.	.	.	.	.	.	.	.	H	H	.		H	H	H	HA	HA	H	H	HA		
CerPed	.	.	.	.	.	.	.	.	H	H	H	.	H	HA	HA	HA	HA	HA	HA	HA		
CerNuc	.	.	.	.	.	.	.	.	H	H			H	H	H	.		H	HA	HA		
Coll	.	.	.	.	.	.	.	.	.	.	.	.	H	H	H	H	.	H	H	H		
MLF	.	.	.	.	H	H	H	H	H	H	H	H	H	H	HA	HA	HA	HA	HA			
MRN	.	.	.	.	.	.	.	.	H	H	H	H	H	HA	HA	HA	HA	H	HA			
LatThal	.	.	.	.	H	.	.	.	H	H	H	H	H	H	H	HA	HA	H	HA	HA	HA	
MidThal	.	.	.		H	H	.	.	H	H	H	H	H	H	H	H	HA	H	H	HA	HA	
Hypothal	.	.	.	.	.	.	.	.	H	.	.	.	H	H	H	H	.	H	H	.	.	
HDG	.	.	.	.	.	.	.	.	H	.	.	.	H	H	H	H	H	H	H	H	HA	
HCA1	.	.	.		.	.	.	.	.	.	.	.	H	H	H	H		H	H	HA		
IntCap	.	.	.	.	H	H	.		H	H	H	H	H	HA	HA	HA	HA	HA	HA	HA	HA	HA
Cthal	.	.	.	.	.	.	.	.	H	.	.		H	H	H	H	H	H	H	H	H	
SepNuc	.				.	.	.	.	.	.	.		H	H	H	H	H	H	H	H		
Csep	.	.	.	.	.	.	.	.	.	.	.		H	H	H	H	H	H	H	H	H	H

Figure 13. Temporal changes in microglial morphology in response to prion infection. Representative images of ramified quiescent microglia (**13a**, control thalamus, 155 DPI), hypertrophied microglia (**13b**, RML-infected hippocampus, 120 DPI) and amoeboid microglia (**13c**, RML-infected cerebellar nuclei, 155 DPI). 400x, IHC for Iba1, AEC. Table documents appearance of hypertrophied and amoeboid microglial populations over time across 15 brain regions. Columns represent a single RML-infected animal at each collection timepoint. . - only ramified microglia observed. H - hypertrophied microglia present. HA - both hypertrophied and amoeboid microglia present. - Brain region not present in tissue section.

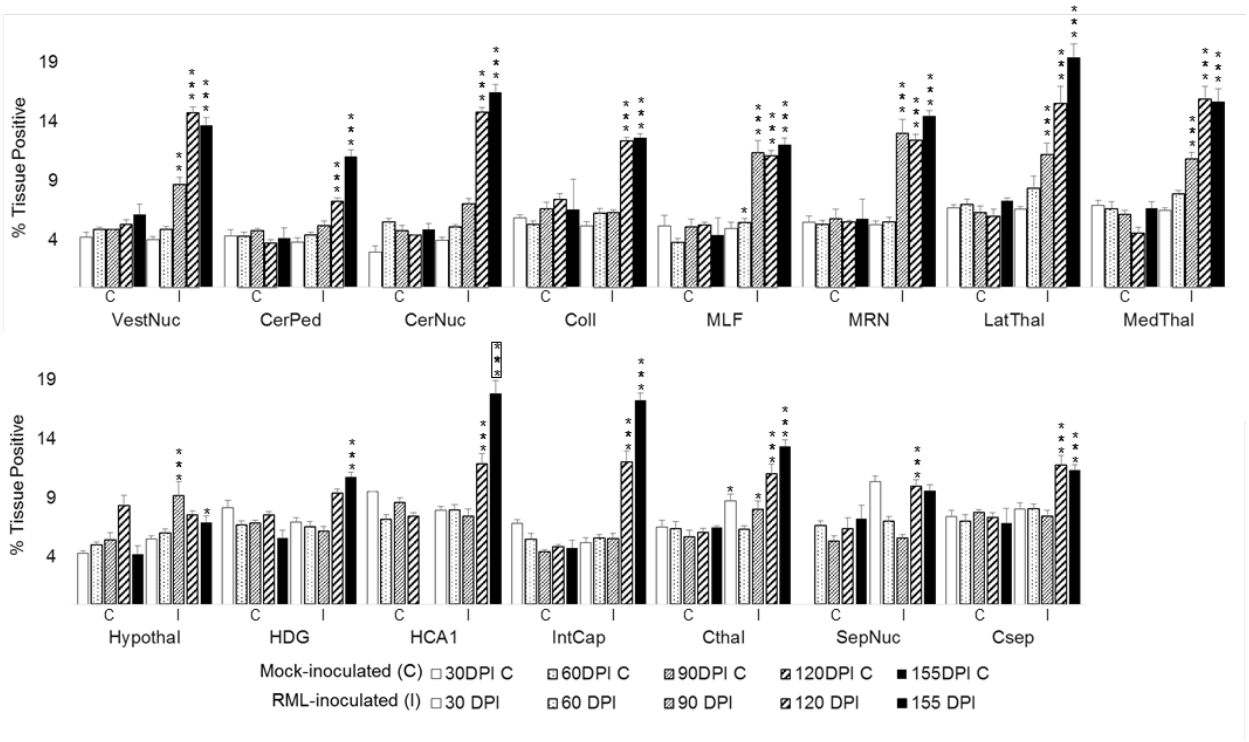

Figure 14. Iba1 immunoreactivity in 15 brain regions over RML infection timecourse. Iba1 labeling quantified in brain regions as % tissue positive for Iba1 immunoreactivity. Bars represent mean ±SE values for control (C) and RML-inoculated (I) animal cohorts at each sacrifice timepoint. *$p < 0.05$, **$p < 0.01$, ***$p < 0.001$; significant differences compared with control animals. *** $p<.001$, significant difference compared to 30DPI RML-infected animals. Vestibular nuclei (VestNuc), cerebellar peduncles (CerPed), cerebellar nuclei (CerNuc), superior colliculus (Coll), medial longitudinal fasciculus (MLF), midbrain reticular nucleus (MRN), lateral thalamus (LatThal), medial thalamus (MedThal), hypothalamus (Hypothal), dentate gyrus of hippocampus (HDG), CA1 of hippocampus (HCA1), internal capsule (IntCap), cerebral cortex at level of thalamus (Cthal), septal nuclei (SepNuc), cerebral cortex at level of septal nuclei (Csep).

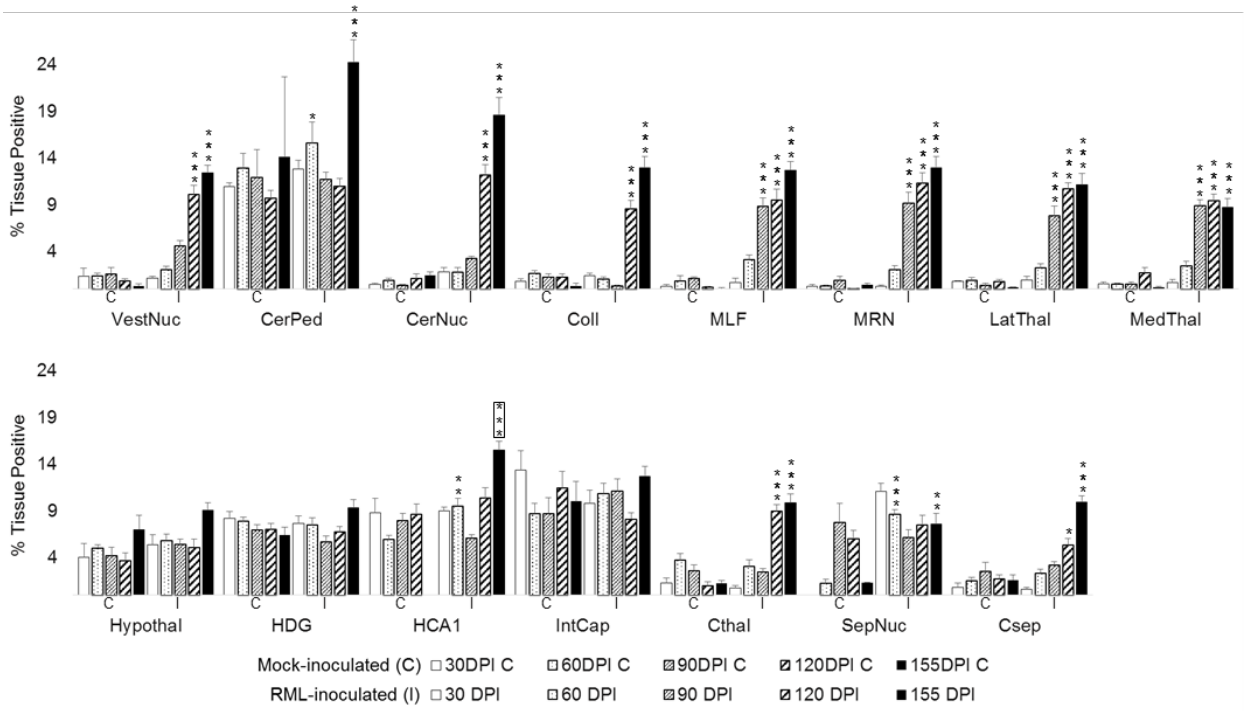

Figure 15. GFAP immunoreactivity in 15 brain regions over RML infection timecourse. GFAP labeling quantified in brain regions as % tissue positive for AEC chromogen deposition. Bars represent mean±SE values for control (C) and RML-inoculated (I) animal cohorts at each sacrifice timepoint. *$p < 0.05$, **$p < 0.01$, ***$p < 0.001$; significant differences compared with control animals. *** $p<.001$, significant difference compared to 30DPI RML-infected animals. Vestibular nuclei (VestNuc), cerebellar peduncles (CerPed), cerebellar nuclei (CerNuc), superior colliculus (Coll), medial longitudinal fasciculus (MLF), midbrain reticular nucleus (MRN), lateral thalamus (LatThal), medial thalamus (MedThal), hypothalamus (Hypothal), dentate gyrus of hippocampus (HDG), CA1 of hippocampus (HCA1), internal capsule (IntCap), cerebral cortex at level of thalamus (Cthal), septal nuclei (SepNuc), cerebral cortex at level of septal nuclei (Csep).

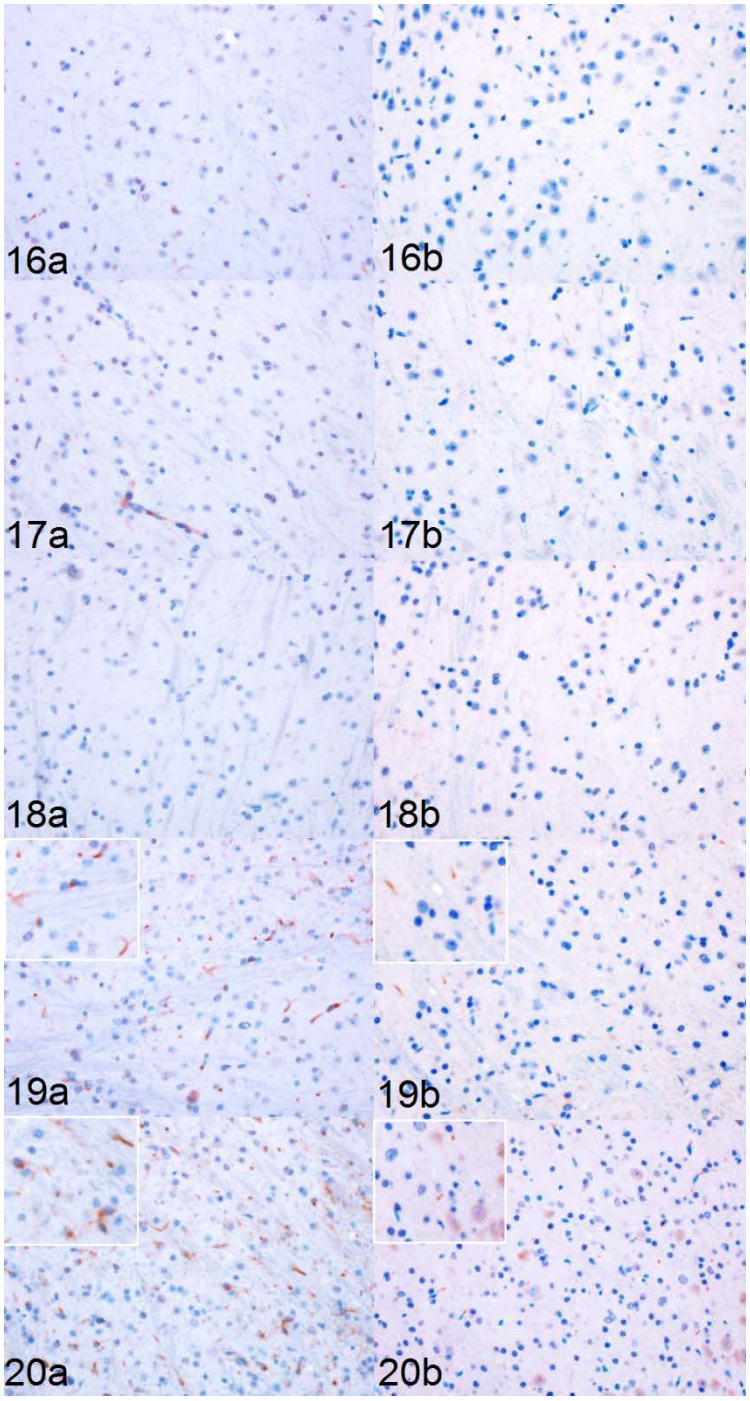

Figures 16-20. Representative images of iNOS and Arg1 immunoreactivity in the thalamus of infected mice 30 (Figure 16), 60 (Figure 17), 90 (Figure 18), 120 (Figure 19) and 155 DPI (Figure 20). **16a-20a.** Immunohistochemistry for iNOS. Occasional immunoreactivity in endothelium.

Filamentous labeling reminiscent of glial processes present at later timepoints (insets, 19-20a). Lateral thalamus, 400x, AEC. **16b-20b.** Immunohistochemistry for Arg1. Faint linear and neuronal cytoplasmic labeling present in late timepoints (insets, 19-20b). Lateral thalamus, 400x, AEC.

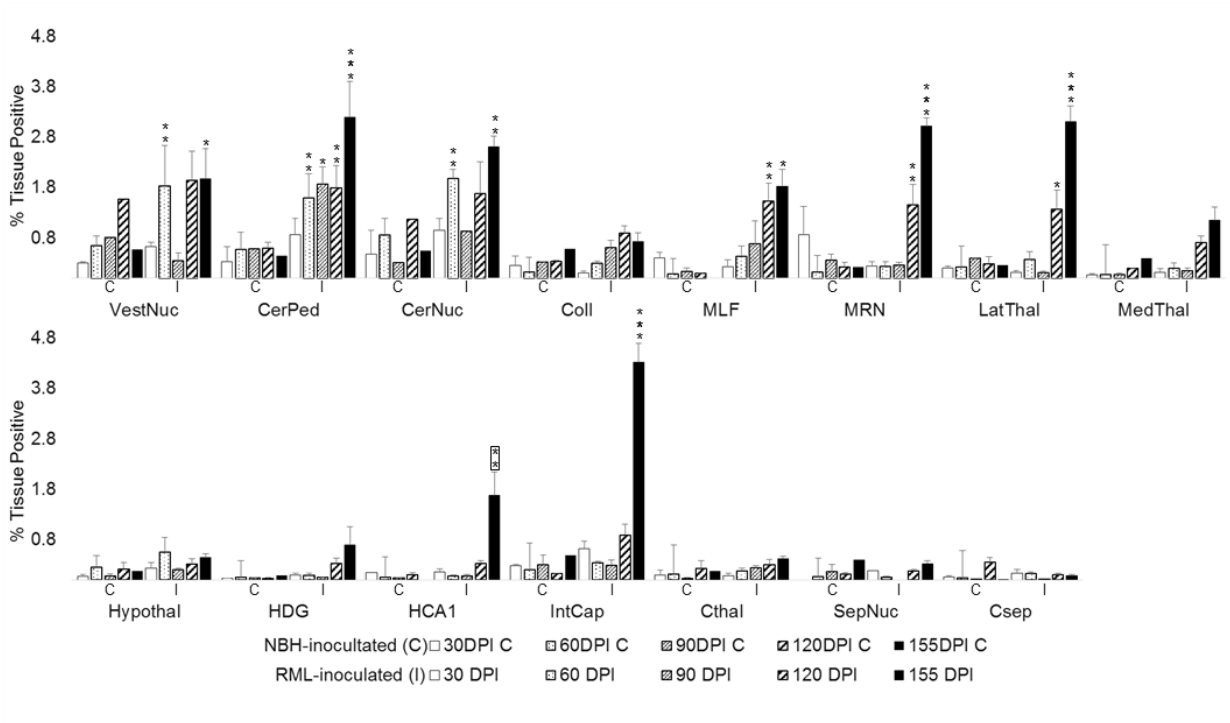

Figure 21. Total iNOS immunoreactivity in 15 brain regions over RML infection timecourse. Bars represent mean±SE values for mock-inoculated (C) and RML-inoculated (I) animal cohorts at each sacrifice timepoint. *$p < 0.05$, **$p < 0.01$, ***$p < 0.001$; significant differences compared with control (mock-inoculated) animals. ** $p<.01$, significant difference compared to 30 DPI infected. Vestibular nuclei (VestNuc), cerebellar peduncles (CerPed), cerebellar nuclei (CerNuc), superior colliculus (Coll), medial longitudinal fasciculus (MLF), midbrain reticular nucleus (MRN), lateral thalamus (LatThal), medial thalamus (MedThal), hypothalamus (Hypothal), dentate gyrus of hippocampus (HDG), CA1 of hippocampus (HCA1), internal capsule (IntCap), cerebral cortex at level of thalamus (Cthal), septal nuclei (SepNuc), cerebral cortex at level of septal nuclei (Csep).

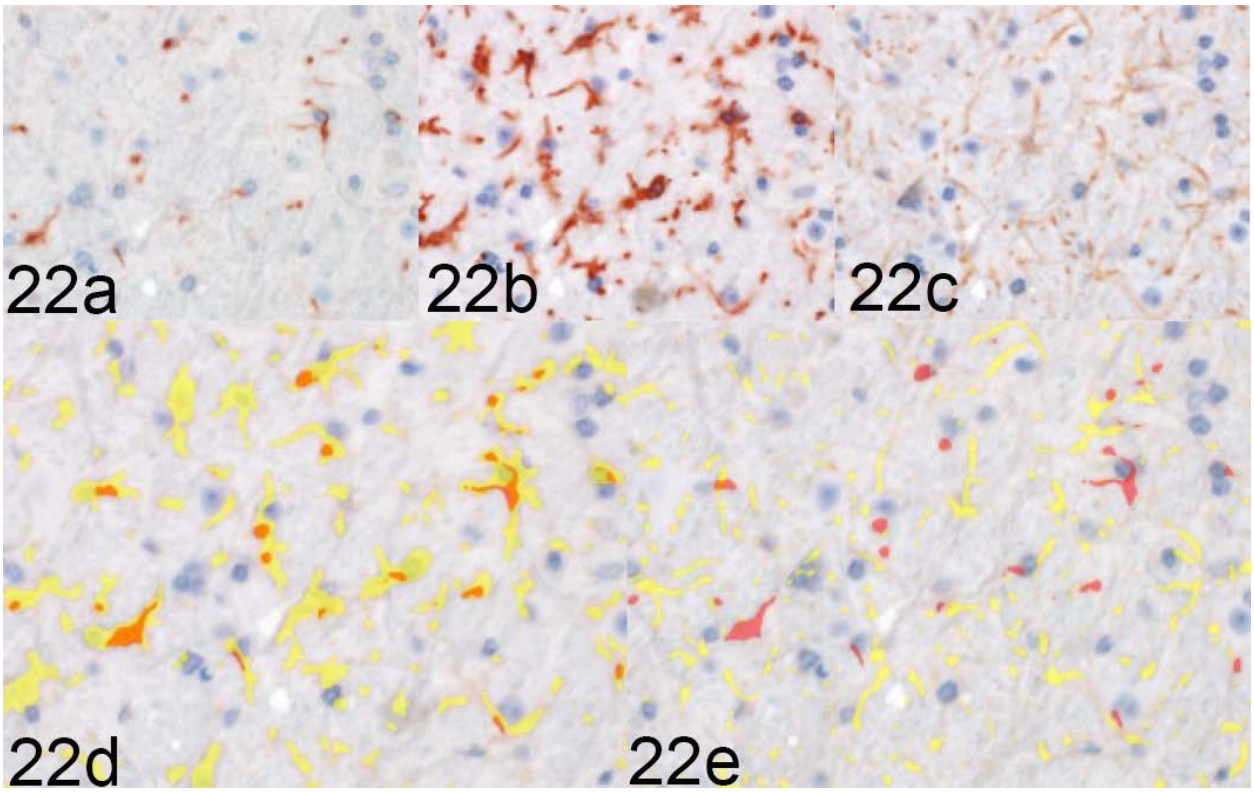

Figure 22. iNOS colocalization with Iba1 and GFAP in a clinical RML-infected mouse, MRN, representative image. Sequential immunohistochemical labeling for iNOS (22a), Iba1 (22b), and GFAP (22c) was performed on the same section of brain. iNOS colocalizes with Iba1 (22d), but fails to demonstrate overlap with GFAP expression in this section (22e). Red – iNOS; yellow – Iba1, 22d; GFAP, 22e; orange – colocalization of iNOS and glial labeling. MRN, 400x, immunohistochemistry.

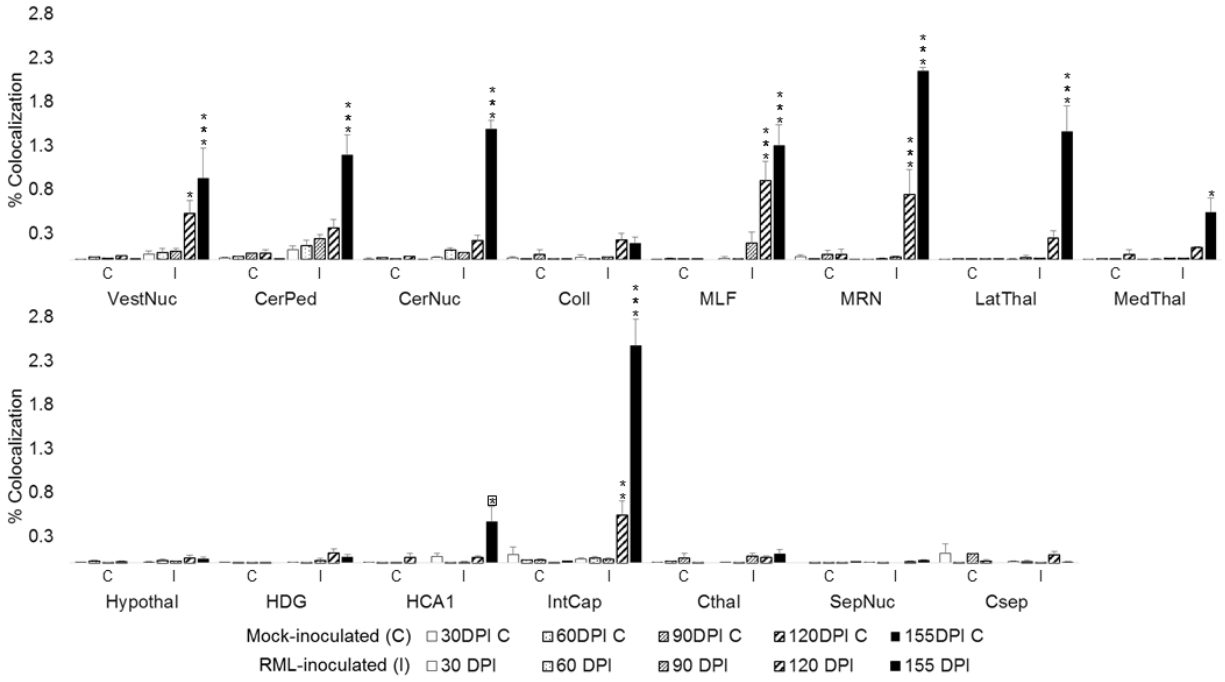

Figure 23. iNOS colocalization with Iba1 in 15 brain regions over RML infection timecourse. Colocalization was quantified in brain regions as % tissue positive for both iNOS and Iba1 immunoreactivity in composite images. Bars represent mean±SE values for mock-inoculated (C) and RML-inoculated (I) animal cohorts at each sacrifice timepoint. *$p < 0.05$, **$p < 0.01$, ***$p < 0.001$; significant differences compared with control (mock-inoculated) animals. * $p<.05$, significant difference compared to 30 DPI RML-infected animals. Vestibular nuclei (VestNuc), cerebellar peduncles (CerPed), cerebellar nuclei (CerNuc), superior colliculus (Coll), medial longitudinal fasciculus (MLF), midbrain reticular nucleus (MRN), lateral thalamus (LatThal), medial thalamus (MedThal), hypothalamus (Hypothal), dentate gyrus of hippocampus (HDG), CA1 of hippocampus (HCA1), internal capsule (IntCap), cerebral cortex at level of thalamus (Cthal), septal nuclei (SepNuc), cerebral cortex at level of septal nuclei (Csep).

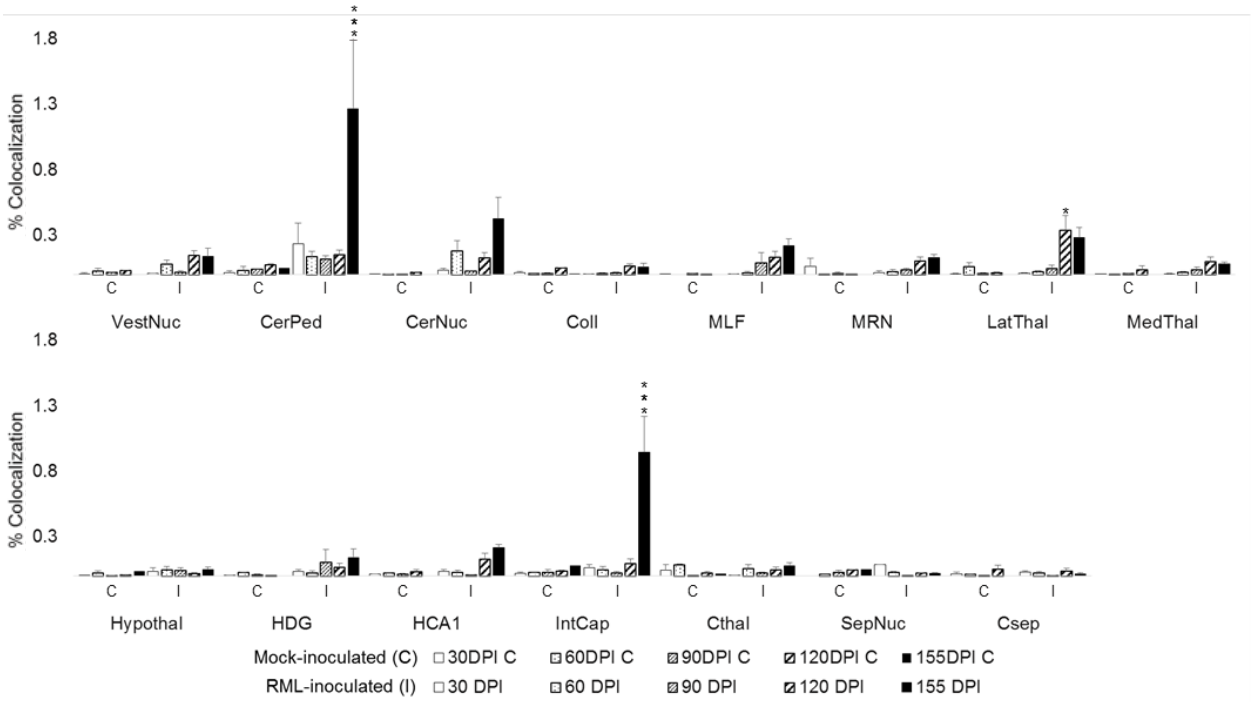

Figure 24. iNOS colocalization with GFAP in 15 brain regions over RML infection timecourse. Colocalization was quantified in brain regions as % tissue positive for both iNOS and GFAP immunoreactivity in composite images. Bars represent mean±SE values for mock-inoculated (C) and RML-inoculated (I) animal cohorts at each sacrifice timepoint. *$p < 0.05$, **$p < 0.01$, ***$p < 0.001$; significant differences compared with control (mock-inoculated) animals. Vestibular nuclei (VestNuc), cerebellar peduncles (CerPed), cerebellar nuclei (CerNuc), superior colliculus (Coll), medial longitudinal fasciculus (MLF), midbrain reticular nucleus (MRN), lateral thalamus (LatThal), medial thalamus (MedThal), hypothalamus (Hypothal), dentate gyrus of hippocampus (HDG), CA1 of hippocampus (HCA1), internal capsule (IntCap), cerebral cortex at level of thalamus (Cthal), septal nuclei (SepNuc), cerebral cortex at level of septal nuclei (Csep).

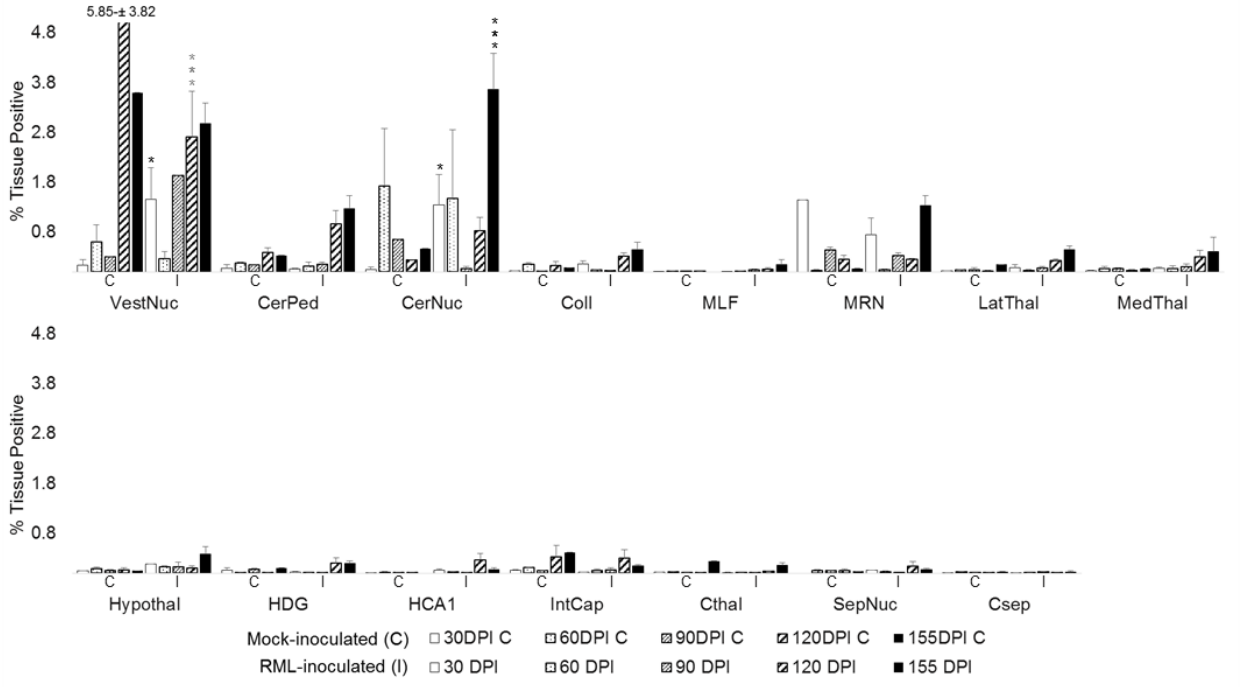

Figure 25. Total Arg1 immunoreactivity in 15 brain regions over RML infection timecourse. Bars represent mean±SE values for control (C) and RML-inoculated (I) animal cohorts at each sacrifice timepoint. *$p < 0.05$, **$p < 0.01$, ***$p < 0.001$; grey ***p<.001 represents negative difference between C and I means due to outlier in control brains. Significant differences compared with control animals. Vestibular nuclei (VestNuc), cerebellar peduncles (CerPed), cerebellar nuclei (CerNuc), superior colliculus (Coll), medial longitudinal fasciculus (MLF), midbrain reticular nucleus (MRN), lateral thalamus (LatThal), medial thalamus (MedThal), hypothalamus (Hypothal), dentate gyrus of hippocampus (HDG), CA1 of hippocampus (HCA1), internal capsule (IntCap), cerebral cortex at level of thalamus (Cthal), septal nuclei (SepNuc), cerebral cortex at level of septal nuclei (Csep).

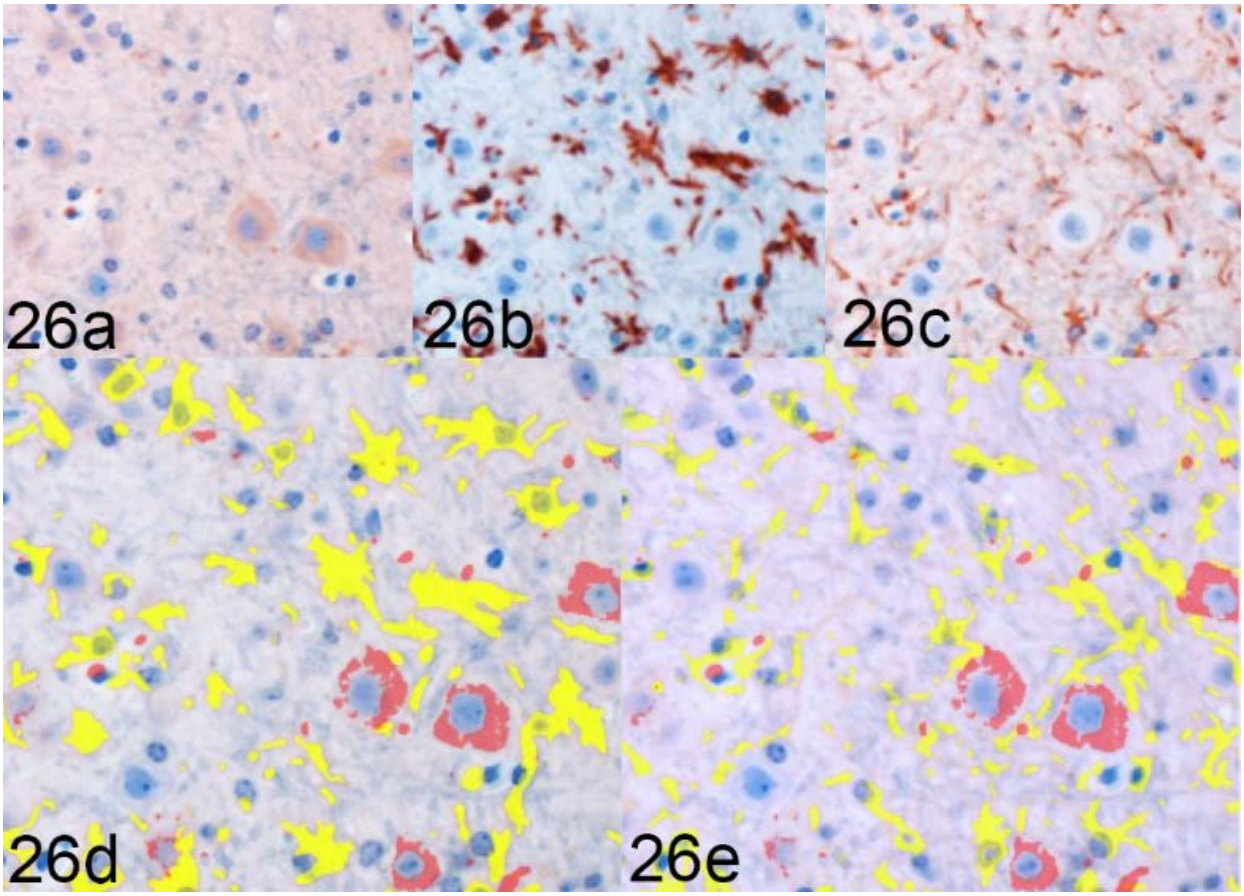

Figure 26. Arg1 colocalization with Iba1 and GFAP in the vestibular nucleus from a clinical RML-infected mouse, representative image. Sequential immunohistochemical labeling for Arg1 (26a), Iba1 (26b), and GFAP (26c) was performed on the same section of RML-infected murine brain. Arg1 is largely expressed in neuronal cytoplasm, and fails to demonstrate significant overlap with either Iba1 (26d) or GFAP (26e) labeling in this section. Red – Arg1 labeling. Yellow – glial cytoplasmic protein labeling (Iba1, 26d; GFAP, 26e). Orange – colocalization of Arg1 and glial labeling. Vestibular nucleus, 400x, immunohistochemisty.

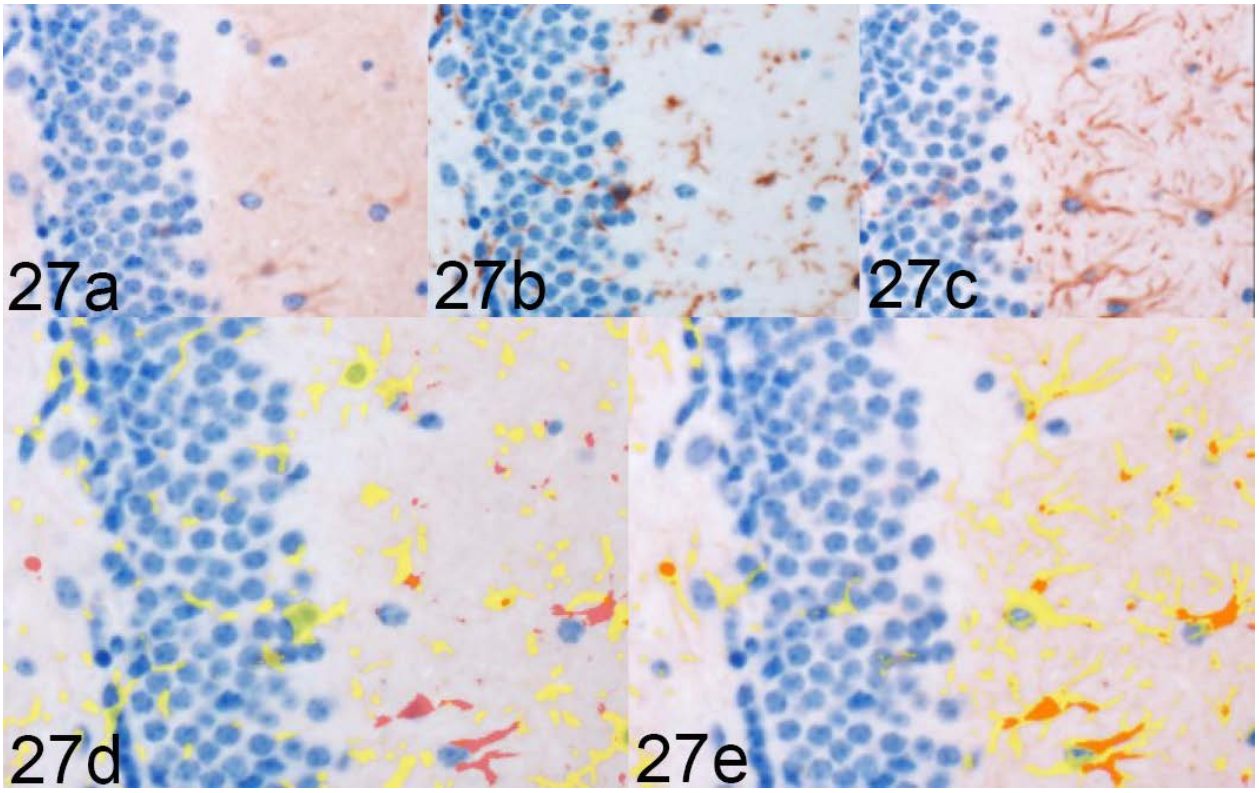

Figure 27. Arg1 colocalization with Iba1 and GFAP in a single hippocampal section from a 120DPI RML-infected mouse, representative image. Sequential immunohistochemical labeling for Arg1 (27a), Iba1 (27b), and GFAP (27c) was performed on the same section of RML-infected murine brain. Here, Arg1 fails to demonstrate overlap with Iba1 labeling (27d), but displays colocalization with GFAP expression (27e). Red – Arg1 labeling. Yellow – glial cytoplasmic protein labeling (Iba1, 27d; GFAP, 27e). Orange – colocalization of Arg1 and glial labeling (here, only in 27e). CA1 of hippocampus, 400x, mmunohistochemistry.

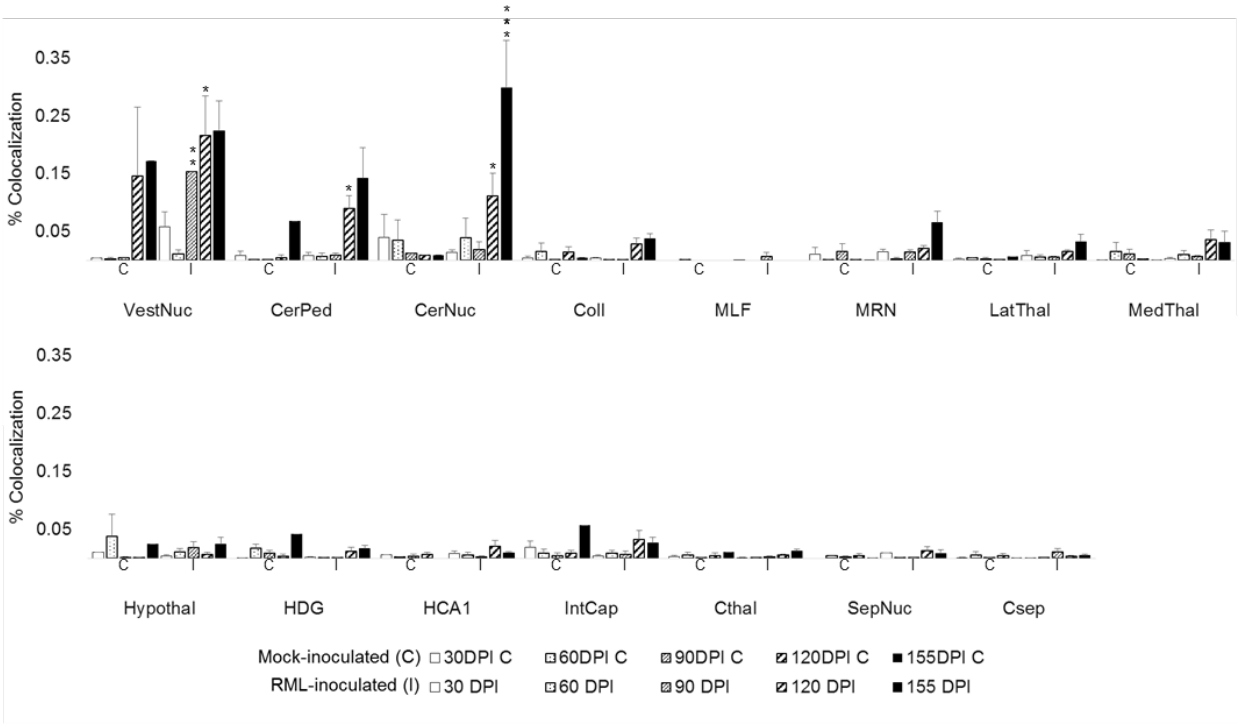

Figure 28. Arg1 colocalization with Iba1 in 15 brain regions over RML infection timecourse. Colocalization was quantified in brain regions as % tissue positive for both Arg1 and Iba1 immunoreactivity in composite images. Bars represent mean±SE values for control (C) and RML-inoculated (I) animal cohorts at each sacrifice timepoint. *$p < 0.05$, **$p < 0.01$, ***$p < 0.001$; significant differences compared with control animals. Vestibular nuclei (VestNuc), cerebellar peduncles (CerPed), cerebellar nuclei (CerNuc), superior colliculus (Coll), medial longitudinal fasciculus (MLF), midbrain reticular nucleus (MRN), lateral thalamus (LatThal), medial thalamus (MedThal), hypothalamus (Hypothal), dentate gyrus of hippocampus (HDG), CA1 of hippocampus (HCA1), internal capsule (IntCap), cerebral cortex at level of thalamus (Cthal), septal nuclei (SepNuc), cerebral cortex at level of septal nuclei (Csep).

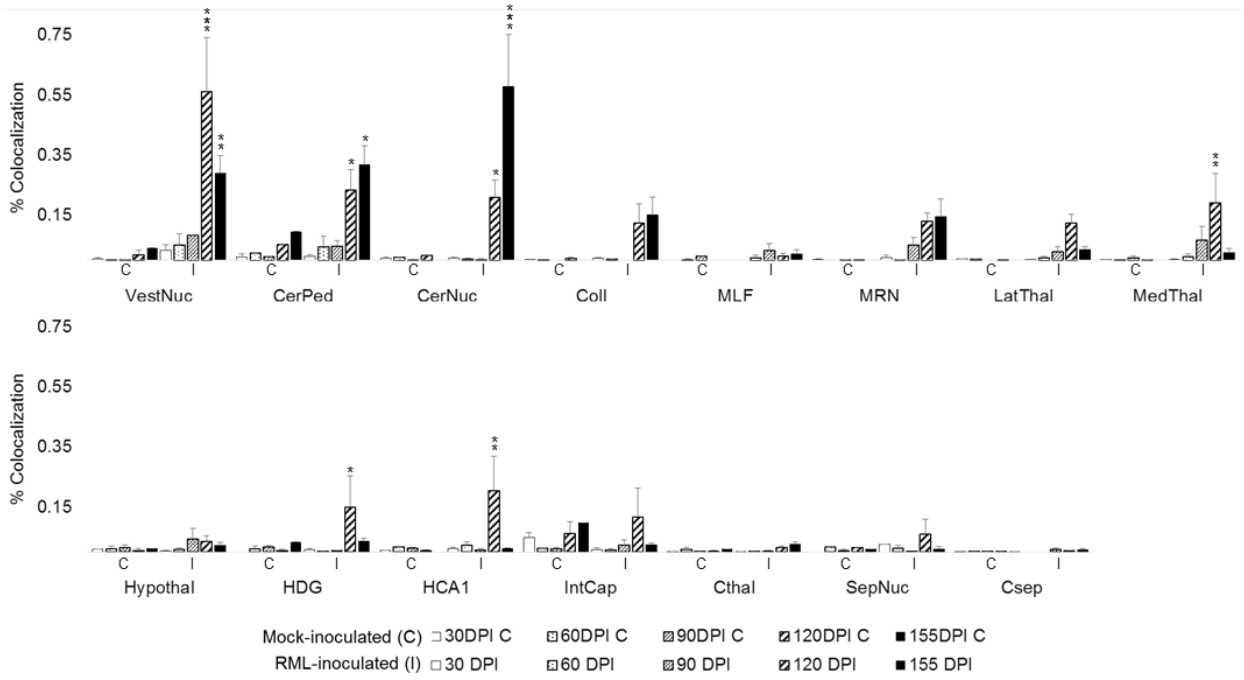

Figure 29. Arg1 colocalization with GFAP in 15 brain regions over RML infection timecourse. Colocalization was quantified in brain regions as % tissue positive for both Arg1 and GFAP immunoreactivity in composite images. Bars represent mean±SE values for control (C) and RML-inoculated (I) animal cohorts at each sacrifice timepoint. *$p < 0.05$, **$p < 0.01$, ***$p < 0.001$; significant differences compared with control animals. Vestibular nuclei (VestNuc), cerebellar peduncles (CerPed), cerebellar nuclei (CerNuc), superior colliculus (Coll), medial longitudinal fasciculus (MLF), midbrain reticular nucleus (MRN), lateral thalamus (LatThal), medial thalamus (MedThal), hypothalamus (Hypothal), dentate gyrus of hippocampus (HDG), CA1 of hippocampus (HCA1), internal capsule (IntCap), cerebral cortex at level of thalamus (Cthal), septal nuclei (SepNuc), cerebral cortex at level of septal nuclei (Csep).

CHAPTER 3. TEMPOROSPATIAL DISTRIBUTION OF PSMB10 EXPRESSION IN PRION INFECTION

A manuscript to be submitted to *BMC Veterinary Research*

Alyona V. Michael[1], Justin J. Greenlee[2], Min Zhang[3], M. Heather West Greenlee[4], Jodi D. Smith[1]

Author affiliations
[1] Department of Veterinary Pathology, College of Veterinary Medicine, Iowa State University, Ames, IA
[2] Virus and Prion Research Unit, National Animal Disease Center, Agricultural Research Service, US Department of Agriculture, Ames, IA
[3] Department of Statistics, College of Liberal Arts and Sciences, Iowa State University, Ames, IA
[4] Department of Biomedical Sciences, College of Veterinary Medicine, Iowa State University, Ames, IA

Abstract

The accumulation of misfolded prion particles in transmissible spongiform encephalopathies (TSEs) stimulates a neuroinflammatory response characterized by activation and proliferation of astrocytes and microglia. Misfolded proteins in the healthy cell are degraded, in part, by the 26S ubiquitin proteasome system, whose dysfunction has been documented in prion infection. As part of the neuroinflammatory response, human neurodegenerative "prionopathies", such as Alzheimer's disease, additionally upregulate the expression of inducible proteasome subunits, called immunoproteasomes. The effect of immunoproteasome induction on the pathology of protein misfolding diseases is uncertain, and mixed clinical outcomes are associated with their inhibition. This study used in-situ hybridization to characterize expression of PSMB10, an immunoproteasome subunit, over a timecourse of a murine model of scrapie infection, and correlate any changes to markers of prion-associated neuropathology, including spongiform change, PrP^{sc} deposition, Iba1, GFAP, iNOS, and Arg1. We successfully demonstrated PSMB10

expression in 16 brain regions, however no significant temporal upregulation of PSMB10 transcription was observed, and there was no correlation to prion neuropathology.

Introduction

Transmissible spongiform encephalopathies are mediated by the toxic aggregation of misfolded analogs of cellular prion protein, PrP^{c}. PrP^{c} is composed of a 208 amino acid chain that, after maturation in the golgi, is trafficked to the plasma membrane, where it becomes associated with the outer leaflet of lipid rafts (Castle et al., 2017). While defunct PrP^{c} undergoes recycling via constitutive endocytosis (Campana et al., 2005), dysmature PrP^{c} can be redirected into the cytosol, where it undergoes degradation by the 26S proteasome (Ma et al., 2001). Inhibition of cellular proteolysis can not only accelerate aggregation of misfolded PrP conformers (PrP^{sc}), but can furthermore trigger the cell's endoplasmic reticulum stress response (Orsi et al., 2006). This mechanism further promotes both misfolding (Orsi et al., 2006) and neuronal apoptosis (Kristiansen et al., 2005). Moreover, misfolded oligomers of PrP^{sc}, have been shown to inhibit the 26S proteasome directly, potentially by stabilizing the proteolytic barrel in the closed position (Kristiansen et al., 2007).

Antigen-presenting and non-immune cells under stress can substitute an inducible subset of proteasomal subunits, β1i (LMP2, PSMB9), β2i (MECL1, PSMB10), β5i (LMP7, PSMB8), in place of constitutive 26S proteasomal subunits β1, β2 and β3, respectively. The resulting immunoproteasome is capable of higher rates of proteolysis and displays an altered cleavage pattern that favors degradation of oxidized proteins and MHC class I presentation (Ferrington et al., 2012; Seifert et al., 2010). Immunoproteasomes are expressed at low levels in healthy brains

(Stohwasser et al., 1997), and can be upregulated in microglia in response to IFNγ stimulation (Stohwasser et al., 2000).

Immunoproteasome induction has been demonstrated in neurodegenerative diseases, such as Alzheimer's(AD), Huntington's (HD) and amyotrophic lateral sclerosis (ALS) (Gavilan et al., 2009; Orre et al., 2013; Cheroni et al., 2009; Mishto et al., 2006; Diaz-Hernandez et al., 2003). Like prion diseases, these entities share a common element of toxic accumulation of self-propagating misfolded proteinaceous particles. Investigations into the role of immunoproteasomal induction in sterile neuroinflammatory disorders has yielded mixed, entity-specific results, with evidence for both protection and exacerbation of pathology (Orre et al., 2013; Wagner et al., 2017; X. Chen et al., 2015; Moritz et al., 2017; Ahtoniemi et al., 2007).

Prion infection is known to stimulate a neuroinflammatory response, characterized by microglial and astrocytic hypertrophy and proliferation. Recent transcriptomic studies suggest that prion infections are associated with a proinflammatory cytokine milieu (Vincenti et al., 2015; Carroll et al., 2016; Tribouillard-Tanvier et al., 2009; Newsom et al., 2011; Moody et al., 2011; Song et al., 2012). Despite the inflammatory nature of prion disease and evidence of expression in analogous neurodegenerative entities, investigations into prion-mediated immunoproteasomal induction are limited in the literature. A single report by Amici et al. failed to demonstrate increased immunoproteasomal subunit expression in brainstem homogenates of scrapie-infected sheep (Amici et al., 2010). Spatiotemporal analyses of immunoproteasomal expression in prion disease have not been represented in the literature.

In the current study, we used quantitative in situ hybridization to determine the temporospatial distribution of immunoproteasome subunit PSMB10 (MECL1, β2i) mRNA expression over the course of prion disease using a murine intracranial RML scrapie infection

model. We also correlated PSMB10 expression to glial activation, PrPsc deposition and vacuolation data generated from a parallel timecourse study. We found that, while PSMB10 transcripts are present in healthy and diseased brain, there were no significant trends in expression over time and no correlation to of PSMB10 to RML scrapie neuropathology in this model.

Materials and Methods

Animals and tissue preparation

This study used archived tissue blocks of murine brain from the previous study (Chapter 2). Briefly, C57BL/6 mice, aged 6 to 8 weeks, were inoculated intracranially into the right cerebral hemisphere with 20 μL of 10% w/v brain homogenate in PBS pooled from C57BL/6 mice terminally ill with the mouse-adapted Rocky Mountain Laboratories (RML) strain of the scrapie agent. Groups of four mice were euthanized at predetermined time points of 30, 60, 90 and 120 days post inoculation (DPI), along with a group of animals that were allowed to survive until clinical signs necessitated euthanasia at 155 DPI. Age-matched C57BL/6 negative control mice inoculated with 10% w/v normal C57BL/6 brain homogenate in PBS were also included at each time point. Brains were collected into 10% neutral buffered formalin. After 24 hours of fixation, brains were transversely sectioned at four levels: mid-cerebellum, rostral colliculus, thalamus and hypothalamus, and rostral cerebrum at level of septal nuclei. Tissues were processed by routine histologic methods, embedded in paraffin, sectioned at 5 μm, and mounted on glass slides for in-situ hybridization. For this study, we analyzed a subset of n=3 infected and n=1 control brains from animals sacrificed at 30, 60, 120, and 155DPI in the archived timecourse.

RNAscope in-situ hybridization

RNAscope® (ACDbio), a proprietary in-situ hybridization platform, was used to visualize transcribed immunoproteasomal mRNA. We obtained a custom probe from ACDbio specific to the murine transcript of immunoproteasomal subunit PSMB10 (Cat#452541, NCBI Reference Sequence NM_013640.3, target region 120-1226). This probe was applied to deparaffinized tissue sections following the manufacturer's protocol for the RNAscope® 2.5 HD Assay (RED) kit. Briefly, slides were baked for 1hr at 60C and deparaffinized through a xylene/alcohol series. Tissues were incubated with hydrogen peroxide for 10 minutes, washed and boiled in RNAscope® target retrieval solution for 15 minutes. A protease solution was applied to tissues and incubated for 30min at 40C in the HybEz™ oven. After washing in distilled water, tissues were incubated with the hybridization probe for 2 hours at 40C. After removing unbound probe with RNAscope® wash buffer, signal was enhanced through a series of incubations with 6 amplification probes with intervening washes. Incubation times and temperatures followed the manufacturer's protocol, with exception of Amp 5, which was extended to 60 minutes. Signal detection solution was applied to tissues for 10 minutes at room temperature. After washing slides in distilled water, tissues were redirected into an immunohistochemistry procedure to label Iba1.

Immunohistochemistry

Washed slides from the completed RNAscope® protocol were blocked with 5% BSA for 60 minutes, and incubated with rabbit anti-Iba1 antibody at a 1:250 dilution (019-19741, Wako) for 24 hours at 4C. After washing with TBST, slides were incubated with goat-anti-rabbit IgG secondary HRP-conjugated polymer (ab2891, Abcam) for 30 minutes at room temperature, washed and developed with Vector Nova Red HRP substrate (SK-4800, Vector Laboratories), per

kit instructions. Slides were then counterstained with 50% Gill's #2 hematoxylin and dried in a 60C oven prior to coverslipping with Ecomount permanent mounting medium (EM897L, Biocare).

Image Analysis

The chromogenic probe in the RNAscope® 2.5HD Red kit can be visualized both in brightfield and under fluorescent excitation, a property that was exploited to enhance signal recognition in brightfield images. Immunohistochemical labeling was captured using an Olympus DP73 camera mounted on an Olympus BX53 fluorescence microscope, operated with cellSens imaging software (Olympus, USA). 2400x1800 brightfield images were generated at 400x for all brain regions, except medial thalamus (20x). ISH signal was captured at the same location as the brightfield image by switching to fluorescence excitation with an X-Cite 120LED illuminator (Lumen Dynamics Group) at a wavelength of 550nm (red fluorescent protein filter). Select brightfield and fluorescent image pairs were superimposed in cellSens by using the Image>Combine Channels command. Captured fluorescence images were processed using the Area Quantification module v1.0 FL within the HALO image analysis platform (v2.0.1145.19, Indica Labs). Briefly, the red probe signal was selected as Dye 1. A base threshold intensity value was assigned to image sets and manually adjusted, as needed, for images with higher autofluorescence to accurately reflect probe distribution in the regions of interest. Total probe signal was quantified in each region of interest as % Dye 1 Positive Tissue.

Statistical analysis

Data were analyzed using a generalized linear model to detect significant differences in quantified PSMB10 probe signal between mock-inoculated and RML-infected animal groups.

DPI, brain location and treatment condition were included as fixed effects in the model. Simple effect comparisons between the least squares (LS) means of mock-inoculated and infected animal groups were conducted at each DPI for each brain region to determine the degree of significance. Pearson correlation analysis was used to evaluate temporal associations between PSMB10 and previously presented immunoreactivity data for PrP^{sc}, Iba1, GFAP, iNOS and Arg1. Results were considered statistically significant if $p<0.05$. The software for conducting statistical analysis was SAS version 9.4.

No statistical significance was calculated for temporal trends in control animals due to inclusion of a single mock-inoculated animal per collection timepoint. Evaluation of relative total PSMB10 expression between brain regions, probe distribution and cellular colocalization were based on qualitative visual assessment of trends in data and images

Results

PSMB10 transcript distribution

The ISH signal was interpreted in both brightfield and fluorescence images as 1 transcript per punctate fluorescent dot (Figure 1). PSMB10 expression was quantified as % area positive for probe (Figure 2). Signal puncta appeared reasonably evenly distributed through the brain regions on visual evaluation of acquired images, with exception of increased probe density in the granular layer of the dentate gyrus, pyramidal layer of CA1, and Purkinje layer of the cerebellum (Figure 1). PSMB10 transcript levels were overall lower in white matter of cerebellar peduncles and the internal capsule, and were present at the highest level in the vestibular nuclei.

PSMB10 probe expression over time

There was a temporal upregulation of PSMB10 expression in control animals, with age-associated increases in the vestibular nuclei, cerebellar nuclei, colliculus and cortex at the level of the thalamus (Figure 2). Because control groups only featured an n=1 for each location:timepoint combination, statistical significance could not be calculated through-pair-wise comparison of means. PSMB10 expression in RML-infected mice did not change significantly over time compared to mock-inoculated controls. Similarly, pair-wise comparisons of 60, 120 and 155 DPI animals to the 30 DPI infected group did not yield significant increases in PSBM10 expression.

Pearson's correlation coefficients were calculated to evaluate any temporal association between PSMB10 expression in control and infected animals over time (Table 1). A strong positive linear relationship was only observed in the colliculus, indicating that the temporal increase in controls was likely reproduced in the infected animals only at this location.

PSMB10 expression and microglia

Microglial expression of PSMB10 was evaluated at 30 and 150DPI by dual microglial Iba1 IHC and PSMB10 ISH. PSMB10 does not exclusively colocalize with microglia (Figure 4). Although sporadic signal puncta overlie microglial processes (Fig. 4, insets), the vast majority of transcripts are found in unlabeled neuropil or in neuronal cytoplasm. This distribution does not subjectively appear significantly different between early and late infection timepoints.

Correlation analysis between PSMB10 expression and markers of prion neuropathology.

Prion disease is associated with spongiform change, deposition of PrP^{sc}, microgliosis and astrocytosis. These changes were recapitulated in a parallel infection timecourse using archived

tissues from this model. Additionally, we have previously demonstrated induction of the glial polarization markers iNOS and Arg1 late in disease incubation. Pearson's correlation coefficients were calculated to evaluate association between PSMB10 expression and data documenting temporal trends in PrP^{sc}, Iba1, GFAP, iNOS and Arg1 immunoreactivity over the infection timecourse at each of the 16 brain regions. Stain pairs with $r>.8$ were considered to have a strong positive linear relationship. Only pairs with a strong positive relationship were found to have a $p<0.5$.

Overall, due to lack of temporal changes in expression, PSMB10 exhibited minimal correlation to any markers of neuropathology. No statistically significant associations were present between PSMB10, spongiform change, and gliosis. Strong positive relationships were observed between PSMB10 and PrP^{sc} and the internal capsule ($p<.05$) and septal nuclei ($p<.001$). PSMB10 and iNOS had positive relationships at the same locations ($p<.05$). A statistically significant relationship between iNOS and Arg1 was only present in the colliculus ($p<.01$). These few correlations are not compelling in impact, as the modest temporal trends for the two diencephalic structures did not achieve statistical significance on pairwise comparisons and the septal correlation was the consequence of a relative flat-line in values over time for all 3 stains.

Discussion

This timecourse attempted to characterize temporospatial changes in the expression of PSMB10, an immunoproteasome subunit, over the course of prion infection. We successfully demonstrated expression of immunoproteasome subunit PSMB10 transcripts in all 16 brain regions over time in healthy C57Bl/6 control mice, but did not detect temporal trends suggestive of upregulation in infected animals.

Immunoproteasomes are present at low levels in healthy human and murine neural tissues (Stohwasser et al., 1997; Boegel et al., 2018), and expression is upregulated in ageing and inflamed brains (Mishto et al., 2006). Cellular colocalization varies by stimulus. Mice infected with lymphocytic choriomeningitis virus, an established model of sterile neuroinflammation (Kang et al., 2008), demonstrate increased expression of PSMB10 and LMP2 in microglial processes and astrocytic nuclei (Kremer et al., 2010). Little to no immunoproteasomal induction was observed in neurons or astrocytic cytoplasm in this infection model (Kremer et al., 2010). Upregulation of LMP2 and LMP7 has been demonstrated in neurons, astrocytes and plaque-associated amoeboid microglia in Alzheimer's disease (Mishto et al., 2006; Orre et al., 2013), and neurons of Huntington's disease (Diaz-Hernandez et al., 2003). Increased immunoproteasome expression has been reported in reactive glia in ALS (Puttaparthi et al., 2005; Ahtoniemi et al., 2007; Cheroni et al., 2009), and was recently documented in neurons, astrocytes and microglia of a PD model (Ugras et al., 2018). Thus, immunosubunit upregulation has been documented in multiple neurodegenerative protein misfolding disorders.

In this timecourse, PSMB10 transcription was documented in all 16 analyzed brain regions of both control and infected animals. White matter tracts of the cerebellar peduncles and the internal capsule had the lowest level of quantified PSMB10 signal. The highest signal density relative to other brain regions was observed in the vestibular nuclei. Signal puncta were associated with Iba1-positive microglial processes, neuronal cytoplasm and unlabeled neuropil throughout the brain in both 30 and 150DPI animals, and no overt differences in cell association were observed between early and late disease. There were increased numbers of signal puncta in areas of high neuronal density, such as the granular layer of the dentate gyrus, pyramidal layer of CA1, and

Purkinje layer of the cerebellum. However, these locations were not overall associated with increased PSMB10 expression relative to other brain regions.

Immunoproteasome subunit incorporation is stimulated by inflammatory cytokines including TFNα and IFNγ (Ferrington et al., 2012), and upregulation in response to NO has been demonstrated in vascular endothelium (Kotamraju et al., 2006). Both TNFα (Vincenti et al., 2015; Carroll et al., 2016) and IFNγ (Tribouillard-Tanvier et al., 2009; Newsom et al., 2011) secretion has been demonstrated in response to prion infection in the brain, and we have previously documented increased iNOS expression in the late stages of scrapie incubation in this model. Thus, upregulation of PSMB10 was anticipated in our model. However, quantification of PSMB10 expression over time across all brain regions failed to demonstrate temporal upregulation of this subunit in infected animals. Additionally there was no visually apparent increase in colocalization of PSMB10 with Iba1-positive microglia over time, and no significant temporal correlation with data quantifying Iba1, GFAP, iNOS or Arg1 immunoreactivity in a parallel timecourse of this infection model. These results suggest that microglia do not upregulate PSMB10 transcription in response to prion infection. Although unexpected, our findings corroborate Amici et al's 2010 report describing an absence of increased immunoproteasome subunit induction in the brainstem of scrapie-infected sheep.

Immunoproteasome expression is reported to increase in the ageing brain (Mishto et al., 2006; Gavilan et al., 2009). In mice, upregulation of immunosubunits was reported at 15-18 months of age, compared to animals aged 3-6 months (Orre et al., 2013). Although our animals did not exceed ~211 days of age (7.5 months) at the final timepoint, we observed apparent temporal increases in PSMB10 expression in control animals in several locations including the vestibular nuclei, cerebellar nuclei, colliculus, and cortex at the level of the thalamus. If there was truly no

effect of prion infection on immunoproteasome expression in infected brains, we would anticipate a similar temporal trend at these locations and a strong positive linear relationship between mock and RML-inoculated animals. Interestingly, correlation analysis between temporal expression in control and infected brains at each of these location revealed a strong positive relationship only in the colliculus ($p<.05$). No complementary ageing trends were observed at the other 3 locations exhibiting significant temporal upregulation in control mice. Combined, these findings suggest that normal age-associated upregulation of PSMB10 expression in some areas of the brain may be disrupted in infected animals, however higher numbers of control replicates would be necessary to substantiate this claim.

Thus, no strong evidence of prion-associated temporal PSBM10 transcriptional upregulation was demonstrated in our infection model. Several explanations for these findings were considered, including shifts in microglial immunophenotypes over time, asymmetric subunit incorporation, and the limitation of transcript quantification as a measurement of subunit induction.

Unlike proinflammatory M1 macrophages, M2, or “alternatively activated”, monocytes do not appear to upregulate immunoproteasome subunit mRNA transcription in response to experimental polarization (S. Chen et al., 2016). M2 microglia have been reported to cluster around amyloid plaques in Alzheimer’s disease (Jimenez et al., 2008), thus we questioned whether a potential shift in microglial immunophenotype could be responsible for the lack of PSMB10 upregulation. However, previous work by our laboratory did not detect a significant Arg1-positive microglial population indicative of M2 phenotype predominance, thus alternative polarization does not account for the lack of PSMB10 induction in this model.

Synthesis of mixed proteasomes containing both constituent and inducible subunits is possible (Kaur et al., 2016). Studies of immunoproteasome expression in neurodegenerative disease frequently report increases in LMP2 (PSMB8) and LMP7 (PSMB9) (Cheroni et al., 2009; Diaz-Hernandez et al., 2003; Puttaparthi et al., 2005), but MECL1 (PSMB10) upregulation is inconsistent (Diaz-Hernandez et al., 2003; Cheroni et al., 2009; Orre et al., 2013). Our preliminary studies demonstrated relatively more PSMB10 expression in control brains, leading to the selection of this probe for evaluation in infected tissues. PSMB8 and PSMB9 quantification may have yielded different expression patterns and should be explored in the future.

Finally, it is important to consider the limitations of evaluating only transcriptional fluctuations as a measure of protein upregulation. Transcript levels are estimated to predict only approximately 40% of the change in cellular protein levels, with the rest likely accounted for by post-transcriptional regulatory mechanisms (Vogel et al.). This discrepancy has been demonstrated in studies of immunoproteasome expression. Chen et al. noted that macrophages polarized towards an M2 phenotype in-vitro show an upregulation of LMP2 and LMP7 protein levels by Western blot analysis, with no corresponding changes in mRNA transcript levels (S. Chen et al., 2016). Similarly, Orre et al. found no difference in murine PSMB10 (MECL-1) plaque-adjacent transcript levels in a model of AD, but demonstrated an increase in immunoreactivity against the translated protein in the same regions (Orre et al., 2013). Additionally, proteolytic activity of all three subunits was increased in diseased areas of both murine and human brain samples (Orre et al., 2013). Thus, post-translational regulation of protein expression has been documented both in experimental monocyte polarization and in vivo. We were unable to achieve satisfactory immunoreactivity against subunits when conducting preliminary IHC experiments, thus ISH was selected as the best method for in-situ evaluation of

subunit expression. However, our lack of transcriptional PSMB10 induction may not reflect subunit protein levels or activity.

In summary, while we did not observe temporal upregulation of PSMB10 mRNA in evaluated regions of infected brains, we successfully demonstrated relative expression across 16 brain regions and provided evidence for potential disruption of age-related immunoproteasomal upregulation. The results of this study highlight the need for protein-level and, potentially, functional analysis of immunoproteasome expression in prion disease. Thus, we believe that future investigation into immunoproteasome involvement in prion infection would benefit from in-situ evaluation of protein expression for all three subunits with correlation to local cytokine milieus and cellular colocalization of target expression.

References

Ahtoniemi, T., Goldsteins, G., Keksa-Goldsteine, V., Malm, T., Kanninen, K., Salminen, A., & Koistinaho, J. (2007). Pyrrolidine dithiocarbamate inhibits induction of immunoproteasome and decreases survival in a rat model of amyotrophic lateral sclerosis. *Mol Pharmacol, 71*(1), 30-37. doi:10.1124/mol.106.028415

Amici, M., Cecarini, V., Cuccioloni, M., Angeletti, M., Barocci, S., Rossi, G., . . . Eleuteri, A. M. (2010). Interplay between 20S proteasomes and prion proteins in scrapie disease. *J Neurosci Res, 88*(1), 191-201. doi:10.1002/jnr.22186

Boegel, S., Löwer, M., Bukur, T., Sorn, P., Castle, J. C., & Sahin, U. (2018). HLA and proteasome expression body map. *BMC Med Genomics, 11*. doi:10.1186/s12920-018-0354-x

Campana, V., Sarnataro, D., & Zurzolo, C. (2005). The highways and byways of prion protein trafficking. *Trends Cell Biol, 15*(2), 102-111. doi:10.1016/j.tcb.2004.12.002

Carroll, J. A., Striebel, J. F., Rangel, A., Woods, T., Phillips, K., Peterson, K. E., . . . Chesebro, B. (2016). Prion Strain Differences in Accumulation of PrPSc on Neurons and Glia Are Associated with Similar Expression Profiles of Neuroinflammatory Genes: Comparison of Three Prion Strains. *PLoS Pathog, 12*(4), e1005551. doi:10.1371/journal.ppat.1005551

Castle, A. R., & Gill, A. C. (2017). Physiological Functions of the Cellular Prion Protein. *Front Mol Biosci, 4*, 19. doi:10.3389/fmolb.2017.00019

Chen, S., Kammerl, I. E., Vosyka, O., Baumann, T., Yu, Y., Wu, Y., . . . Stoeger, T. (2016). Immunoproteasome dysfunction augments alternative polarization of alveolar macrophages. *Cell Death Differ, 23*(6), 1026-1037. doi:10.1038/cdd.2016.3

Chen, X., Zhang, X., Wang, Y., Lei, H., Su, H., Zeng, J., . . . Huang, R. (2015). Inhibition of immunoproteasome reduces infarction volume and attenuates inflammatory reaction in a rat model of ischemic stroke. *Cell Death Dis, 6*, e1626. doi:10.1038/cddis.2014.586

Cheroni, C., Marino, M., Tortarolo, M., Veglianese, P., De Biasi, S., Fontana, E., . . . Bendotti, C. (2009). Functional alterations of the ubiquitin-proteasome system in motor neurons of a mouse model of familial amyotrophic lateral sclerosis. *Hum Mol Genet, 18*(1), 82-96. doi:10.1093/hmg/ddn319

Diaz-Hernandez, M., Hernandez, F., Martin-Aparicio, E., Gomez-Ramos, P., Moran, M. A., Castano, J. G., . . . Lucas, J. J. (2003). Neuronal induction of the immunoproteasome in Huntington's disease. *J Neurosci, 23*(37), 11653-11661.

Ferrington, D. A., & Gregerson, D. S. (2012). Immunoproteasomes: Structure, Function, and Antigen Presentation. *Prog Mol Biol Transl Sci, 109*, 75-112. doi:10.1016/b978-0-12-397863-9.00003-1

Gavilan, M. P., Castano, A., Torres, M., Portavella, M., Caballero, C., Jimenez, S., . . . Ruano, D. (2009). Age-related increase in the immunoproteasome content in rat hippocampus: molecular and functional aspects. *J Neurochem, 108*(1), 260-272. doi:10.1111/j.1471-4159.2008.05762.x

Jimenez, S., Baglietto-Vargas, D., Caballero, C., Moreno-Gonzalez, I., Torres, M., Sanchez-Varo, R., . . . Vitorica, J. (2008). Inflammatory response in the hippocampus of PS1M146L/APP751SL mouse model of Alzheimer's disease: age-dependent switch in the microglial phenotype from alternative to classic. *J Neurosci, 28*(45), 11650-11661. doi:10.1523/jneurosci.3024-08.2008

Kang, S. S., & McGavern, D. B. (2008). Lymphocytic choriomeningitis infection of the central nervous system. *Front Biosci, 13*, 4529-4543.

Kaur, G., & Batra, S. (2016). Emerging role of immunoproteasomes in pathophysiology. *Immunol Cell Biol, 94*(9), 812-820. doi:10.1038/icb.2016.50

Kotamraju, S., Matalon, S., Matsunaga, T., Shang, T., Hickman-Davis, J. M., & Kalyanaraman, B. (2006). Upregulation of immunoproteasomes by nitric oxide: potential antioxidative mechanism in endothelial cells. *Free Radic Biol Med, 40*(6), 1034-1044. doi:10.1016/j.freeradbiomed.2005.10.052

Kremer, M., Henn, A., Kolb, C., Basler, M., Moebius, J., Guillaume, B., . . . Groettrup, M. (2010). Reduced immunoproteasome formation and accumulation of immunoproteasomal precursors in the brains of lymphocytic choriomeningitis virus-infected mice. *J Immunol, 185*(9), 5549-5560. doi:10.4049/jimmunol.1001517

Kristiansen, M., Deriziotis, P., Dimcheff, D. E., Jackson, G. S., Ovaa, H., Naumann, H., . . . Tabrizi, S. J. (2007). Disease-associated prion protein oligomers inhibit the 26S proteasome. *Mol Cell, 26*(2), 175-188. doi:10.1016/j.molcel.2007.04.001

Kristiansen, M., Messenger, M. J., Klohn, P. C., Brandner, S., Wadsworth, J. D., Collinge, J., & Tabrizi, S. J. (2005). Disease-related prion protein forms aggresomes in neuronal cells leading to caspase activation and apoptosis. *J Biol Chem, 280*(46), 38851-38861. doi:10.1074/jbc.M506600200

Ma, J., & Lindquist, S. (2001). Wild-type PrP and a mutant associated with prion disease are subject to retrograde transport and proteasome degradation. *Proc Natl Acad Sci U S A, 98*(26), 14955-14960. doi:10.1073/pnas.011578098

Mishto, M., Bellavista, E., Santoro, A., Stolzing, A., Ligorio, C., Nacmias, B., . . . Franceschi, C. (2006). Immunoproteasome and LMP2 polymorphism in aged and Alzheimer's disease brains. *Neurobiol Aging, 27*(1), 54-66. doi:10.1016/j.neurobiolaging.2004.12.004

Moody, L. R., Herbst, A. J., & Aiken, J. M. (2011). Upregulation of interferon-gamma-induced genes during prion infection. *J Toxicol Environ Health A, 74*(2-4), 146-153. doi:10.1080/15287394.2011.529064

Moritz, K. E., McCormack, N. M., Abera, M. B., Viollet, C., Yauger, Y. J., Sukumar, G., . . . Burnett, B. G. (2017). The role of the immunoproteasome in interferon-gamma-mediated microglial activation. *Sci Rep, 7*(1), 9365. doi:10.1038/s41598-017-09715-y

Newsom, D. M., Liggitt, H. D., O'Rourke, K., Zhuang, D., Schneider, D. A., & Harrington, R. D. (2011). Cytokine antibody array analysis in brain and periphery of scrapie-infected Tg338 mice. *Comp Immunol Microbiol Infect Dis, 34*(5), 387-397. doi:10.1016/j.cimid.2011.06.001

Orre, M., Kamphuis, W., Dooves, S., Kooijman, L., Chan, E. T., Kirk, C. J., . . . Hol, E. M. (2013). Reactive glia show increased immunoproteasome activity in Alzheimer's disease. *Brain, 136*(Pt 5), 1415-1431. doi:10.1093/brain/awt083

Orsi, A., Fioriti, L., Chiesa, R., & Sitia, R. (2006). Conditions of endoplasmic reticulum stress favor the accumulation of cytosolic prion protein. *J Biol Chem, 281*(41), 30431-30438. doi:10.1074/jbc.M605320200

Puttaparthi, K., & Elliott, J. L. (2005). Non-neuronal induction of immunoproteasome subunits in an ALS model: possible mediation by cytokines. *Exp Neurol, 196*(2), 441-451. doi:10.1016/j.expneurol.2005.08.027

Seifert, U., Bialy, L. P., Ebstein, F., Bech-Otschir, D., Voigt, A., Schroter, F., . . . Kruger, E. (2010). Immunoproteasomes preserve protein homeostasis upon interferon-induced oxidative stress. *Cell, 142*(4), 613-624. doi:10.1016/j.cell.2010.07.036

Song, K., Na, J. Y., Oh, M. H., Kim, S., Kim, Y. H., Park, B. Y., . . . Kwon, J. (2012). Synthetic Prion Peptide 106-126 Resulted in an Increase Matrix Metalloproteinases and Inflammatory Cytokines from Rat Astrocytes and Microglial Cells. *Toxicol Res, 28*(1), 5-9. doi:10.5487/tr.2012.28.1.005

Stohwasser, R., Giesebrecht, J., Kraft, R., Muller, E. C., Hausler, K. G., Kettenmann, H., . . . Kloetzel, P. M. (2000). Biochemical analysis of proteasomes from mouse microglia: induction of immunoproteasomes by interferon-gamma and lipopolysaccharide. *Glia, 29*(4), 355-365.

Stohwasser, R., Standera, S., Peters, I., Kloetzel, P. M., & Groettrup, M. (1997). Molecular cloning of the mouse proteasome subunits MC14 and MECL-1: reciprocally regulated tissue expression of

interferon-gamma-modulated proteasome subunits. *Eur J Immunol, 27*(5), 1182-1187. doi:10.1002/eji.1830270520

Tribouillard-Tanvier, D., Striebel, J. F., Peterson, K. E., & Chesebro, B. (2009). Analysis of protein levels of 24 cytokines in scrapie agent-infected brain and glial cell cultures from mice differing in prion protein expression levels. *J Virol, 83*(21), 11244-11253. doi:10.1128/jvi.01413-09

Ugras, S., Daniels, M. J., Fazelinia, H., Gould, N. S., Yocum, A. K., Luk, K. C., . . . Ischiropoulos, H. (2018). Induction of the Immunoproteasome Subunit Lmp7 Links Proteostasis and Immunity in alpha-Synuclein Aggregation Disorders. *EBioMedicine*. doi:10.1016/j.ebiom.2018.05.007

Vincenti, J. E., Murphy, L., Grabert, K., McColl, B. W., Cancellotti, E., Freeman, T. C., & Manson, J. C. (2015). Defining the Microglia Response during the Time Course of Chronic Neurodegeneration. *J Virol, 90*(6), 3003-3017. doi:10.1128/jvi.02613-15

Vogel, C., & Marcotte, E. M. Insights into the regulation of protein abundance from proteomic and transcriptomic analyses. *Nat Rev Genet, 13*(4), 227-232. doi:10.1038/nrg3185

Wagner, L. K., Gilling, K. E., Schormann, E., Kloetzel, P. M., Heppner, F. L., Kruger, E., & Prokop, S. (2017). Immunoproteasome deficiency alters microglial cytokine response and improves cognitive deficits in Alzheimer's disease-like APPPS1 mice. *Acta Neuropathol Commun, 5*(1), 52. doi:10.1186/s40478-017-0453-5

Figures and Figure Legends

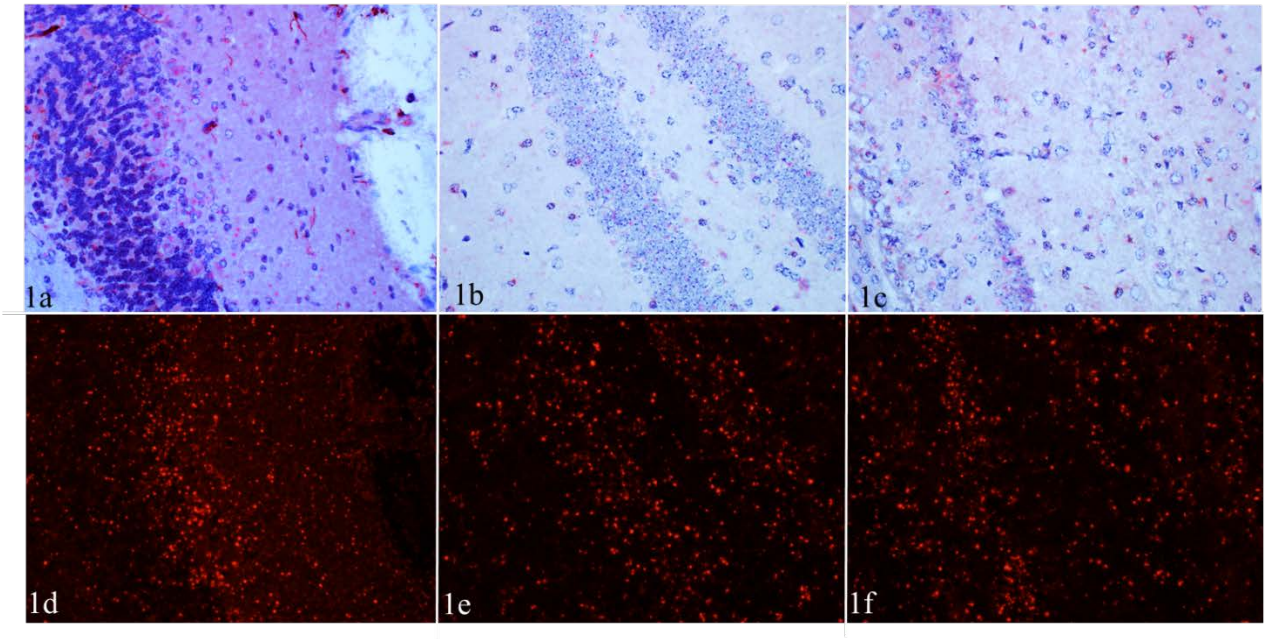

Figure 1. PSMB10 mRNA expression in brain. Red puncta each correspond to a hybridized transcript copy. Increased PSMB10 probe density is observed in the Purkinje layer of the cerebrum (1a,d), granular layer of the dentate gyrus (1b,e) and pyramidal layer of CA1 (1c,f). In-situ hybridization, RNAscope, 400x, brightfield hematoxylin counterstain (a-c), RFP fluorescence (d-e).

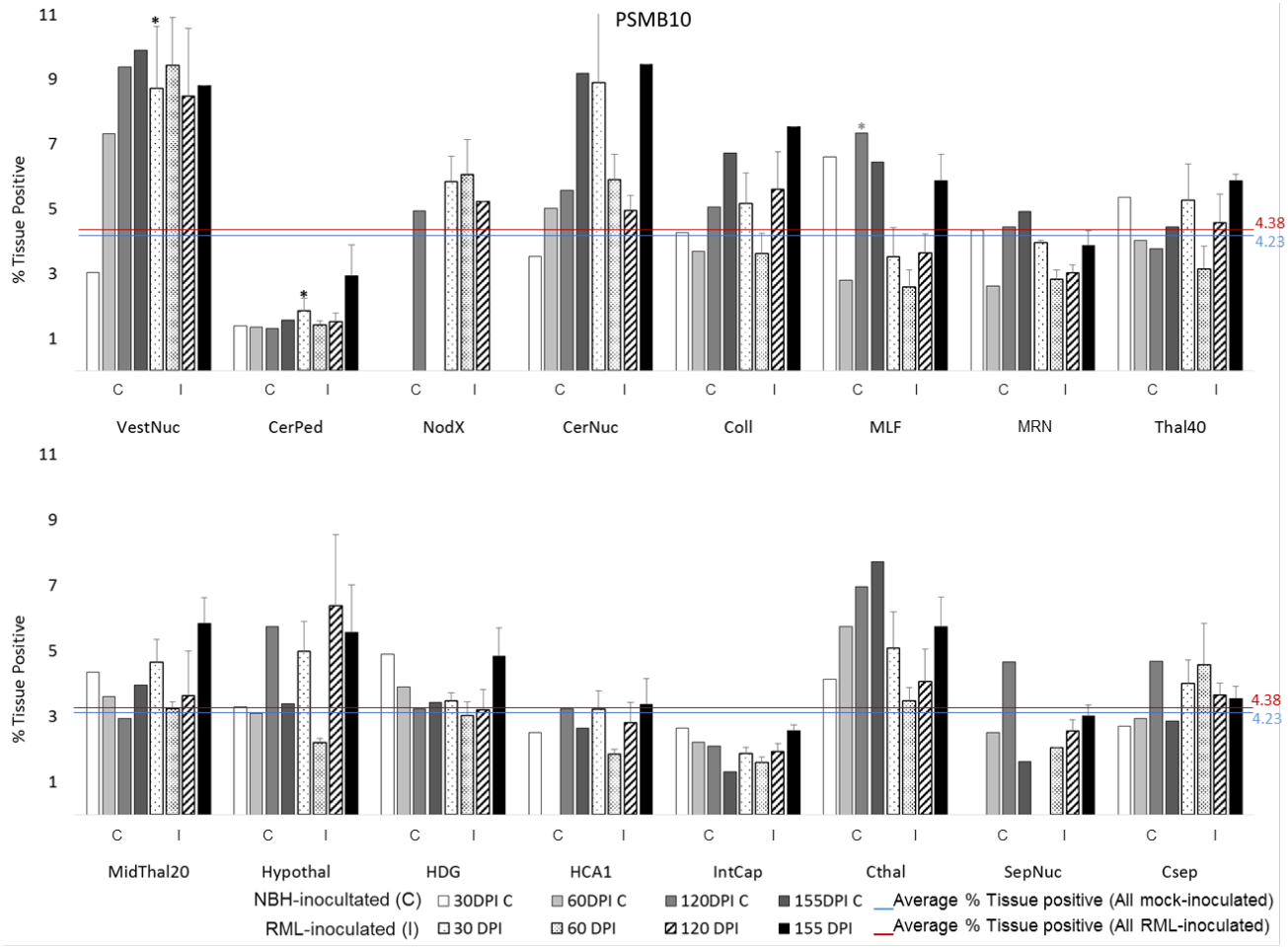

Figure 2. Total PSMB10 hybridization probe signal in 16 brain regions over RML infection timecourse. PSMB10 expression quantified as % tissue positive for red hybridization signal. Bars represent mean±SE values for mock-inoculated and RML-inoculated animal cohorts at each timepoint. *$p < 0.05$; significant differences compared with control (mock-inoculated) animals. Horizontal lines represent mean % tissue positive for PSMB10 for all mock-inoculated (blue) and all RML-inoculated animals (red). Vestibular nuclei (VestNuc), cerebellar peduncles (CerPed), cerebellar cortex (nodulus X, NodX), cerebellar nuclei (CerNuc), colliculus (Coll), medial longitudinal fasciculus (MLF), midbrain reticular nucleus (MRN), lateral thalamus (LatThal),

medial thalamus (MedThal), hypothalamus (Hypothal), dentate gyrus of hippocampus (HDG), CA1 of hippocampus (HCA1), internal capsule (IntCap), cerebral cortex at level of thalamus (Cthal), septal nuclei (SepNuc), cerebral cortex at level of septal nuclei (Csep).

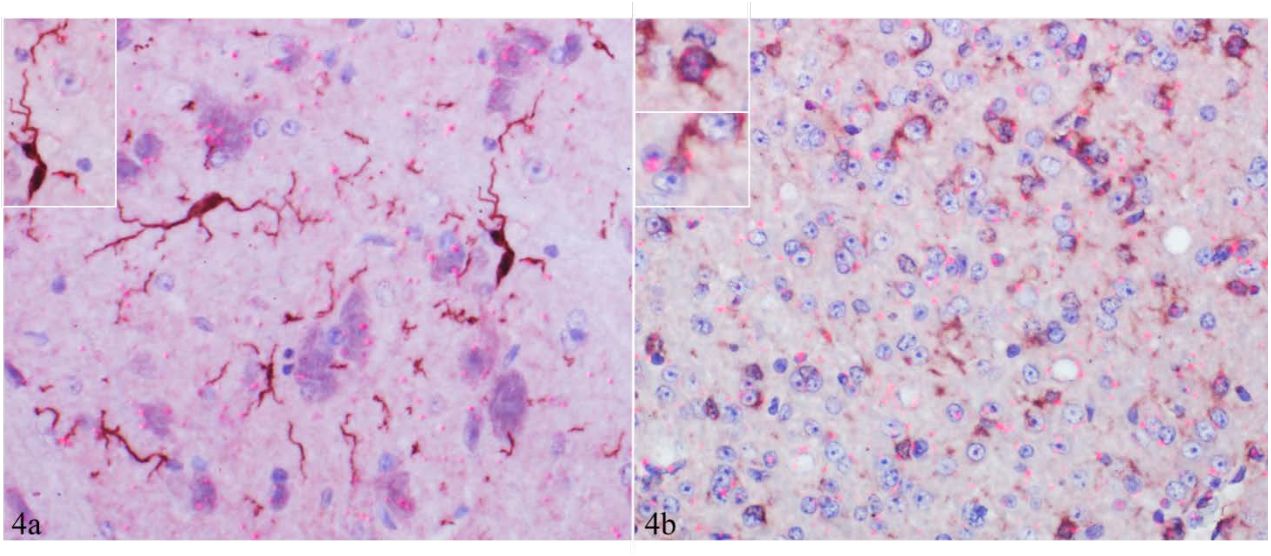

Figure 3. Immunoreactivity for Iba1 with concurrent ISH for PSMB10 in a 30DPI animal (4a) and a 155DPI animal (4b). Sporadic signal puncta overlie microglial processes (insets). While hypertrophy of microglial processes is visible in the clinical animal, the majority of PSMB10 signal is present in the neuropil and around neurons, as in the 30DPI animal. Brainstem (4a), cerebellar peduncle (4b), NovaRed, hematoxylin and RNAscope® 2.5 HD Assay (RED), 400x.

Psmb10 Control vs	Infected	p<
VestNuc	-0.01482	0.9852
CerPed	0.9741	0.0259
CerNuc	0.34767	0.6523
Coll	0.97664	0.0234
MLF	0.54168	0.4583
DMN	0.69238	0.3076
Thal40	0.51597	0.484
MidThal20	0.58637	0.4136
Hypothal	0.66056	0.3394
HDG	-0.23401	0.766
HCA1	-0.95709	0.1872
IntCap	-0.83077	0.1692
Cthal	0.17133	0.8287
SepNuc	-0.25761	0.8341
Csep	-0.33099	0.669

Table 1. Pearson's correlation coefficients (r=) for PSMB10 expression in control and infected animals at each timepoint. Vestibular nuclei (VestNuc), cerebellar peduncles (CerPed), cerebellar nuclei (CerNuc), colliculus (Coll), medial longitudinal fasciculus (MLF), midbrain reticular nucleus (MRN), lateral thalamus (LatThal), medial thalamus (MedThal), hypothalamus (Hypothal), dentate gyrus of hippocampus (HDG), CA1 of hippocampus (HCA1), internal capsule (IntCap), cerebral cortex at level of thalamus (Cthal), septal nuclei (SepNuc), cerebral cortex at level of septal nuclei (Csep). No correlation for cerebellar cortex (nodulus X, NodX) due to lack of control data.

Psmb10 vs	Iba1	GFAP	iNOS	Arg1	SE	PrPSc
VestNuc	-0.53557	-0.40831	0.20596	-0.75826	-0.50467	-0.42187
CerPed	0.79655	0.8695	0.8132	0.55975	0.79405	0.81339
NodX	-0.98576	0.69452	0.76046	-0.52515	-0.98767	-0.98642
CerNuc	0.26602	0.26602	0.10939	0.74259	-0.19863	0.08393
Coll	0.76548	0.90606	0.60003	0.97937	0.84591	0.90154
MLF	0.76711	0.79617	0.76569	0.91792	0.56688	0.33841
DMN	0.10864	-0.00047	0.2846	0.84962	0.01254	-0.19432
Thal40	0.49641	0.44046	0.60527	0.74423	0.50055	0.33999
MidThal20	0.25275	0.26954	0.62234	0.59456	0.30173	0.68392
Hypothal	0.60024	0.12179	-0.70631	0.28087	0.70624	0.34422
HDG	0.74322	0.94445	0.90707	0.54555	0.72098	0.91649
HCA1	0.52872	0.52343	0.55918	0.1969	0.46349	0.5274
IntCap	0.90278	0.56756	0.96973	0.26543	0.89091	0.96057
Cthal	0.73643	0.30371	0.34285	0.74526	0.43603	0.65924
SepNuc	0.80855	-0.90864	0.99936	0.36854	0.83045	0.99994
Csep	-0.8197	-0.71302	0.8507	-0.84917	-0.84917	-0.49881

Significance (p value)	
p<0.05	p<0.001

Table 2. Pearson's correlation coefficients (r=) comparing PSMB10 expression with IHC stains from neuroinflammatory timecourse at each timepoint. Vestibular nuclei (VestNuc), cerebellar peduncles (CerPed), cerebellar nuclei (CerNuc), colliculus (Coll), medial longitudinal fasciculus (MLF), midbrain reticular nucleus (MRN), lateral thalamus (LatThal), medial thalamus (MedThal), hypothalamus (Hypothal), dentate gyrus of hippocampus (HDG), CA1 of hippocampus (HCA1), internal capsule (IntCap), cerebral cortex at level of thalamus (Cthal), septal nuclei (SepNuc), cerebral cortex at level of septal nuclei (Csep). No correlation for cerebellar cortex (nodulus X, NodX) due to lack of control data.

CHAPTER 4. GENERAL CONCLUSIONS

Summary

Transmissible spongiform encephalopathies and human neurodegenerative protein misfolding diseases exhibit parallels in the molecular identity, mechanism of propagation and neuroinflammatory response to their respective causative agents. Both deleterious and neuroprotective functions have been attributed to activated glial cells. Microglia and astrocytes are heterogeneously distributed throughout the brain, with regional variations in density and physiology. Different glial reactive phenotypes have been described in neurodegenerative diseases. An additional feature of neuroinflammation and accumulation of misfolded cellular proteins in these entities is variable impairment of proteolysis and induction of immunoproteasomes, a functional subtype of the ubiquitin proteasome system. Prion diseases exhibit strain-specific lesion distribution patterns, and the immunophenotypes of reacting glia have not been resolved throughout the brain. The goal of this dissertation was to characterize the temporospatial glial response to prion infection and to evaluate tissues for disease-associated changes in immunoproteasome expression. We found that microglia and astrocytes express different activation markers in late disease incubation, and that closely apposed anatomic locations can display variable patterns of neuropathology. We also demonstrated variation in expression of immunoproteasome subunit PSMB10 throughout the brain. This work lays a foundation for resolving glial immunophenotypes in prion infection and underscores the value of in-situ analysis of protein expression.

Chapter 2 presented a comprehensive spatiotemporal investigation of neuropathology associated with intracranial infection with RML scrapie. We characterized vacuolation, PrP^{sc} deposition and glial activation in 15 locations across the murine brain, and we utilized quantitative

immunohistochemistry to evaluate the expression of iNOS and Arg1, canonical markers of glial activation, and demonstrated upregulation of both in late disease incubation. Our findings support the existence of a primarily proinflammatory microglial profile, characterized by upregulation of iNOS, with negligible Arg1 expression. Astrocytes, however, were found to upregulate iNOS primarily in two white matter tracts, but display either transient or sustained increases in Arg1 expression in multiple brain regions. These results suggest that astrocytes may assume variable location-dependent activation phenotypes, and, to our knowledge, constitute the first such report in experimental prion infection.

In chapter 3, we used RNAscope®, an in-situ hybridization platform, to analyze expression of PSMB10 transcripts across a parallel timecourse of the same RML infection model described in chapter 2. PSMB10 encodes MECL1/$\beta 2_i$, the second subunit incorporated in immunoproteasome assembly. We demonstrated heterogeneous transcription levels across the healthy murine brain, but did not detect changes in transcript numbers in infected animals over time. To date, this represents the first comprehensive anatomically resolved characterization of PSMB10 expression in the healthy murine brain. Additionally, we detected potential temporal increases in PSMB10 at several locations in control animals that were not reproduced in infected animals. Age-related upregulation of immunoproteasome subunits has been demonstrated in murine and human brains, and our findings may provide evidence towards disruption of normal expression in prion disease.

Recommendations for Future Research

Expanding the marker pool: A(n even more) comprehensive analysis of the neuroinflammatory response to prion infection

Our findings demonstrate the utility of in-situ analysis of marker expression on a subanatomic scale. Whole or even partially dissected brain homogenates frequently used in cytokine and transcriptomic analysis in prion research are unlikely to have detected the nuanced expression of glial activation markers we described in anatomically apposed locations. However, our study accommodated evaluation of only two glial activation markers, which carries the risk of grossly underrepresenting glial heterogeneity and oversimplifying phenotype complexity (Ransohoff, 2016b). Additionally, the limited insight yielded by the PSMB10 ISH timecourse underscored the need for complementary protein-level analysis. Contextualization of these findings would furthermore have benefited from concurrent evaluation of the local cytokine milieu.

Ideally, these shortcomings would be resolved with the use of a comprehensive in-situ proteomics modality. However, multiplex analysis, especially that targeting protein expression, is limited either by availability of effective antibodies, such as with immunohistochemistry, or by the lack of microanatomic specificity, such as with Western blotting, which necessitates use of tissue homogenates. Laser dissection microscopy and subsequent proteomic and transcriptomic analysis of select cells is an option, however this modality does not easily support mass-throughput, as would be desired for a comprehensive anatomic timecourse.

We believe that the above requirements can be satisfied by MALDI imaging mass-spectrometry (IMS), a platform used for direct proteomic analysis of even paraffin-fixed

formalin-embedded tissues, with demonstrated applications in cancer classification, pharmacokinetics, and neurodegenerative disease research (Norris et al., 2013). Using this technique to analyze infection timecourses would yield the most relevant and comprehensive profile of the neuroinflammatory response to prion infection due to IMS's capacity to resolve in-situ protein expression down to a subcellular level. Furthermore, this modality is label-free and tissue-sparing, and can thus not only provide an expression profile for an unlimited number of protein targets across a tissue section, but leaves the sample essentially unaltered and available for redirection towards subsequent counterstaining or immunohistochemical analysis (Norris et al., 2013). Thus, we would propose to use IMS on the remaining archived tissues from this timecourse to generate the first truly exhaustive temporospatial profile of neuroinflammatory marker and proteasome subunit expression

Functional contribution of immunoproteasomes to prion pathology

Constitutive proteasome inhibition has been documented in prion disease. Even successful demonstration of immunoproteasome transcript or protein expression fluxes in prion-infected tissues would not address the functionality of these proteasomes. Additional insight into any potential role of immunoproteasomes in the pathophysiology of prion infection may be gained from timecourse studies using immunoproteasome inhibitors. Subunit-specific and pan-immunoproteasomal inhibitors are commercially available, and some are actively used in cancer therapeutics (Miller et al., 2013). Immunoproteasome inhibition in other neurodegenerative protein misfolding diseases has yielded mixed clinical outcomes (Orre et al., 2013; Wagner et al., 2017; Moritz et al., 2017; Ahtoniemi et al., 2007), but no similar study has been undertaken in prion research. We believe assessment of disease progression in the absence of functional

immunosubunits would complement expression analysis and supply valuable mechanistic insight.

Concluding remarks

Neuroinflammation has been proposed as a therapeutic target for protein misfolding diseases (Ransohoff, 2016a; Venigalla et al., 2016; Rizzo et al., 2014). Modulation of glial activation and population ablation in prion disease has been investigated, but yielded mixed clinical outcomes (Gomez-Nicola et al., 2013; Carroll et al., 2018; Zhu et al., 2016). Understanding glial dynamics in prion disease may identify targets for a more nuanced therapeutic approach. Our findings establish a baseline glial activation profile in prion infection, characterized by a proinflammatory microglial population, and a mixed spatially segregated astrocytic profile. Additionally, this work represents the first known characterization of PSMB10 expression across the murine brain, demonstrates the advantage of in-situ subanatomic marker expression analysis, and establishes the application of sequential chromogenic immunohistochemistry and RNAscope® in-situ hybridization in prion disease research.

REFERENCES

Ahtoniemi, T., Goldsteins, G., Keksa-Goldsteine, V., Malm, T., Kanninen, K., Salminen, A., & Koistinaho, J. (2007). Pyrrolidine dithiocarbamate inhibits induction of immunoproteasome and decreases survival in a rat model of amyotrophic lateral sclerosis. *Mol Pharmacol, 71*(1), 30-37. doi:10.1124/mol.106.028415

Carroll, J. A., Race, B., Williams, K., Striebel, J., & Chesebro, B. (2018). Microglia Are Critical in Host Defense Against Prion Disease. *J Virol*. doi:10.1128/jvi.00549-18

Gomez-Nicola, D., Fransen, N. L., Suzzi, S., & Perry, V. H. (2013). Regulation of microglial proliferation during chronic neurodegeneration. *J Neurosci, 33*(6), 2481-2493. doi:10.1523/jneurosci.4440-12.2013

Miller, Z., Ao, L., Kim, K. B., & Lee, W. (2013). Inhibitors of the Immunoproteasome: Current Status and Future Directions. *Curr Pharm Des, 19*(22), 4140-4151.

Moritz, K. E., McCormack, N. M., Abera, M. B., Viollet, C., Yauger, Y. J., Sukumar, G., . . . Burnett, B. G. (2017). The role of the immunoproteasome in interferon-gamma-mediated microglial activation. *Sci Rep, 7*(1), 9365. doi:10.1038/s41598-017-09715-y

Norris, J. L., & Caprioli, R. M. (2013). Analysis of tissue specimens by matrix-assisted laser desorption/ionization imaging mass spectrometry in biological and clinical research. *Chem Rev, 113*(4), 2309-2342. doi:10.1021/cr3004295

Orre, M., Kamphuis, W., Dooves, S., Kooijman, L., Chan, E. T., Kirk, C. J., . . . Hol, E. M. (2013). Reactive glia show increased immunoproteasome activity in Alzheimer's disease. *Brain, 136*(Pt 5), 1415-1431. doi:10.1093/brain/awt083

Ransohoff, R. M. (2016a). How neuroinflammation contributes to neurodegeneration. *Science, 353*(6301), 777-783. doi:10.1126/science.aag2590

Ransohoff, R. M. (2016b). A polarizing question: do M1 and M2 microglia exist? *Nat Neurosci, 19*(8), 987-991. doi:10.1038/nn.4338

Rizzo, F., Riboldi, G., Salani, S., Nizzardo, M., Simone, C., Corti, S., & Hedlund, E. (2014). Cellular therapy to target neuroinflammation in amyotrophic lateral sclerosis. *Cell Mol Life Sci, 71*(6), 999-1015. doi:10.1007/s00018-013-1480-4

Venigalla, M., Sonego, S., Gyengesi, E., Sharman, M. J., & Munch, G. (2016). Novel promising therapeutics against chronic neuroinflammation and neurodegeneration in Alzheimer's disease. *Neurochem Int, 95*, 63-74. doi:10.1016/j.neuint.2015.10.011

Wagner, L. K., Gilling, K. E., Schormann, E., Kloetzel, P. M., Heppner, F. L., Kruger, E., & Prokop, S. (2017). Immunoproteasome deficiency alters microglial cytokine response and improves cognitive deficits in Alzheimer's disease-like APPPS1 mice. *Acta Neuropathol Commun, 5*(1), 52. doi:10.1186/s40478-017-0453-5

Zhu, C., Herrmann, U. S., Falsig, J., Abakumova, I., Nuvolone, M., Schwarz, P., . . . Aguzzi, A. (2016). A neuroprotective role for microglia in prion diseases. *J Exp Med, 213*(6), 1047-1059. doi:10.1084/jem.20151000

APPENDIX. ADDITIONAL MATERIAL

Table A1. Pearson's correlation matrices comparing temporal trends in markers of prion-associated neuropathology in RML-infected animals at each brain location. Pearson's correlation coefficients (r=) are given in the table, and cell fill indicates significance (p<). Spongiform change (SE), Iba1, GFAP, iNOS, Arg1, colocalization of Arg1 with microglia (Arg1Iba1) and astrocytes (Arg1GFAP), colocalization of iNOS with microglia (iNOSIba1) and astrocytes (iNOSGFAP). Vestibular nuclei (VestNuc), cerebellar peduncles (CerPed), cerebellar nuclei (CerNuc), superior colliculus (Coll), medial longitudinal fasciculus (MLF), midbrain reticular nucleus (MRN), lateral thalamus (LatThal), medial thalamus (MedThal), hypothalamus (Hypothal), dentate gyrus of hippocampus (HDG), CA1 of hippocampus (HCA1), internal capsule (IntCap), cerebral cortex at level of thalamus (Cthal), septal nuclei (SepNuc), cerebral cortex at level of septal nuclei (Csep).

SE vs	PrPsc	Iba1	GFAP	iNOS	Arg1	Arg1Iba1	Arg1GFAP	iNOSIba1	iNOSGFAP
VestNuc	0.95102	0.9687	0.99329	0.60063	0.89089	0.9217	0.85765	0.92898	0.86427
CerPed	0.99289	0.98286	0.72204	0.87809	0.95183	0.98246	0.96901	0.93922	0.86939
CerNuc	0.76251	0.96144	0.89117	0.6347	0.38764	0.76544	0.78245	0.60424	0.6078
Coll	0.83169	0.98986	0.98685	0.79645	0.94204	0.99023	0.99559	0.98684	0.98676
MLF	0.14466	0.68477	0.71233	0.91989	0.69583	-0.41257	0.18532	0.90383	0.78505
MRN	0.70148	0.85874	0.93035	0.861	0.42151	0.73515	0.9962	0.8155	0.97877
LatThal	0.89402	0.94254	0.88397	0.86634	0.88772	0.82928	0.7676	0.72197	0.98494
MedThal	0.66681	0.97971	0.85807	0.80222	0.87959	0.91647	0.756	0.62358	0.97608
Hypothal	0.24941	0.03675	0.68806	0.21469	0.63795	0.39081	0.2854	0.91013	-0.09183
HDG	0.93475	0.99007	0.61769	0.94542	0.97036	0.99955	0.61023	0.84676	0.68766
HCA1	0.81294	0.91468	0.77942	0.75589	0.69747	0.70287	0.55541	0.7008	0.93659
IntCap	0.89348	0.99787	0.21764	0.87661	0.67591	0.8999	0.45047	0.91565	0.84467
Cthal	0.88128	0.91107	0.95883	0.93327	0.81035	0.89017	0.94464	0.86406	0.61335
SepNuc	0.8983	0.54976	-0.35007	0.6715	0.79872	0.6462	0.58642	0.79346	-0.28948
Csep	0.82592	0.98096	0.87914	0.02897	0.51381	0.04116	0.40056	0.55758	0.38723
Significance (p value)									
p<0.05	p<0.01	p<0.001							

PrPsc vs	Iba1	GFAP	iNOS	Arg1	Arg1Iba1	Arg1GFAP	iNOSIba1	iNOSGFAP	SE
VestNuc	0.92855	0.96128	0.41249	0.9043	0.94736	0.69927	0.89547	0.72527	0.95102
CerPed	0.99718	0.7454	0.92383	0.93076	0.96394	0.95489	0.96346	0.89016	0.99289
CerNuc	0.83353	0.83353	0.54777	0.31421	0.77002	0.77497	0.72626	0.61416	0.76251
Coll	0.78308	0.89989	0.52856	0.89711	0.88983	0.878	0.74666	0.75747	0.83169
MLF	0.56933	0.66157	0.44172	0.56624	0.31681	0.73599	0.35995	0.52834	0.14466
MRN	0.82632	0.85741	0.71602	0.29355	0.65386	0.71179	0.7248	0.74426	0.70148
LatThal	0.96813	0.98781	0.78553	0.78566	0.71108	0.69575	0.67845	0.87463	0.89402
MedThal	0.73704	0.75761	0.84704	0.84762	0.64055	0.09973	0.902	0.64572	0.66681
Hypothal	0.73972	0.45849	-0.23577	0.40893	0.89672	0.71196	0.16935	0.41624	0.24941
HDG	0.92793	0.79613	0.99864	0.8249	0.93626	0.29027	0.60963	0.78108	0.93475
HCA1	0.97739	0.94425	0.99463	0.1741	0.21099	-0.02347	0.97623	0.94717	0.81294
IntCap	0.91738	0.61184	0.99655	0.28053	0.61783	0.00603	0.99859	0.99452	0.89348
Cthal	0.91988	0.8884	0.88725	0.9862	0.994	0.98676	0.72152	0.69435	0.88128
SepNuc	0.38372	-0.377	0.59343	0.5447	0.35822	0.28282	0.87477	-0.39301	0.8983
Csep	0.75843	0.94639	0.03782	0.82592	0.02412	0.38624	0.13615	0.08239	0.82592
Significance (p value)									
p<0.05	p<0.01	p<0.001							

Iba1vs	GFAP	iNOS	Arg1	Arg1Iba1	Arg1GFAP	PrPSc	SE
VestNuc	0.94843	0.53023	0.87471	0.94862	0.90695	0.92855	0.9687
CerPed	0.73941	0.94374	0.92414	0.95316	0.95107	0.99718	0.98286
CerNuc	0.97236	0.68619	0.51073	0.8861	0.90184	0.83353	0.96144
Coll	0.95901	0.86228	0.88528	0.96275	0.9763	0.78308	0.98986
MLF	0.96511	0.85249	0.81233	0.31857	0.83037	0.56933	0.68477
MRN	0.98022	0.71423	0.41149	0.6968	0.87141	0.82632	0.85874
LatThal	0.95565	0.90935	0.91512	0.86357	0.61372	0.96813	0.94254
MedThal	0.89728	0.83103	0.8924	0.93792	0.72737	0.73704	0.97971
Hypothal	-0.18966	-0.46112	-0.24958	0.42165	0.96399	0.73972	0.03675
HDG	0.67889	0.94334	0.96674	0.99364	0.60951	0.92793	0.99007
HCA1	0.94233	0.95411	0.37692	0.4093	0.1879	0.97739	0.91468
IntCap	0.2794	0.89979	0.63768	0.8782	0.39975	0.91738	0.99787
Cthal	0.86599	0.77921	0.89084	0.92847	0.9499	0.91988	0.91107
SepNuc	0.5687	0.7314	0.79151	0.92599	0.66837	0.38372	0.54976
Csep	0.77985	0.16569	0.347	-0.10103	0.246	0.75843	0.98096
Significance (p value)							
p<0.05	p<0.01	p<0.001					

GFAP vs	iNOS	Arg1	Arg1Iba1	Arg1GFAP	PrPSc	SE	Iba1
VestNuc	0.62736	0.85899	0.89589	0.80528	0.96128	0.99329	0.94843
CerPed	0.82935	0.49597	0.58731	0.56173	0.7454	0.72204	0.73941
CerNuc	0.75119	0.68156	0.96411	0.97669	0.83353	0.89117	0.97236
Coll	0.7094	0.97607	0.99888	0.99734	0.89989	0.98685	0.95901
MLF	0.91221	0.91243	0.17227	0.77644	0.66157	0.71233	0.96511
MRN	0.78845	0.38647	0.71845	0.93475	0.85741	0.93035	0.98022
LatThal	0.74879	0.78132	0.69563	0.70409	0.98781	0.88397	0.95565
MedThal	0.61412	0.70118	0.69418	0.65733	0.75761	0.85807	0.89728
Hypothal	0.41895	0.9617	0.82073	0.04014	0.45849	0.68806	-0.18966
HDG	0.80261	0.4727	0.63197	-0.07538	0.79613	0.61769	0.67889
HCA1	0.94285	0.25572	0.32575	0.04889	0.94425	0.77942	0.94233
IntCap	0.60927	-0.47529	-0.1555	-0.70175	0.61184	0.21764	0.2794
Cthal	0.91302	0.80055	0.86618	0.93865	0.8884	0.95883	0.86599
SepNuc	-0.26416	0.12113	0.37441	0.19911	-0.377	-0.35007	0.5687
Csep	-0.19263	0.76389	0.26233	0.61427	0.94639	0.87914	0.77985
Significance (p value)							
p<0.05	p<0.01	p<0.001					

iNOS vs	Arg1	Iba1	GFAP	SE	PrPsc
VestNuc	0.19065	0.53023	0.62736	0.60063	0.41249
CerPed	0.76606	0.94374	0.82935	0.87809	0.92383
CerNuc	0.83074	0.68619	0.75119	0.6347	0.54777
Coll	0.57222	0.86228	0.7094	0.79645	0.52856
MLF	0.91266	0.85249	0.91221	0.91989	0.44172
MRN	0.74122	0.71423	0.78845	0.861	0.71602
LatThal	0.97732	0.90935	0.74879	0.86634	0.78553
MedThal	0.98803	0.83103	0.61412	0.80222	0.84704
Hypothal	0.21277	-0.46112	0.41895	0.21469	-0.23577
HDG	0.84382	0.94334	0.80261	0.94542	0.99864
HCA1	0.09532	0.95411	0.94285	0.75589	0.99463
IntCap	0.23838	0.89979	0.60927	0.87661	0.99655
Cthal	0.83529	0.77921	0.91302	0.93327	0.88725
SepNuc	0.38859	0.7314	-0.26416	0.6715	0.59343
Csep	-0.75923	0.16569	-0.19263	0.02897	0.03782
Significance (p value)					
p<0.05	p<0.01	p<0.001			

Arg1 vs	Iba1	GFAP	iNOS	SE	PrPsc
VestNuc	0.87471	0.85899	0.19065	0.89089	0.9043
CerPed	0.92414	0.49597	0.76606	0.95183	0.93076
CerNuc	0.51073	0.68156	0.83074	0.38764	0.31421
Coll	0.88528	0.97607	0.57222	0.94204	0.89711
MLF	0.81233	0.91243	0.91266	0.69583	0.56624
MRN	0.41149	0.38647	0.74122	0.42151	0.29355
LatThal	0.91512	0.78132	0.97732	0.88772	0.78566
MedThal	0.8924	0.70118	0.98803	0.87959	0.84762
Hypothal	-0.24958	0.9617	0.21277	0.63795	0.40893
HDG	0.96674	0.4727	0.84382	0.97036	0.8249
HCA1	0.37692	0.25572	0.09532	0.69747	0.1741
IntCap	0.63768	-0.47529	0.23838	0.67591	0.28053
Cthal	0.89084	0.80055	0.83529	0.81035	0.9862
SepNuc	0.79151	0.12113	0.38859	0.79872	0.5447
Csep	0.56217	0.76389	-0.75923	0.51381	0.82592
Significance (p value)					
p<0.05	p<0.01	p<0.001			

iNOSIba1 vs	Iba1NIG	GFAPNIG	Arg1Iba1coloc
VestNuc	0.8137	0.95501	0.76811
CerPed	0.96246	0.87791	0.86184
CerNuc	0.7758	0.89191	0.97349
Coll	0.98242	0.95308	0.96322
MLF	0.80295	0.87424	-0.29332
MRN	0.69919	0.7636	0.9706
LatThal	0.82514	0.6517	0.97384
MedThal	0.6598	0.50413	0.70137
Hypothal	0.13203	0.57164	0.31822
HDG	0.81642	0.13706	0.84037
HCA1	0.92378	0.93923	0.09745
IntCap	0.93695	0.57344	0.65833
Cthal	0.71526	0.71589	0.7764
SepNuc	0.377	-0.62453	0.23815
Csep	0.6767	0.14655	-0.12613
Significance (p value)			
p<0.05	p<0.01	p<0.001	

iNOSGFAP vs	Iba1NIG	GFAPNIG	Arg1GFAPcoloc
VestNuc	0.81385	0.87755	0.81115
CerPed	0.8793	0.93562	0.72522
CerNuc	0.71892	0.81991	0.89534
Coll	0.99786	0.94895	0.96916
MLF	0.91678	0.96881	0.6184
MRN	0.82327	0.90445	0.98656
LatThal	0.89332	0.86393	0.86406
MedThal	0.98981	0.8438	0.78594
Hypothal	-0.17343	0.65745	-0.27331
HDG	0.61262	0.37014	0.07653
HCA1	0.99116	0.94627	0.2801
IntCap	0.87285	0.67104	-0.0954
Cthal	0.42649	0.75756	0.67569
SepNuc	0.64	0.96637	0.21988
Csep	0.55152	-0.03847	-0.62397
Significance (p value)			
p<0.05	p<0.01	p<0.001	